January 2020

Investigation Of The Neurological Manifestations Of Lyme Disease And The Impact Of Borrelia Burgdorferi On The Epigenetic Landscape Of Astrocytes

Derick Thompson

INVESTIGATION OF THE NEUROLOGICAL MANIFESTATIONS OF LYME DISEASE AND THE IMPACT OF *BORRELIA BURGDORFERI* ON THE EPIGENETIC LANDSCAPE OF ASTROCYTES

by

Derick Kahn-Shung Thompson

Bachelor of Science, University of Minnesota - Twin Cities, 2011

A Dissertation

Submitted to the Graduate Faculty

of the

University of North Dakota

In partial fulfillment of the requirements

for the degree of Doctor of Philosophy in Biomedical Sciences

Grand Forks, North Dakota

August

2020

Name: Derick Thompson

Degree: Doctor of Philosophy

This document, submitted in partial fulfillment of the requirements for the degree from the University of North Dakota, has been read by the Faculty Advisory Committee under whom the work has been done and is hereby approved.

DocuSigned by:
Catherine Brissette
Catherine Brissette

DocuSigned by:
John Watt
John Watt

DocuSigned by:
Archana Dhasarathy
Archana Dhasarathy

DocuSigned by:
Junguk Hur
Junguk Hur

DocuSigned by:
Diane Darland
Diane Darland

This document is being submitted by the appointed advisory committee as having met all the requirements of the School of Graduate Studies at the University of North Dakota and is hereby approved.

DocuSigned by:
Chris Nelson
Chris Nelson
Dean of the School of Graduate Studies

7/14/2020
Date

PERMISSION

Title: Investigation of the Neurological Manifestations of Lyme Disease and the Impact of *Borrelia Burgdorferi* on the Epigenetic Landscape of Astrocytes

Department: Biomedical Sciences

Degree: Doctor of Philosophy

In presenting this dissertation in partial fulfillment of the requirements for a graduate degree from the University of North Dakota, I agree that the library of this University shall make it freely available for inspection. I further agree that permission for extensive copying for scholarly purposes may be granted by the professor who supervised my dissertation work, or in her absence, by the Chairperson of the department or the dean of the School of Graduate Studies. It is understood that any copying or publication or other use of this dissertation or part thereof for financial gain shall not be allowed without my written permission. It is also understood that due recognition shall be given to me and to the University of North Dakota in any scholarly use which may be made of any material in my dissertation.

Derick Kahn-Shung Thompson
August, 2020

TABLE OF CONTENTS

LIST OF TABLES

LIST OF FIGURES

ACKNOWLEDGEMENTS

I would like to extend my sincerest appreciation to my advisors, Dr. Catherine A. Brissette and Dr. John A. Watt, for their guidance, support, and providing the best educational and professional opportunity during my time at the University of North Dakota. Through their kindness, patience, encouragement, and mentorship, they provided a basis for my scientific career, and the work within this dissertation would not have been possible without this guidance. They have helped me grow not only as a professional but as a person as well. During these past five years they have been involved in several milestones of my life and were present during my marriage to my best friend, Monica Sohrabi Thompson. Thank you for all your support and for all the wisdom and knowledge you have imparted upon me.

To my committee members: Dr. Archana Dhasarathy, Dr. Junguk Hur, and Dr. Diane Darland, I still remember the day in which this committee was first formed. In the early days of my graduate career and with the next few years of my dissertation work laid out before me, the idea of accomplishing this work seemed like an impossibility. Through your support, assistance, and advisory commitment, you have all helped make this work a reality. To Dr. Dhasarathy, your knowledge of epigenetics has been invaluable to all my projects spanning my graduate career. To Dr. Hur, your expertise in bioinformatics has provided the tools necessary for the analysis of my work and has instilled a newfound passion

within me to pursue these analytical skills. To Dr. Darland, your knowledge of neuroscience and epigenetics provided the groundwork that bridged these two fields to form the backbone of my dissertation. Thank you all for your patience and wisdom that aided in my development to become a scientist.

To the Biomedical Sciences faculty and staff at the University of North Dakota, thank you for your support in providing a phenomenal educational experience. Thank you to Dr. Sergei Nechaev for your guidance in the technical and analytical aspects of my projects. I am very appreciative for the help of the specialized cores within the Department of Biomedical Sciences. Thank you to Sarah Abrahamson of the Imaging Core, and Beth Ann DeMontigny of the Histology Core. Additionally, I would like to thank the members of the Bioinformatics Core for providing guidance of the development of my projects – Dr. Bony De Kumar, Danielle Perley, and Hannah Huffman. A special thanks to all supportive staff – Jennifer Hershey, Jennifer Henry, Joyce Rice, Julie Horn, and Michael Ullrich. Thank you to Bonnie Kee for all your support and patience during these years.

I would like to extend my gratitude to all past and present lab members. To Dr. Tim Casselli and Dr. Yvonne Tourand – we joined the lab around the same time several years ago and during these years you both have been phenomenal colleagues. You have both helped in the development of many of the technical skills required for my work and you always made time to answer all my questions. Thank you for all your help.

I would like to give a special thank you to all my friends that I grew up with and made during my graduate career. Thank you to Sema Oncel, Dr. Emily Biggane, Dr. Joe Biggane, and Dr. Gaurav Datta for the time we have spent together and for brightening up the most stressful days of research. I would like to thank a group of friends that I have grown up with – The UbErs. Our time spent playing games together have been invaluable and necessary in providing a work-life balance that has brought many late nights of fun into my life.

Finally, I would like to express my gratitude and love to my family – My parents Randy and Soo-Yin; My brother Ryan, his wife Stephanie, and their son Oliver; And my parents-in-law Majid and Minoo, and brother-in-law Soheil. To my parents, and with all sincerity, you have provided a life filled with love, support, and happiness that is unmatched in this world – all of my past and future accomplishments are in part due to your hard work and devotion. During the pursuit of my PhD, I most unexpectedly found love – this is to my wife Monica, you are the love of my life and my best friend. Through the stressful days and the sleepless nights, you have always been there for me and I am forever grateful and enamored for your support during my graduate career. I am doubtlessly excited for all the adventures of our life that we will share together.

With love and admiration, I dedicate this work to my family.

You are the foundation of my life and the guiding light of my future.

ABSTRACT

Lyme disease, caused by the spirochete *Borrelia burgdorferi* (*Bb*), is the most commonly reported vector-borne disease in the United States – with 30,000 cases being reported to the CDC annually, though it is estimated that 300,000 individuals are infected each year in the U.S [1–4]. Due to the medical treatment of the disease, this equates to an estimated $712 million - $1.3 billion in medical costs each year [5]. Conclusively, due to the continued geographical spread and increasing incidence rate, Lyme disease is becoming a greater public health threat throughout the world.

The symptoms of Lyme disease can range from erythema migrans to more systematic disorders such as arthritis and neurological complications, termed neuroborreliosis [6,7]. Manifestations of neuroborreliosis include radiculoneuritis, meningitis, and facial palsy [8–10]. Interestingly, *B. burgdorferi* does not produce any known toxins, and it is thought that the resulting host immune response leads to cellular and tissue damage associated with clinical symptoms. Although many individuals will be effectively treated through the administration of antibiotics, up to 20% of patients will experience on-going symptoms termed Post-treatment Lyme Disease Syndrome (PTLDS). PTLDS is marked by persistent musculoskeletal pain and neurological complications. Inflammatory states have been associated to these symptoms with the invasion of peripheral immune cells and an increase of inflammatory cytokines.

Furthermore, the neurological complications of PTLDS has been associated with an increase in glial inflammation. It is well-documented that *B. burgdorferi* is capable of penetrating into the central nervous system (CNS); however, it is unknown how and where the bacterium does so. Additionally, the exact pathogenetic mechanisms of neuroborreliosis and PTLDS are poorly understood. The work within this dissertation aims to provide novel insight into these gaps in knowledge.

This dissertation is laid out into three sections relating to understanding the pathogenesis of the neurological effects of Lyme disease. In the first study, we aimed to provide an explanation for the dissemination of *B. burgdorferi* and peripheral immune cells into the central nervous system. Clinical presentations of neuroborreliosis is associated with an increase of peripheral immune cells, inflammatory chemokines, and live *B. burgdorferi* in the cerebrospinal fluid (CSF). To this end, we sought to investigate a direct route from hematogenous dissemination into the CSF. The choroid plexus (CP) is a structure within the ventricles of the brain that is responsible for the production of CSF, the formation of the blood-CSF barrier, and regulation of the immune response. This barrier allows for the exchange of specific nutrients, waste, and peripheral immune cells between the blood stream and CSF. We hypothesize that during infection of the choroid plexus, *Borrelia burgdorferi* will induce an immune response conducive to the chemotaxis of immune cells and subsequently lead to a pro-inflammatory state within the CNS. To investigate this hypothesis, we cultured primary human choroid plexus epithelial cells and infected with the *B. burgdorferi* strain B31 MI-

16 for 48 hours. RNA was isolated and used for RNA sequencing and RT-qPCR validation. Secreted proteins in the supernatant were analyzed via ELISA. Transcriptome analysis based on RNA sequencing determined a total of 160 upregulated genes and 98 downregulated genes. Pathway and biological process analysis determined a significant upregulation in immune and inflammatory genes specifically in chemokine and interferon related pathways. Further analysis revealed downregulation in genes related to cell to cell junctions including tight and adherens junctions. Protein analysis of secreted factors showed an increase in inflammatory chemokines, corresponding to our transcriptome analysis. These data further demonstrate the role of the CP in the modulation of the immune response in a disease state and give insight into the mechanisms by which *Borrelia burgdorferi* may disseminate into, and act upon, the CNS. Future experiments aim to detail the impact of *B. burgdorferi* on the blood-CSF-barrier (BCSFB) integrity and inflammatory response within animal models.

The second and third study aim to elucidate the pathogenic mechanisms of neuroborreliosis and PTLDS, specifically the manifestations of a persistent inflammatory state. As *B. burgdorferi* has previously been shown to elicit an inflammatory response in astrocytes, and glial inflammation is associated with PTLDS, we sought to investigate the epigenetic modifications associated with the astrocytic response in order to determine a mechanistic explanation to these disorders. In the second study, we investigated the differential DNA methylation of astrocytes in response to three strains of *B. burgdorferi* – B31 MI-16, B31 e2,

and 297 through the use of beadchip array. This study utilized primary human astrocytes *in vitro*. This study was met with a limiting factor in biological replicate variability that led to diminished results. Nevertheless, differential methylation within specific genes involving vesicle trafficking and cell communication were observed. This suggests that DNA methylation may be a mechanistic explanation for the changes in gene expression of astrocytes in response to *B. burgdorferi*.

In the third study, we utilized the same astrocyte model of the second study to investigate the effects of *B. burgdorferi* on chromatin structure of astrocytes. We performed *in vitro* infection of astrocytes with the B31 MI-16 strain for 24, 48, 72, and 96 hours. Following infection, ATAC-seq was performed to interrogate the chromatin structure of astrocytes in response to *B. burgdorferi*. We observed a robust change in chromatin accessibility at 24-hours with 25,464 differential peaks. At 48, 72, and 96 hours, these peaks were reduced to 7,266, 3,376, and 3,015 respectively. Additionally, while many of the differential peaks were associated with open chromatin at 24, 48, and 72 hours, the 96-hour time point was marked by a dramatic decrease in chromatin accessibility. Many of the peaks within gene bodies at the first three time points were associated with changes in anatomical and morphological alterations, while the 96-hour time point was highlighted by metabolic and cellular stress. This suggests that astrocytes undergo an acute response following infection observed by a large change in chromatin structure associated with inflammation and immune response genes, which later decrease in accessibility. Motif enrichment analysis

provides greater insight into the overall response of astrocytes across time points. The AP-1 transcription factor is involved in the transcription of genes in response to inflammatory stimuli, stress signals, and infection. This transcription factor is made up of a heterodimer that includes the FOS, JUN, ATF, and JDP families. Motif analysis indicated significant enrichment of these family members at each time point, and in fact, analysis of peaks shared amongst all time points indicated AP-1 motif as being the most significantly enriched. These data suggest that the response of astrocytes to *B. burgdorferi* is in part due to the changes in chromatin accessibility that provides an environment for the transcription of genes associated with the inflammatory and immune response. Furthermore, AP-1 has been implicated as a potential transcription factor responsible for these changes in gene expression.

Together, the work within this dissertation demonstrates potential mechanisms for the pathogenesis of neuroborreliosis and PTLDS. This is highlighted by the potential of the choroid plexus as a route of dissemination for *B. burgdorferi* and peripheral immune cells into the CNS as an explanation for the clinical manifestations of neuroborreliosis. Additionally, these studies are the first to implicate *B. burgdorferi* as an epimutagen which provides insight into the mechanisms and development of the neurological and persistent symptoms of Lyme disease. In conclusion, this work provides novel insights for the pathogenesis of the neurological effects of Lyme disease which may aid in the development of future therapeutics.

CHAPTER I

AN INTRODUCTION TO LYME DISEASE

A Brief History of Lyme Disease

In 3300 BCE, a man colloquially known as Ötzi the Iceman died in the Ötztal Alps on the Austrian-Italian border, with evidence indicating he had likely died a violent death, and it wouldn't be until 1991 when his body was first discovered [6,7]. Following three decades of work and the advent of next-generation sequencing technologies, researchers were able to uncover a detailed medical history of Ötzi which included musculoskeletal abnormalities associated with arthritis and the presence of *Borrelia burgdorferi* (*Bb*) DNA from a bone biopsy of Ötzi's pelvis – evidence of the earliest human case of Lyme disease [8,9]. Though the Iceman may hold the record for the first known case of Lyme disease, he most likely was not the first individual to have contracted the pathogen, as recent phylogenetic research in the U.S. suggests that *B. burgdorferi* may have first diverged from a common ancestor 60,000 years ago [10]. However ancient *Borrelia burgdorferi* may be, it wasn't until the 1970's when doctors and scientists first identified Lyme disease.

In 1975 a cluster of cases originally thought to be juvenile rheumatoid arthritis were identified in the towns of Lyme and Old Lyme, Connecticut [11]. This epidemic form of arthritis was initially investigated by Steere et al. and

ultimately led to the recognition of what is now known as Lyme disease [12]. Upon this investigation, it was initially suggested that a tick was the main vector of Lyme arthritis, and in 1978 the first epidemiological evidence was found, showing the tick, *Ixodes scapularis*, was the main vector for the disease [13,14]. Though the characterization of the disease and its vector were being investigated, the infectious agent was still unknown. It was in 1982 in which Burgdorfer and his colleagues first isolated the infectious agent, now known as the spirochete bacterium *Borrelia burgdorferi* [15].

Since its discovery, Lyme disease has seen a consistent increase in the number of reported cases in the United States, with approximately 30,000 cases being reported each year (Figure I-1A) [16]. However, since only a small percentage of cases are reported, the total number of individuals who contract Lyme disease are estimated to be around 300,000 annually in the US. This estimation comes from two studies from the Centers for Disease Control and Prevention (CDC) that utilized clinical laboratory testing results of people who tested positive for Lyme disease and used medical claims from insurance databases [3,4]. These cases are not uniformly distributed throughout the US. In fact, 93% of reported illnesses are within 15 states, concentrated within the Northeast and upper Midwest regions, but are expanding into other states (Figure I-1C, Table I-1) [16]. As the most reported vector-borne disease in the US, the economic burden of medical costs are estimated to be between $712 million to $1.3 billion each year – these figures are attributed to initial testing and treatment of Lyme disease and ongoing healthcare associated with post-

Figure I - 1. Incidence and geographical distribution of confirmed Lyme disease.

An infographic of Lyme disease incidence and geographical distribution. **A)** The number of reported cases in the United States by year from 1996-2018. Changes to case definition were made in 2008 to strengthen requirements of a confirmed case. The definition for a confirmed case is a positive culture for *B. burgdorferi* and a positive two-tier IgM or IgG serological test or a single-tier positive IgG immunoblot. A probable case requires evidence of infection and clinical diagnosis of Lyme disease, but does not fully meet the confirmed disease definition. **B)** The average number of confirmed cases in the US by month from 2008-2018. Peak disease onset is in June and July. **C)** A geographical map of the United States indicating the distribution of the average annual rate of confirmed Lyme disease from 2008-2015. High incidence regions are found in the Northeast and Upper Midwest regions. Associated values for each state can be found in Table 1-1. All data was obtained from the Center for Disease Control and Prevention [1].

A

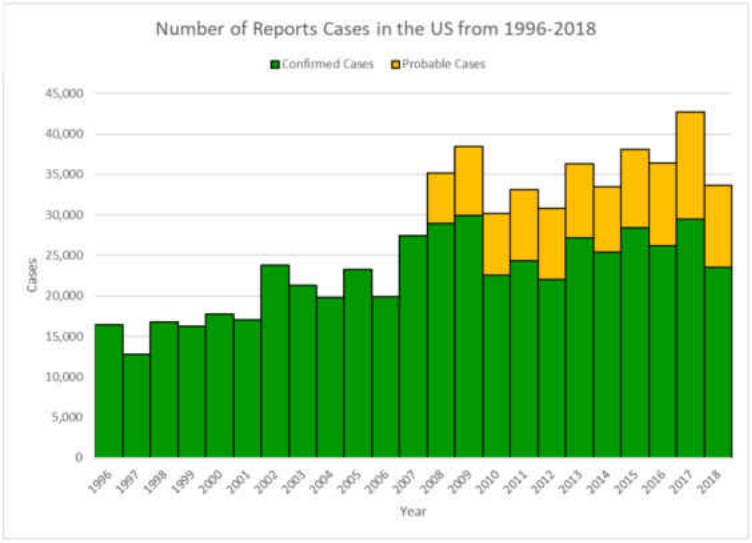
Number of Reports Cases in the US from 1996-2018
Confirmed Cases
Probable Cases
45,000
40,000
35,000
30,000
25,000
20,000
15,000
10,000
5,000
0
Cases
1996
1997
1998
1999
2000
2001
2002
2003
2004
2005
2006
2007
2008
2009
2010
2011
2012
2013
2014
2015
2016
2017
2018
Year

B

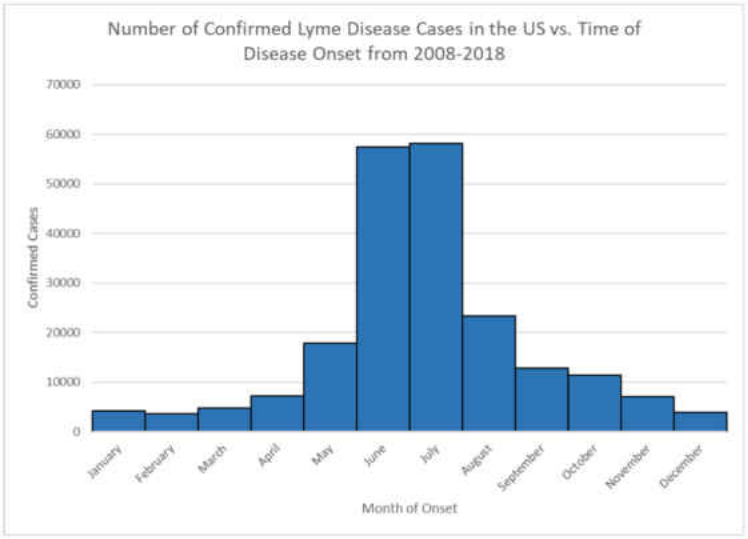
Number of Confirmed Lyme Disease Cases in the US vs. Time of Disease Onset from 2008-2018
70000
60000
50000
40000
30000
20000
10000
0
Confirmed Cases
January
February
March
April
May
June
July
August
September
October
November
December
Month of Onset

C

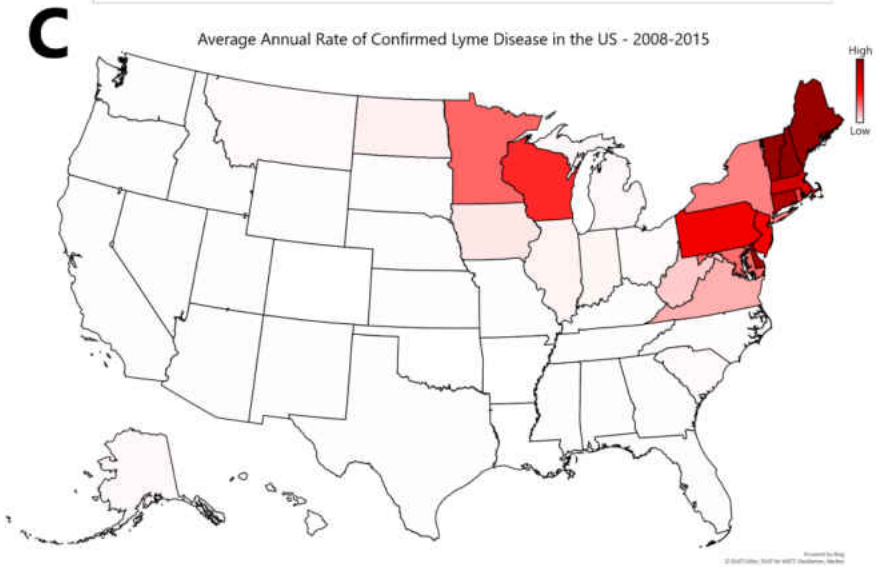
Average Annual Rate of Confirmed Lyme Disease in the US - 2008-2015
High
Low

Table I - 1. Incidence rates of confirmed Lyme disease per 100,000 individuals in each state and district. From 2008-2015

	Year								
State/Area	2008	2009	2010	2011	2012	2013	2014	2015	Average
High Incidence									
Connecticut	77.2	77.2	54.9	55.8	46	58.7	47.8	52.2	58.7
Delaware	87.3	110.3	72.9	84.5	55.3	43.2	36.4	35.3	65.2
Maine	58.6	59.5	42.1	60.3	66.6	84.8	87.9	74.7	66.8
Maryland	30.7	25.6	20.1	16.1	18.9	13.5	16	20.8	20.1
Massachusetts	61.2	61.7	36.3	27.2	51	56.9	54	43	48.9
Minnesota	19.9	20.1	24.3	22.2	16.9	26.4	16.4	21.4	21
New Hampshire	92	75.7	63	67.3	75.8	100.1	46.8	32.8	69.1
New Jersey	36.9	52.5	37.7	38.4	30.8	31.3	29	43.9	37.5
New York	29.9	21.4	12.3	16	10.4	17.8	14.4	16.4	17.3
Pennsylvania	30.3	39.1	25.9	37.2	32.5	39	50.6	57.4	39
Rhode Island	17.6	14.2	10.9	10.6	12.6	42.2	54	53.4	27
Vermont	52.9	51.7	43.3	76	61.6	107.5	70.5	78.4	67.8
Virginia	11.3	8.8	11.4	9.3	9.8	11.2	11.7	13.1	10.8
Wisconsin	26.5	34.4	44	42.2	23.9	25.2	17.2	22.7	29.5
Neighboring									
District of Columbia	12.2	8.9	5.6	N/A	N/A	5.1	5.3	11.6	8.1
Illinois	0.8	1.1	1.1	1.5	1.6	2.6	1.8	2.2	1.6
Indiana	0.7	0.9	1	1.2	1	1.5	1.5	1.5	1.2
Iowa	2.8	2.5	2.2	2.3	3	4.9	3.5	4.2	3.2
Kentucky	0.1	0	0.1	0.1	0.2	0.4	0.2	0.3	0.2
Michigan	0.8	0.8	0.8	0.9	0.8	1.2	0.9	1.3	0.9
North Carolina	0.2	0.2	0.2	0.2	0.3	0.4	0.3	0.4	0.3
North Dakota	1.2	1.5	3.1	3.2	1.4	1.7	0.3	2	1.8
Ohio	0.3	0.4	0.2	0.3	0.4	0.6	0.8	1	0.5
South Dakota	0.4	0.1	0.1	0.2	0.5	0.4	0.2	0.6	0.3
Tennessee	0.1	0.2	0.1	0.1	0	0.2	0.1	0.1	0.1
West Virginia	6.5	7.7	6.9	5.8	4.4	6.3	6.1	13.2	7.1
Low Incidence									
Alabama	0.1	0.1	0	0.2	0.3	0.2	0.6	0.3	0.2
Alaska	0.9	1	1	1.2	0.5	1.9	0.7	0.1	0.9
Arizona	0	0	0	0.1	0.1	0.3	0.2	0.1	0.1
Arkansas	0	0	0	0	0	0	0	0	0
California	0.2	0.3	0.3	0.2	0.2	0.2	0.1	0.2	0.2
Colorado	0	0	0	0	0	0	0	0	0
Florida	0.4	0.4	0.3	0.4	0.3	0.4	0.4	0.6	0.4
Georgia	0.4	0.4	0.1	0.3	0.3	0.1	0	0.1	0.2
Hawaii	0	0	0	0	0	0	0	0	0
Idaho	0.3	0.3	0.4	0.2	0	0.9	0.5	0.2	0.4
Kansas	0.6	0.6	0.2	0.4	0.3	0.6	0.4	0.4	0.4
Louisiana	0.1	0	0	0	0.1	0	0	0	0
Mississippi	0	0	0	0.1	0	0	0.1	0.1	0.1
Missouri	0.1	0.1	0.1	0.1	0	0	0.1	0	0.1
Montana	0.6	0.3	0.3	0.9	0.6	1.6	0.5	0.2	0.6
Nebraska	0.4	0.2	0.4	0.4	0.3	0.4	0.3	0.3	0.3
Nevada	0.3	0.4	0.1	0.1	0.4	0.4	0.1	0.2	0.2
New Mexico	0.2	0	0.1	0.1	0	0	0	0	0.1
Oklahoma	0	0.1	0	0.1	0	0	0	0	0
Oregon	0.5	0.3	0.2	0.2	0.1	0.3	0.1	0.1	0.2
South Carolina	0.3	0.5	0.4	0.5	0.7	0.7	0.4	0.3	0.5
Texas	0.4	0.4	0.2	0.1	0.1	0.2	0.1	0.1	0.2
Utah	0.1	0.2	0.1	0.2	0.1	0.3	0.2	0.1	0.2
Washington	0.3	0.2	0.2	0.2	0.2	0.2	0.1	0.2	0.2
Wyoming	0.2	0.2	0	0.2	0.5	0.2	0.3	0	0.3

treatment Lyme disease syndrome (PTLDS) [10]. Though many individuals will recover through effective treatment, Lyme disease can lead to a wide range of symptoms that can be long lasting and detrimental to the patient.

The Genetics of *Borrelia burgdorferi*

In 1997, the genomic sequence of *B. burgdorferi* strain B31 was sequenced, making it the third microbial genome to be sequenced, behind *Haemophilus influenzae* and *Mycoplasma genitalium* [17–19]. The genome of B. burgdorferi is highly complex and quite unusual with respect to other bacterial genomes – it consists of a nearly 1 megabase linear chromosome (~950 kb) with a highly variable set of circular and linear plasmids that range in size from 5 kb (linear plasmid 5, lp5) to 56 kb (lp56) [19,20]. While some plasmids are quite evolutionarily stable (i.e. lp54, cp26), many have undergone non-homologous and duplicative recombination, accounting for the wide diversity in plasmid number and content [21]. The strain B31 MI was shown to contain 21 plasmids (12 linear and 9 circular), though a recent study of 14 *B. burgdorferi* sensu stricto (s.s.) strain isolates showed that the bacteria can carry between 9 and 23 plasmids [20,21].

Selective pressure from the environment in which the bacteria persists has been shown to cause changes in plasmid content. In fact, one consideration researchers must take is the number of *in vitro* passages that *B. burgdorferi* undergoes, as continual cultivation can lead to loss of plasmids [22–24]. Furthermore, plasmid loss, such as lp25, has been shown to be correlated to loss of infectivity in *in vivo* models, suggesting specific genes within these plasmids

are required for successful infection but not necessary for survival within *in vitro* environments [23,25]. With regards to plasmid content, changes in gene expression have been documented during each stage of the bacterial life cycle from tick to host.

During its life cycle, *B. burgdorferi* encounters a wide range of environments and has been observed to undergo adaptions to gene expression in response to changes in pH, carbon dioxide, oxygen, osmolarity, and nutrients [26–31]. The bacteria utilize two major systems to regulate the expression of genes during its enzootic life cycle between tick and host: Rrp2-RpoN-RpoS regulatory system and histidine kinase (Hk)1-Rrp1 two-component transduction system (TCS). RpoS is an alternative RNA polymerase σ-factor necessary for transcription of a large number of genes that encode proteins necessary for transmission between the tick and host, maintenance of infection within the host, as well as persistence within the tick [32,33]. RpoN, another alternative RNA polymerase σ-factor, is responsible for the transcription of RpoS, which requires an open *rpoS* promoter complex that is mediated by phosphorylated response regulatory protein 2 – Rrp2 [34–36]. TCS proteins generally mediate bacterial adaptation to their surroundings. The Hk1/Rrp1 system controls the transcription of genes that are essential for survival during enzootic cycle transitions, that occur during tick feeding with the uptake or deposition of *B. burgdorferi* [37]. Binding of ligands to the periplasmic domains of Hk1 leads to the initiation of a signaling cascade that activates Rrp1, which in turn leads to the production of cyclic di-GMP, a secondary messenger. Hk1/Rrp1 is required for the colonization

of the tick midgut, and spirochetes that lack either component do not survive [37,38].

During infection of a host, the Rrp2-RpoN-RpoS system is activated, allowing host genes to be expressed, while inversely, genes required within the tick are repressed. The outer surface proteins (Osps) of *B. burgdorferi* exemplify these changes in gene expression. Within the host, OspC, allows for the initial establishment of early infection, but is later repressed when no longer required to maintain the infection. During the uptake of the bacteria from host to tick, the Rrp2-RpoN-RpoS system is inactive, and the Hk1/Rrp1 system activates expression of tick-phase genes such as OspA, leading to colonization of the tick midgut via binding of Tick Receptor for OspA (TROSPA). Spirochetes that lack OspA fail to colonize the tick and are later expelled [39–41]. During this initial tick phase, Hk1/Rrp1 induces gene expression within the *glp* operon allowing for utilization of glycerol[42]. During the unfed nymphal stage, *B. burgdorferi* encounters a nutrient-deficient environment, where both *Bb* gene expression systems become inactive while tick-phase genes remain expressed [34,35]. During the next blood meal, the large influx of nutrients mediates a robust change in *Bb* gene expression that allows *B. burgdorferi* to take advantage of the new environment. Activation of the Rrp2-RpoN-RpoS and Hk1/Rrp1 systems provides a shift in gene expression towards mammalian infection and transmission, respectively [35]. OspA is subsequently downregulated, allowing for the detachment and transmission from tick to host. OspC, conversely is

upregulated and required for the initial dissemination and immune evasion necessary for the establishment of early infection in mammals [43,44].

The Enzootic Life Cycle of *Borrelia burgdorferi* and *Ixodes scapularis*

B. burgdorferi sensu lato (s.l.). is primarily transmitted by four species of *Ixodes* tick throughout the world: *Ixodes scapularis* in upper Midwestern and Northeastern North America, *Ixodes pacificus* in Western North America, *Ixodes persulcatus* in Asia, and *Ixodes ricinus* in Europe [45–47]. The life cycle of *B. burgdorferi* and *Ixodes scapularis* is depicted in Figure I-2. There are three stages of the tick life cycle, in which a blood meal is taken at each stage: larva, nymph, and adult. As *B. burgdorferi* cannot be transovarially transmitted, the larva hatch from eggs uninfected, requiring each generation to re-acquire the pathogen from infected reservoir hosts [48]. Larva will typically hatch in the spring and begin seeking a blood meal and acquire *B. burgdorferi* if feeding on an infected reservoir host. Following its first blood meal, infected larva will begin molting to the nymph stage, and retain the infection transstadially, that is, the infection is maintained between each life stage. Nymphs will emerge in the spring, and again, the tick will begin questing for a blood meal by climbing grass or other tall structures to increase the likelihood of encountering a host. Though nymphs tend to feed on small to medium animals, this provides the first opportunity for *B. burgdorferi* to be transmitted to reservoir species to maintain a constant transmission cycle or to be transmitted to dead-end hosts such as humans. Following this feeding, the nymphs will detach and molt to adults in the fall of the same year. At this stage, adults will find medium to large mammals to

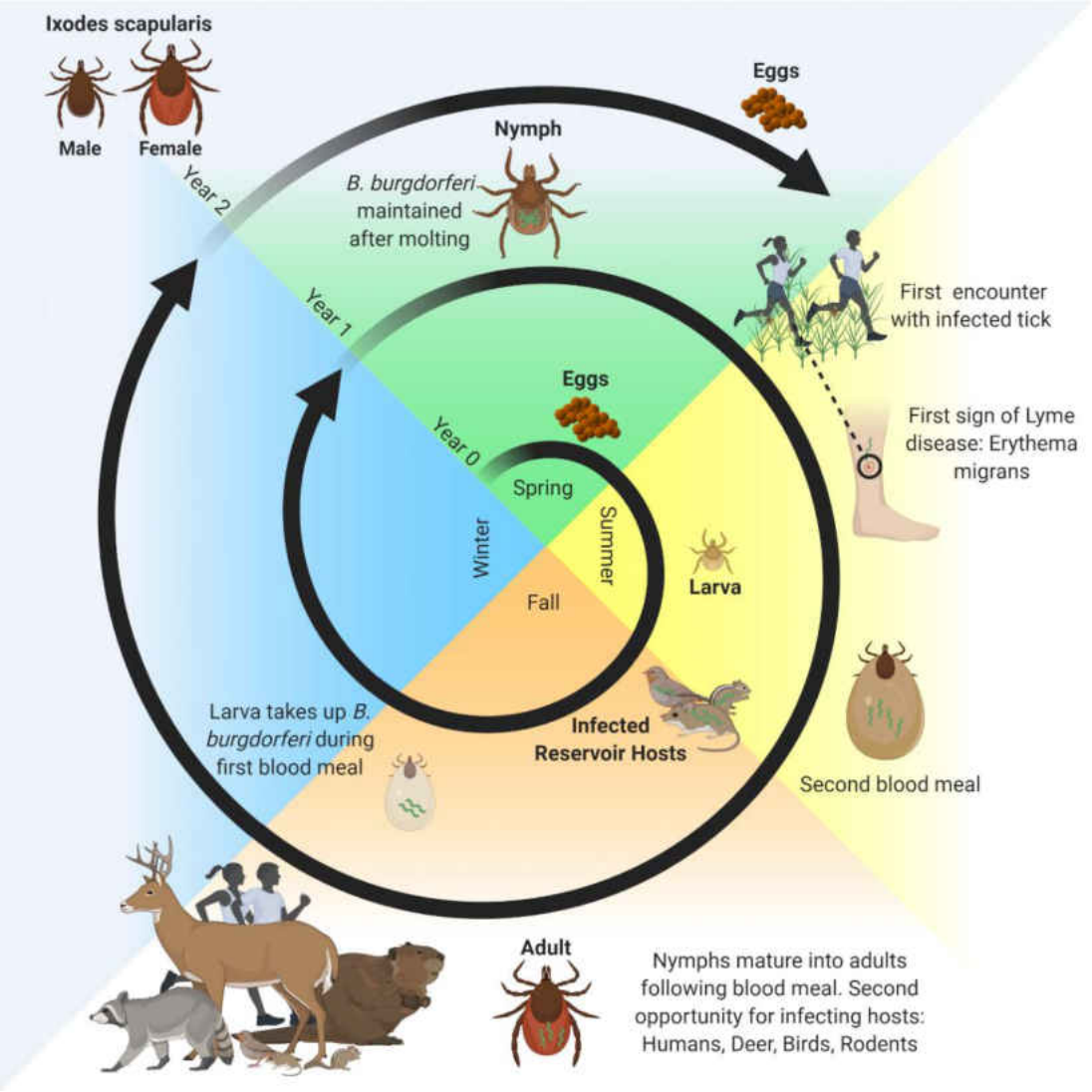

Figure I - 2. The enzootic life cycle of *Borrelia burgdorferi.* *Ixodes scapularis*, is the predominant vector for *B. burgdorferi* in the United States. The life cycle of I. scapularis generally spans two years. There is no transovarian transmission of *B. burgdorferi,* thus eggs and larva are uninfected. Between each life stage, the tick must take a blood meal. Larvae acquire infection from feeding on an infected reservoir host. The larva then molts to a Nymph, maintaining the infection. This is the first stage that the tick can transmit the bacteria to a naïve host, such as humans, leading to the onset of Lyme disease. Following a second blood meal, the tick will mature into an adult. The adult tick can infect another host and reestablish the reservoir of *B. burgdorferi* in specific animals such as the white-footed mouse. Ticks will mate at this stage, lay uninfected eggs, and the cycle repeats.

feed – a common host is *Odocoileus virgiianus* (white-tailed deer). Females and males will then mate, and females will find a suitable environment to lay eggs, thus starting the cycle again.

As illustrated, *Ixodes* will feed once during each stage of life. Though each stage shows an inclination to specific hosts, the ticks are considered generalist feeders and will feed on a wide variety of animals, including rodents, birds, racoons, and deer [49–53]. Typically, larva and nymphs will show a propensity towards smaller to medium mammals such as mice, shrews, or birds, while adults will feed on larger animals like the white-tailed deer or coyotes [54,55]. Activity of *I. scapularis* at all stages is based on seasonality and climate, and peak activity is observed in spring and summer, though larval activity may occur later than nymphs or adults [45,47,56,57]. This correlates with the seasonality of confirmed cases of Lyme disease in which peak onset of disease occurs in June and July (Figure 1-1B).

Furthermore, while *B. burgdorferi* can infect a wide range of animals due to the generalist feeding behavior of *Ixodes* ticks, only a few animals have been observed to maintain a persistent infection, allowing for a natural reservoir for the spirochete. One of the most prevalent reservoir species in North America is the white-footed mouse *Peromyscus leucopus* [58–60]. Though white-foot mice can harbor the bacteria, they do not exhibit pathology associated with Lyme disease, suggestive of co-evolution between the species. This allows for the modulation of the host immune response that is beneficial to the bacteria [35,61–63]. Understanding the life cycle, preferential hosts, and reservoir species for *Ixodes*

scapularis and *B. burgdorferi* provides insight into the increasing incidence of the disease, both in terms of the number of individuals infected and geographical distribution.

Symptoms and Treatments: From Tick Bite to the Doctor's Office

An overview of the symptoms can be found in Figure I-3. Lyme disease is transmitted to humans by a tick bite, typically from *Ixodes scapularis* or *Ixodes pacificus* on the Pacific Coast of the US [64,65]. During the initial localized stages of the disease, the most common and indicative symptom is the erythema migrans (EM) rash which presents in 70%-80% of infected individuals [66]. If treated by antibiotic therapy during this early stage of the disease, most individuals will recover. Typically, an individual will receive a course of antibiotics such as doxycycline or cefuroxime for 2-3 weeks. If a patient does not receive treatment during this early phase of the disease, the bacteria will disseminate via the circulatory system into other tissues and organs. During early *B. burgdorferi* dissemination throughout the body, it commonly enters joints, tendons, or bursae. Patients may initially be asymptomatic, but during the late stages of the disease when the innate and adaptive immune response are present, clinical presentation of arthritis is usually seen within major joints. In a study that followed patients with EM rash who did not receive antibiotic therapy, roughly 60% of patients developed intermittent or chronic arthritis [67]. A more recent surveillance of reported cases by the CDC indicates that approximately 30% of individuals will develop arthritis [66]. While most symptoms will resolve following

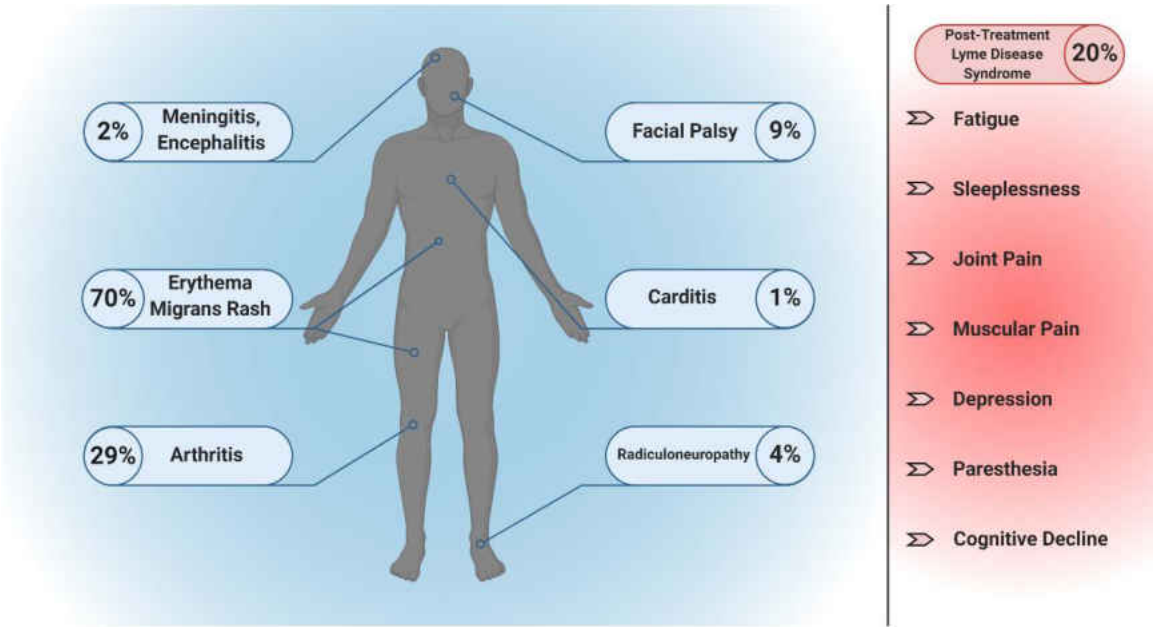

Figure I - 3. The symptoms of Lyme disease and post-treatment Lyme disease syndrome.
Lyme disease is a multi-systemic disease. Symptom severity can be variable but increases the longer the disease is left untreated. Erythema migrans, also known as the bullseye rash, is a common and indicative sign of Lyme disease, appearing in 70% of cases. Arthritis occurs in 29% of individuals, and usually affects major joints such as the knee. Carditis is rare,1%, but is a serious symptom that leads to atrioventricular block, a disruption in the electric signals of the heart. The invasion of the central nervous system results in neuroborreliosis, with associated symptoms including facial palsy, radiculoneuropathy, and meningitis. Post-treatment Lyme disease syndrome occurs in up to 20% of Lyme disease patients and is defined by the continuation or appearance of symptoms after treatment, in which an active infection is no longer detectable. Symptoms include fatigue, musculoskeletal pain, depression, and cognitive decline.

treatment, some patients will continue to experience persistent synovial inflammation that may last for months to years [68].

During the dissemination phase, *B. burgdorferi* may enter cardiac tissue causing 1-4% of patients to develop carditis [66,69]. Involvement in cardiac tissue can impair electrical signals between the atria and ventricles of the heart, termed atrioventricular block [70]. Clinical manifestations of Lyme carditis present as shortness of breath, light-headedness/fainting, heart palpitations, or chest pains [70].

While many patients will recover from Lyme disease following an appropriate antibiotic intervention, the pathophysiology of the disease ranges drastically from person to person. Because *B. burgdorferi* does not produce or secrete any known toxins that can be attributed to the manifestations of the disease, it is suggested that the host immune and inflammatory response elicited by the infection plays a major contributing factor to the pathogenesis of the disease.

Neuroborreliosis

The involvement of the central nervous system (CNS) is usually seen in the later stages of delayed or untreated Lyme disease but has been observed in patients that still present with EM rash [71]. When *B. burgdorferi* does disseminate into the CNS, neurological complications, termed “neuroborreliosis”, are typically observed. Neurological manifestations include radiculoneuritis, meningitis, and facial palsy [72–74]. It is well-documented that *B. burgdorferi* is capable of penetrating the central nervous system (CNS). This is evident from

the direct detection of the pathogen within the cerebrospinal fluid, usually performed by lumbar puncture, followed by bacterial culture or PCR [75]. Furthermore, other methods suggest of CNS invasion - the detection of intrathecal antibodies, an increase in peripheral immune cells, such as lymphocytic pleocytosis, and the presence of the chemoattractant *cxcl13* [76–79]. Though methods of detection and diagnosis of neuroborreliosis continue to grow, very little is known about the mechanisms by which *B. burgdorferi* enters the CNS and the pathophysiology of neuroborreliosis. Explants and primary cultures of dorsal root ganglia tissue from rhesus macaques that were incubated with *Borrelia burgdorferi* showed an increase in inflammatory cytokines *ccl2*, *il-6*, and *il-8*, as well as the apoptosis of sensory neurons [80]. The correlation between inflammation and the pathology of the disease is also observed in the inflammation and subsequent apoptosis of oligodendrocyte cultures following *Bb* infection [81]. This is further seen in the cerebrospinal fluid (CSF) of patients with confirmed neuroborreliosis that show increases in chemokines such as *ccl2*, *ccl5*, and *cxcl1* [82–84]. The presence of these chemokines may indicate a role for these factors in the host immune response, notably immune cell trafficking.

A major point of contention within the realm of neuroborreliosis is the mechanism by which *B. burgdorferi* enters the CNS. As stated previously, the bacteria have been found in the CSF and indeed the commonly used *B. burgdorferi* 297 strain is an isolate from the CSF of a patient [85]. There are two possible routes of dissemination into the CNS, retrogradely via peripheral nerves or hematogenous dissemination [86]. However, it is more likely that

dissemination occurs hematogenously, as it is the major route of dissemination to secondary systemic organs after the establishment of localized infection[87,88]. Transportation and successful immune evasion through the bloodstream are only half of the story. The next hurdle *B. burgdorferi* has to overcome to enter the CNS is successfully passing through the blood-brain barrier. Some researchers advocate for the penetration of endothelial cells while others argue the transcellular migration of the spirochete [89–91]. Clearly, major work is still required to elucidate the mechanisms of CNS entry and pathogenesis of neuroborreliosis. One aspect of the work presented herein aims to provide an alternative route of entry into the CNS.

Post-Treatment Lyme Disease Syndrome

Several studies have shown that the majority of patients who are treated with antibiotics successfully recover; however, individuals presenting with late manifestations of Lyme disease may respond more slowly to the antibiotic therapy [92–97]. Approximately 10-20% of individuals who complete treatment for Lyme disease experience persistent or intermittent symptoms at least 12 months post-treatment [94,98,99]. Originally named “Chronic Lyme Disease” to describe individuals with persistent and non-specific symptoms seen in suspected Lyme disease patients, the term has come under considerable scrutiny for its failure in specificity and consistency for diagnosis and has since been further refined to a more accurate term, Post-Treatment Lyme Disease Syndrome [99]. Common symptoms of PTLDS include fatigue, sleeplessness, joint and muscular pain, headache, paresthesia, and overall cognitive decline

involving difficulties in memory and concentration [93,100]. PTLDS is defined as a syndrome in which an individual with a documented diagnosis of Lyme disease and associated symptoms, received the generally accepted treatment regimen of antibiotics, but has shown persistent symptoms such as fatigue, musculoskeletal pain, or cognitive deficits for at least 6 months following the completion of treatment with no evidence of an on-going infection or co-morbidities that would otherwise explain the individual's symptoms [77,99,101]. The likelihood of a PTLDS diagnosis is correlated to the delay of antibiotic treatment and therefore the extent of *B. burgdorferi* dissemination into other tissue such as the joints or central nervous system [102,103].

Currently, there are no effective treatments for PTLDS or strict guidelines for clinical care. The complexity of the biological systems involved in PTLDS (i.e. CNS, musculoskeletal), the generality of symptoms (i.e. pain, cognitive decline), and on-going controversy worsens the ability to provide adequate care. Furthermore, studies have shown that extending the duration of antibiotic therapy from the typical 2-4 weeks does not provide any additional benefits and is associated with adverse side effects that include diarrhea and sepsis, leading to hospitalization in some cases [104–106].

There is currently no known explanation for the underlying mechanisms of post-treatment Lyme disease syndrome, though the cause of PTLDS may be multifactorial. There are a number of hypotheses that attempt to explain the on-going symptoms: persistent *B. burgdorferi* infection at undetectable levels, autoimmune mechanisms, the Amber hypothesis, or epigenetic manipulation

within the host as outlined in this work [107,108]. The Amber hypothesis initially sought to describe the pathogenesis of Lyme arthritis that is caused by non-viable *B. burgdorferi* or bacterial debris in regions that are more difficult to clear by resident immune cells [108]. This has been extrapolated to include the CNS, and studies have shown that heat-inactivated or sonicated *Borrelia* induces an inflammatory response in microglia [109]. The work described herein provides an additional explanation for PTLDS, focusing on epigenetic manipulation of host cells in response to *B. burgdorferi* that creates a transcriptome profile that is conducive to a pro-inflammatory state.

The Host Transcriptional Response to *Borrelia burgdorferi* Sensu Lato

With the advent of next-generation sequencing technologies, the ability to perform transcriptome analysis has become much more accessible and affordable. The past several years have seen a dramatic increase in RNA-seq analysis that allows researchers to conduct genome-wide transcriptome profiling of both model and non-model organisms. The impact of this technological innovation is best seen in studies of host-pathogen interactions. The use of RNA-seq and microarray technologies aids in understanding the development of the host response to a disease. This can better illustrate the host immune response towards a pathogen and how the pathogen may overcome these obstacles. Particularly, regarding *B. burgdorferi*, the host immune response and subsequent inflammation, while generally beneficial, poses a deleterious outcome for patients with Lyme disease, especially if such symptoms are persistent. With such a tremendous evolution in sequencing technologies, researchers are able to better

understand this dichotomy in Lyme disease. Furthermore, bioinformatics provides the tools necessary to analyze the large amounts of data available in such experiments. This allows researchers to not only perform transcriptome profiling but to determine functional and pathway analysis to quantitatively identify key targets for future therapeutics. As the goal of my projects revolved around understanding the genetic and epigenetic alterations following *B. burgdorferi* infection, this section highlights many of the past and current studies that have utilized RNA-seq and microarray technologies in Lyme disease models to understand the host transcriptome response.

Transcriptional Response of Early Localized Infection

Lyme disease begins at the site of the tick bite where *B. burgdorferi* and tick saliva are transmitted to the host during feeding [110]. Though many studies cited throughout this review do not utilize ticks as a route of transmission, it is important to note the role of tick saliva in Lyme disease. Tick saliva contains a milieu of immunomodulatory factors that include antihistamines, antioxidants, and anti-complement proteins that promote bacterial survival [111–113]. The saliva has been shown to inhibit neutrophil functions and impedes the killing and clearing of bacteria; the proteins ISL 929 and ISL 1373 have been shown to inhibit neutrophil chemotaxis to the site of infection [114,115]. Furthermore, dendritic cell (DC) migration and maturation are also inhibited by tick saliva, specifically Prostaglandin E2 [116,117]. These anti-inflammatory and immunosuppressive effects aid in the initial establishment of a localized infection at the skin of the host. This section summarizes the transcriptional alterations

within tissue and cells that first encounter *B. burgdorferi* during the early phase of the disease.

Dendritic cells.

Dendritic cells (DCs) are phagocytic and professional antigen-presenting cells that can be found in many tissues including the skin where they monitor for and detect invading pathogens. As a part of the innate immune system, DCs act as a bridge linking the innate and adaptive immune response through their ability to activate naïve T cells following stimulation and migration to lymph nodes [118,119]. DCs are one of the first types of immune cells to interact with *Borrelia* and, upon coming into contact with DCs, are quickly engulfed, allowing for the processing and presentation of *Borrelia* antigens for the activation of $CD4^+$ T cells [120,121]. Due to the limited number of DCs that can be collected for *in vitro* investigation, it is common to derive DCs either through bone marrow or peripheral blood monocytes (PBMCs); however, to date, only one study has investigated the transcriptional effects between *Borrelia* and DCs.

Hartiala et al. utilized PBMCs from healthy donors and generated DCs *in vitro* to determine the transcriptional response to *Borrelia garinii* (*Bg*), a member of the *Borrelia burgdorferi* sensu lato complex [122]. Like *B. burgdorferi, B. garinii* elicits a phagocytic response from DCs, in which they are processed, induce DC maturation, and activate T cells [123]. The microarray experiments performed by Hartiala et al. made two comparisons, *Bg* stimulated vs unstimulated DCs and *Bg* stimulated versus LPS stimulated DCs. In both comparisons, several genes that transcribe chemotactic cytokines were upregulated in response to *Bg* stimulation.

The neutrophil chemoattractants CXCL1, CXCL7, and CXCL2, the latter also showing chemotactic properties for polymorphonuclear leukocytes and hematopoietic stem cells, showed increased expression compared to unstimulated and LPS-stimulated groups, and have been previously been implicated in the inflammatory response in later manifestations of Lyme disease [124–127]. The gene encoding for CSF-1 was induced at greater levels in *Bg* stimulated DCs; CSF-1 functions as a cytokine for hematopoietic stem cell differentiation into macrophages, and activates macrophage phagocytosis as well as inflammatory and chemotactic functions [128,129]. Transcripts for markers of DC maturation and differentiation were found to be upregulated in both the LPS and *Bg* stimulated groups – ADAM19, CD83, and SLAMF1 [130–133]. Further evidence of the DC inflammatory response to these stimuli is observed by the induction of inflammatory cytokine genes – TNF-α, IL-1α, IL-1β, and IL-6. Though it has been previously shown that *B. burgdorferi* sensu lato can stimulate an interferon response, interestingly, such a response was not seen in DCs stimulated by *Bg*. Yet, interferon-inducible genes were upregulated within the LPS group – this includes IFIT1, IRF2, and IRF7. One of the principal findings by Hartiala et al. was the demonstration of a reduced response in CD38 and CCR7 expression in DCs stimulated by *Bg* when compared to LPS. During differentiation to immature DCs, CD38 is downregulated, but expressed following DC maturation and is required for DC chemotaxis and transendothelial migration [134,135]. Similarly, CCR7, a chemokine receptor, is a key promoter for DC migration to the lymph nodes [136]. This results in an impaired and weakened

humoral response and is posited by the authors as a possible cause for the immune abnormalities associated with Lyme disease [122]. This is in line with similar experiments that utilize *ex vivo* skin models injected with *B. burgdorferi* sensu stricto, LPS, or Pam3CSK4 (TLR2 agonist) to measure dendritic cell activation and migration [137]. Here, the authors observe the TLR2-mediated migration of DCs in response to *B. burgdorferi*, however, the expression of CCR7 and CD38 were comparable to PBS controls, while LPS and Pam3CSK4 induced significant upregulation of these markers. Infection of monocyte-derived DCs with *B. burgdorferi*, again, did not show an upregulation of CCR7 and CD38[137].

Macrophages.

A second prominent immune cell found in the skin are macrophages. Historically, macrophages and dendritic cells have been considered distinct cell types based on morphology, phenotypic characteristics, and function; however, current understanding has shown that both cell types, while unique in some respects, share many of the same functional characteristics. Like DCs, macrophages play a central role in the innate immune response during pathogen invasion. While both are antigen-presenting, macrophages are predominantly phagocytic, clearing cellular debris and pathogens while modulating an inflammatory response through the secretion of cytokines to alert the adaptive immune system [138,139].

To study the innate immune response to *B. burgdorferi*, Carreras-González et al. utilized RNA-seq, among other techniques, to investigate the transcriptional profile of primary murine bone marrow-derived macrophages

(BMMs) following infection. Following stimulation, a large number of differentially expressed genes (DEGs) were observed (2,066 upregulated and 2,315 downregulated), with gene expression consistent with an innate immune and inflammatory response. The pattern of gene transcription involved biological processes for the recruitment, differentiation, and activation of leukocytes. A sizable number of DEGs (317) that were regulated by *B. burgdoferi* were directly related to the inflammatory response, and 64 DEGs were found to be involved in phagocytosis, a significant function of macrophages. Transcriptional fingerprint analysis identifies expression profiles of signaling pathways to be compared with the observed profile. Unsurprisingly, the macrophage expression profile following exposure to *B. burgdorferi* resembled the fingerprint for the recognition of bacteria and viruses by pattern recognition receptors (PRRs); more specifically, pathway mediators within toll-like receptor (TLR) signaling showed a significant increase in stimulated BMMs. TLRs are a well-recognized and studied receptor family required for the innate immune response that is activated during *Borrelia* infection, and TLR2 signaling has been extensively shown to be a predominant pathway in the induction of a pro-inflammatory response [140–142]. Nonetheless, due to the numerous TLRs and their ability to form heterodimers such as TLR1/2 and TLR2/6, studies have shown that such an immune response to *B. burgdorferi* is not restricted to only TLR2. TLR2-deficient mice show poor response to *B. burgdorferi* which allowed the bacteria to persist at elevated levels for at least 8 weeks [143]. Furthermore, in the same investigation, though macrophages from $TLR2^{-/-}$ mice showed no response to OspA, an outer surface protein known to

signal through TLR2, sonicated spirochetes did stimulate a macrophage response [143,144]. Additionally, another study showed that in TLR2 knock-out mice, macrophages were still able to activate and respond to spirochete lysates [142]. However, the role of TLRs is diminished in the current study by Carreras-González and colleagues. Though there was a significant overlap in the number of genes between stimulated BMMs and TLR2 or PAM_3CSK_4 (a TLR2 agonist) signaling pathways, the percentage of shared genes was less than 10% - suggesting that a greater diversity in signaling receptors are responsible for the overall response, as seen with an upregulation in receptor Nod2 and overlap with triggering receptor expressed on myeloid cells-1 (TREM-1) receptor signaling. TREM-1 is a receptor that amplifies a pro-inflammatory response, and while a more robust inflammatory response could provide efficient clearing of an invading pathogen, it can lead to substantial cell death and tissue damage – a concept not unfamiliar to the Lyme disease field [80,145–148]. However, in a study using $TREM1^{-/-}$ mice infected with *Leishmania major*, *Legionella pneumophila*, or influenza virus, the mice displayed a significant attenuation of disease pathology in regards to inflammatory infiltrates and a reduction in the expression of pro-inflammatory cytokines, yet were equally capable of clearing the infection compared to controls [149]. In fact, additional studies of *B. burgdorferi* infection implicate the TREM1 pathway as a significant contributor to the pathogen-induced inflammatory response [150,151]. The inflammatory response by BMMs was further highlighted by the reduction in signaling intermediates induced by peroxisome proliferator-activated receptor (PPAR), an inflammatory suppressor,

and the downregulation of *Il10ra*, the receptor for the anti-inflammatory interleukin-10. Furthermore, several pro-inflammatory cytokines were shown to be upregulated including IL-1β, IL-6, IFNβ1, and TNF (a regulator of TREM1). Overall, the study showed an inflammatory response by BMMs following *B. burgdorferi* infection that was characterized by an increase in pro-inflammatory cytokines, a reduction in anti-inflammatory pathways, and an increase in phagocytic related genes.

Monocytes.

In addition to transcriptional profiling of murine macrophages, Carreras-González et al. further characterized the transcriptional response of the interaction between *B. burgdorferi* and human $CD14^+$ peripheral blood monocytes via microarray analysis to determine their relevance in the human innate immune response. A similar number of DEGs were found in the human monocytes compared to BMMs. A significantly reduced number of DEGs were shared between the two cell types, most likely attributed to differences across species – 195 DEGs upregulated and 161 DEGs downregulated in both groups; 168 genes were regulated in opposite directions. However, similarities appeared following functional and pathway analysis in which pathways involving the recruitment of leukocytes, phagocytosis, and endocytosis were increased. Furthermore, analysis regarding upstream regulators indicated similar patterns of gene expression for receptors TLR3, TLR9, TLR, and NOD2, and proinflammatory cytokines TNF, IL-1α, IL-1β, and IFNα2. The gene expression pattern for the inhibition of the anti-inflammatory IL10RA pathway was observed in both BMMs

and human monocytes. While there were distinct differences between the two groups regarding expression of specific genes, it appears that infection with *B. burgdorferi* produces a pro-inflammatory response that overlaps both groups.

Dermal fibroblasts.

The skin represents an important obstacle in the progression of Lyme disease as it forms a complex physical barrier comprised of the epidermis, dermis, and hypodermis. *B. burgdorferi* establishes a local infection within the dermis, and aside from resident immune cells such as DCs and macrophages, dermal fibroblasts are among the first cells to come into contact with the spirochetes [152–154]. Fibroblasts are the main resident cells in the dermis and play an important role in the formation and reorganization of the extracellular matrix (ECM). Moreover, fibroblasts are able to communicate and modulate local immunocompetent cells as a functional part of the innate immune response through the recruitment of leukocytes, inflammatory regulation, and the maturation of dendritic cells [155,156].

To understand the role of dermal fibroblasts in skin inflammation during the early pathogenesis of Lyme disease, Schramm et al. performed microarray analysis of human dermal fibroblasts in response to three different strains of *Borrelia burgdorferi* sensu stricto [154]. The three strains of *B. burdorferi* were isolated from different environments representative of different stages of Lyme disease – strain N40 was isolated from a tick, strain Pbre from an erythema migrans skin biopsy, and strain 1408 from a skin biopsy of acrodermatitis chronica atrophicans (ACA), a late-stage manifestation of Lyme disease. Across

all three infection groups, a total of 241 genes were found to be differentially expressed, with 103 genes upregulated and 138 downregulated. There were 47 upregulated and 28 downregulated DEGs that were shared between all three groups. The authors state that there were no discernable differences in relevant transcriptional pathways across each group and note that while the three *B. burgdorferi* isolates stem from different environments of the pathogen life cycle, the dermal fibroblasts produced similar transcriptional profiles in response to each pathogen isolate. As one of the major functions of fibroblasts, ECM production and remodeling genes were found to be upregulated among the shared genes. These involve the structural components that include integrin ITGA1, laminin LAMA1, microfibrils MFAP3, and collagen fibrils COL8A1. Most importantly, three matrix metalloproteinases (MMPs) were found to be upregulated – MMP-1, MMP-3, and MMP-12. The induction of MMPs by the bacteria has been linked to the development of Lyme arthritis showing similar erosive and inflammatory pathologies to rheumatoid arthritis [157–159]. MMP-1 and MMP-3 have been shown to be elevated in the synovial fluid of Lyme arthritis patients [159,160]. *B. burgdorferi* appears to induce the production of host MMPs to degrade and digest extracellular matrix proteins that allow for greater dissemination [161,162].

In addition to the upregulation of ECM remodeling pathways, the transcriptional response in fibroblasts was largely indicative of a pro-inflammatory profile. A high level of cytokines and chemokines were shown to be upregulated, including CXCL1 and many interleukins. Additionally, many upregulated genes

were representative of signaling mediators that regulate and sustain an inflammatory response such as NF-κB transcription factors (NF-κB1, -2), interferon-related and inducible genes (IRF1, STAT1/2, OAS2, and IFIH1), and genes within the tumor necrosis factor family (TNFSF10, TNFSF13B). Through the release of secreted factors, dermal fibroblasts appear to communicate with innate immune cells that allow for their attraction, activation, and maturation to the site of infection [163–167]. Moreover, during the localized infection phase, dermal fibroblasts inadvertently provide a means for *B. burgdorferi* dissemination by the induction of ECM degradation factors like MMPs [154].

Transcriptional Response of Early Disseminated Infection

The next phase, following the initial localized infection of Lyme disease, is the early dissemination of *B. burgdorferi* to other host tissue and organs. Hematogenous dissemination is the primary mechanism for the spread of the spirochete in the host and the first barrier that the spirochetes interact with is the endothelial barrier of the blood vessels. This is also a primary barrier that must be overcome by innate and adaptive immune cells.

Endothelial/Epithelial.

Dame et al. sought to determine the role of endothelial cells in Lyme disease by performing microarray analysis of a human umbilical vein endothelial cell (HUVEC) *in vitro* system infected with *B. burgdorferi* [168]. T lymphocytes have long been implicated in the pathogenesis of Lyme disease and specifically Th1 cells have been shown to be elevated in the synovial fluids of Lyme arthritis patients [169,170]. Furthermore, Th1 cells which specifically secrete IFN-γ have

shown a migratory affinity towards endothelia that have been stimulated by *B. burgdorferi*, and a significant correlation has been shown between symptom score of LD patients and IFN-γ [169,171]. To this end, Dame and colleagues further sought to identify the synergistic effects of IFN-γ and *B. burgdorferi* on the transcriptional profile of primary human endothelial cells.

In the presence of *B. burgdorferi*, HUVECs showed poor activation and minimal differential gene expression, in which no genes were significantly downregulated, and only 23 genes were significantly identified as upregulated with a greater than 2-fold change. Of these genes, several have already been identified to be induced by *B. burgdorferi* in a number of *in vitro* and *in vivo* models – these genes include immune cell adhesion molecules (ICAM-1, VCAM-1) and leukocyte recruitment chemokines (CXCL8, CCL2), which have been specifically shown to promote the transmigration of leukocytes across endothelia during *B. burgdorferi* infection [171–175]. Stimulation of HUVECs with IFN-γ only produced a larger transcriptional change in both magnitude and number of genes when compared to *B. burgdorferi* only, with a subset of genes being classified as mediators of inflammation. However, the combinatorial effects of IFN-γ and infection revealed several inflammatory and immune-related genes that were significantly upregulated and showed a robust fold change compared to each individual treatment. The authors formulated a synergistic scoring system that indicated 34 genes that were differentially upregulated in both individual treatments. This effect can be clearly seen in the expression of CCL8: IFN-γ only treatment – 17.672 FC; *Bb* only treatment – 1.31 FC; and *Bb*+ IFN-γ treatment –

113.58 FC. Of these 34 genes that were markedly upregulated, 9 are involved in the recruitment of leukocytes which include specifically T lymphocyte chemoattractants CCL7, CCL8, CXCL9, CXCL10, CXCL11, CX3CL1 and also the aforementioned adhesion molecules (ICAM-1, VCAM-1), as well as the neutrophil chemoattractant CXCL2 [124,176–180]. Furthermore, the presence of T lymphocytes has been attributed to more persistent inflammatory syndromes [181–184]. Many of the 34 genes are mediators in both the innate and adaptive immune systems; however, interestingly, the CIITA gene showed downregulation in *Bb* only treatment, but an upregulation in IFN-γ only, and an even greater upregulation with the combination of treatments. *CIITA* encodes for the MHC class II transactivator and acts as a master regulator for MHC class II genes, involved in antigen processing and presentation. This change in gene expression brought upon by IFN-γ treatment is suggestive of a transition towards the adaptive immune response. Together, the transcriptional changes observed indicate a key role of endothelial cells in conjunction with IFN-γ that leads to a greater adaptive immunological response through the selective recruitment of T lymphocytes, and as Th1 cells themselves produce and secrete IFN-γ, a positive-feedback loop would promote a more chronic inflammatory environment which is seen in Lyme disease patients [168–170,185–187].

Peripheral blood mononuclear cells.

During hematogenous dissemination, *B. burgdorferi* encounters a wide variety of immunocompetent cells within the blood circulatory system. Due to the ease of access, availability, and as one of the predominate classes of immune

cells in the blood, peripheral blood mononuclear cells (PBMCs) are commonly used in both *ex vivo* and *in vivo* analysis of Lyme disease. PBMCs are defined as any peripheral blood cell that has a round nucleus, as opposed to anucleur cells such as mature erythrocytes or multi-lobed nucleated cells such as granulocytes. They are predominately comprised of lymphocytes (T cells, B cells, and NK cells) and to a lesser extent monocytes [188,189].

To determine the global and temporal transcriptional pathways involved during *B. burgdorferi* infection in humans, Bouquet et al. performed longitudinal transcriptome analysis (RNA-seq) of PBMCs collected from patients with acute Lyme disease at three time points: time of diagnosis/pre-treatment, treatment completion (3 weeks), and 6 months post-treatment to determine the transcriptional profiles of post-treatment symptoms. 29 individuals with acute Lyme disease that presented with a documented EM rash and flu-like symptoms, such as fever, fatigue, and the onset of muscle or joint pains, were enrolled in addition to 13 healthy control individuals. Following 6 months post-treatment, the 29 individuals were further categorized as having resolved the illness (n=15) or experiencing persistent symptoms (n=13); one patient was lost to follow-up. Of the 13 with persistent symptoms, 4 were diagnosed with post-treatment Lyme disease syndrome. The authors also note that the longer the duration between the onset of symptoms and the time of completed treatment was correlated to PTLDS diagnosis, in which non-PTLDS patients had an average duration of 9.7 days between symptom onset and treatment completion and 19.3 days for PTLDS patients.

Transcriptional analysis showed a consistent decrease in the number of DEGs across the three time points compared to controls – pre-treatment: 1235 DEGS, treatment completion: 1060 DEGs, 6-months post-treatment: 686. Interestingly, when taking into consideration other infectious diseases such as Influenza, the gene expression of patients with Lyme disease failed to return to baseline levels; however, persistent symptoms were not solely dependent on this failure to return to baseline as no DEGs were found between patients with resolved symptoms and those with persistent symptoms. Pathway analysis of the pre-treatment group indicated activation of the inflammatory response, immune cell trafficking, hematological system, as would be expected during the early dissemination phase of *B. burgdorferi*. However, these pathways remained activated at treatment completion and to a lesser extent at the 6-month post-treatment time point. This is reflected in the top 10 enriched pathways in that 8 pathways of the pre-treatment, 10 pathways in treatment completion group, and 4 pathways in 6-month post-treatment group were directly related to the immune response. Furthermore, TREM-1 signaling was the top activated pathway for both pre- and completed treatment groups. As mentioned previously, TREM-1 acts as an amplifier of inflammation, and also acts as a mediator for Th1 activation through factors such as DAP12, IL-6, IL-12 that were upregulated in these two groups. Inversely, the eIF2 signaling pathway was found to be downregulated in all three groups and has been found to be involved in protein synthesis during cellular stress [190]. The pathogen *Legionella pneumophila* was previously shown to disrupt and downregulate mediators of this pathway through

the secretion of effectors, and defective signaling of eIF2 was shown to lead to greater susceptibility to intracellular invasion by *Yersinia pseudotuberculosis*, *Listeria monocytogenes*, and *Chlamydia trachomatis* [191,192]. However, the current mechanism and immunological impact of eIF2 signaling inhibition following *B. burgdorferi* infection is yet to be elucidated. Several TLRs were also found to be either upregulated or predicted to be activated that include TLR-1, -2, -4, -7, and -8. Additionally, within the first two groups, the majority of upstream regulators were proinflammatory cytokines such as CSF2, IFN-γ, TNF-α (a master regulator of eIF2, TREM1, and TLR signaling), anti-inflammatory cytokines IL-6 and IL-110, and the transcription factor NF-κB. In contrast, the top upstream regulators for the 6-month group mainly involved genes associated with the regulation of gene expression such as MYCN, MYC, and FOS. Overall, Bouquet et al. found that the transcriptional profile of acute Lyme disease patients prior to treatment and upon treatment completion shared many characteristics, with many overlapping DEGs involved in the inflammatory and immune process but the activation of inflammatory T-cell apoptosis and B-cell developmental pathways were inhibited when compared to other acute infectious diseases. While the 6-month post-treatment group did not produce a marked inflammatory response, it failed to return to baseline levels; however, when compared to the transcriptional profiles of other immune-mediated chronic diseases such as systemic lupus erythematosus, up to 60% of the pathways overlapped.

Transcriptional Response of Late Disseminated Infection

Joint (mouse).

The late disseminated phase of Lyme disease is characterized by successful invasion of secondary tissue and organs, including joints, heart, and CNS, followed by subsequent clinical presentations associated with affected tissue. A common outcome of dissemination into the joints is Lyme arthritis, in which 30% of patients will develop it and up to 60% if treatment was not administered at the time of infection [66,67,193]. The laboratory mice have long been used as a model for Lyme arthritis, and as such, Crandall et al. used two strains of mice that developed either severe arthritis (C3H) or mild disease (C57BL/6), as well as C578BL/6-IL-$10^{-/-}$ that lacked the anti-inflammatory cytokine IL-10, to study the global gene expression within the joints of these animals in response to *B. burgdorferi* [194–196].

Expression profiles of rear ankle joints were determined by microarray analysis at 1, 2, and 4 weeks of infection. At week 1, C3H, C57BL/6, and C578BL/6-IL-$10^{-/-}$ had an increase in 156 genes, 119 genes, and 419 genes, respectively. Interestingly, only 3 genes overlapped between C3H and C57BL/6. At week 2, significant inflammatory response and immune cell infiltration were evident through gene expression and histological analysis in all three strains; 302 DEGs were shared among the three groups. In agreement with histological evidence of leukocyte recruitment, an increase in the expression of recruiting chemokines was observed: PMN-recruiting (CXCL1, CXCL2, CXCL5), mononuclear cell-recruiting (CCL2, CCL3, CCL7, CCL12), and T cell-recruiting

(CXCL9, CXCL16, CCL2, CCL7). Transcripts for antigen-presenting cells and antigen processing such as MHC, CD1, and TAP1/2 were elevated at 2 and 4 weeks; this is suggestive of an active adaptive immune response.

B. burgdorferi is known to activate the production of several pro-inflammatory cytokines such as TNF-α, IL-1β, or IFN-γ, many of which are mediated by the activation of NF-κB. However, in C3H and C57BL/6 mice, only IL-1β was found to be increased in the joints. This is suggestive that these cytokines fail to be induced by *B. burgdorferi* in the presence of the anti-inflammatory cytokine IL-10, as the production of many of these inflammatory cytokines were robustly induced in IL-$10^{-/-}$ mice, including IL-1β, IFN-γ, IL-15, and members of the TNF family. Due to this response in IL-$10^{-/-}$, these mice were able to more effectively control bacterial growth but at the cost of developing more severe arthritis. Though induction of Type I and II IFN was not detectable in C3H, a robust IFN induced response was displayed – the IFN induced GTPases, Igtp, Iigp2, and Iigp1 saw a fold-change of 128, 123, and 113 respectively when compared to control at week 1. Additional IFN related genes include IFI1, GBP2, OASl2, and signaling molecules Stat1, IRF1, IRF2, IRF7, and IRF8. In the study, the authors note that the cause of IFN-related transcription cannot be determined as the presence of Type I/II IFNs were not detectable in either C3H and C57BL/6. However, more recent studies shed light on this phenomenon that indicate receptors independent of IFN receptors may be responsible, such as TLRs [197]. However, in stark contrast of this, C57BL/6 mice did display any increase of these IFN-inducible genes at week 1, and only minimal expression at week 2, which

corresponded to less severe arthritis. This association with arthritis and gene expression in further observed in IL-10$^{-/}$ mice that saw a robust IFN-induced response that significantly increased according to a longer time point. Furthermore, C57BL/6 mice saw an increase in transcripts related to epidermal differentiation and wound repair, compared to either no change or downregulation of these same genes in the other two strains across all time points. The study performed by Crandall et al., provides transcriptional insight of late dissemination associated with Lyme arthritis, showing a robust inflammatory response corresponding to disease severity, and upregulation of epidermal and wound repair genes correlating to a more protective effect [194].

Astrocytes.

Neuroborreliosis is defined by the invasion of the CNS by *B. burgdorferi* sensu lato, leading to subsequent neurological manifestations. Due to the disease severity and difficulty in treatment of persistent symptoms, many studies have been aimed to understand the mechanisms that lead to this pathology. Another study performed in the Brissette laboratory, Casselli et al., investigated the role of astrocytes in the exacerbation of neuroborreliosis through the use of RNA-seq [198]. Astrocytes, a resident glial cell, are the most abundant cell in the brain and play a role in a wide variety of functions [199]. Their functions include nutrient support, neurotransmitter recycling, aiding in synaptic remodeling and plasticity, structural support which includes the formation of the blood-brain barrier, and responding to CNS injury and infection through inflammatory and immune modulation [199,200].

Casselli et al. used primary human astrocytes *in vitro* stimulated by *Bb* for 24 and 48 hours. 275 transcripts were found to be differentially expressed at both time points with significant overlap between them (221 DEGs). Tumor necrosis factor superfamily, member 18 (TNFSF18) showed the strongest induction with a fold-change of 440 and 580 for 24 hours and 48 hours, respectively. Additional inflammatory and immune-related genes were upregulated that include chemokines CXCL1, CXCL6, and CXCL8 as well as ERAP2 which is involved in innate immunity and antigen processing and presentation [201]. In line with the broad nature of astrocyte functionality, biological and functional analysis indicated genes were involved in nervous system development, angiogenesis, and cell adhesion. While these experiments indicated an inflammatory and immune response following *B. burgdorferi* infection, it seems the response was less concerted compared to more specialized peripheral immune cells. This may suggest and provide credibility to disease severity that correlates to the invasion of peripheral immune cells into the CNS, as seen in the CSF of neuroborreliosis patients. Such an outcome may lead to a dysregulation in astrocytic function and result in exacerbation of a more persistent inflammatory environment within the CNS.

Gap in Knowledge

The work presented herein aims to elucidate the mechanisms underlying two major questions surrounding the neurological manifestations of Lyme disease. They are 1) How does *B. burgdorferi* enter the central nervous system,

and 2) How does *B. burgdorferi* induce persistent neurological symptoms present in PTLDS patients.

Regarding the first question, it is quite evident that *B. burgdorferi* is able to enter the central nervous system, however, where and how this occurs is still a matter of debate. The CNS is a highly regulated system that is selectively permeable through its barriers such as the blood-brain barrier and the blood-CSF barrier. In order to understand the pathogenesis of Lyme disease and how the dissemination into the CNS leads to the clinical presentations of neuroborreliosis, it is important to understand the mechanisms of entry. The choroid plexus forms the blood-CSF barrier, and due to its anatomical position and functions, it is a structure that we have chosen to investigate. The choroid plexus is situated within the ventricles of the brain, with the epithelial cells forming the blood-CSF barrier through tight and adherens junctions, and it is the predominate producer of CSF. Previous studies have shown its predisposition in the transmigration of peripheral immune cells and possibly pathogens into the CSF. It is applicable to note that a defining characteristic of neuroborreliosis is lymphocytic pleocytosis, an abnormal elevation of lymphocytes in the CSF, and *B. burgdorferi* or its DNA is found in the CSF of patients. The next chapter discusses the relevance of the choroid plexus' function, its role in the context of other infectious diseases, and the results of our experiments investigating the impact of *B. burgdorferi* on primary human choroid plexus epithelial cells *in vivo*.

Regarding the second question, the history of post-treatment Lyme disease syndrome has been plagued by controversy and is frequently and

incorrectly referred to as “chronic Lyme disease”, a term since rejected by the scientific community [99,202–204]. Much of the confusion is due to a lack of evidence for a conclusive cause of PTLDS. The Amber hypothesis suggests that the debris of dead *B. burgdorferi* continues to elicit an inflammatory response, and due to the disseminating nature of the bacteria, the debris may be located in difficult to clear regions of the body, such as the extracellular matrix of joints or the CNS [108]. However, as presented in Chapters 3 and 4, we hypothesized a new approach, that is not necessarily mutually exclusive to prevailing lines of thought. Our central hypothesis states that *during active infection and subsequent inflammatory host response, B. burgdorferi induces long-term epigenetic modifications in host cells that are conducive to a persistent inflammatory state*. This hypothesis is extended to our current interests, focusing on the central nervous system and more specifically to a resident glial cell, astrocytes. Two epigenetic alterations, namely DNA methylation and chromatin accessibility, are explored in chapters 3 and 4, respectively.

CHAPTER II

THE LYME DISEASE BACTERIUM, *BORRELIA BURGDORFERI*, STIMULATES AN INFLAMMATORY RESPONSE IN HUMAN CHOROID PLEXUS EPITHELIAL CELLS

Thompson, D, Sorenson, J., Greenmyer, J, Brissette, CA, Watt, JA

Department of Biomedical Sciences
University of North Dakota
School of Medicine and Health Sciences
504 Hamline Street
Grand Forks, ND 58203

Adapted from:

PLoS One 15(7): e0234993. doi:10.1371/journal pone.0234993

Introduction

The choroid plexus (CP) is a complex that has been implicated in the trafficking of immune cells across the blood-CSF-barrier (BCSFB). In addition to its role in the formation of the BCSFB, it is the major producer of CSF [205,206]. The CP is a highly vascularized structure within the ventricles of the brain, and unlike the blood-brain barrier (BBB), the capillaries within the choroid plexus are highly fenestrated. Instead, the choroid epithelial layer is responsible for the selective permeability of the BCSFB through the formation of tight and adherens junctions at the apical lateral surfaces [207]. An interesting characteristic of the choroid plexus is the presence of immune cells on the basolateral side within the stromal matrix – this includes dendritic cells and macrophages (Figure II-1) [208–211]. A further illustration of the immune-surveillance role of the choroid plexus is shown in the presence of cell adhesion molecules on CP epithelium and not the neighboring endothelium, which mediate the binding of immune cells [212]. The transmigration of macrophages and peripheral blood mononuclear cells (PBMCs) across the choroid plexus epithelium was observed in transwell and explant cultures in the presence of feline immunodeficiency virus [213]. In a human barrier model of the choroid plexus, the transepithelial migration of polymorphonuclear neutrophils and monocytes was observed following bacterial infection (*Neisseria meningitidis*) [213]. It is understood that the context of a

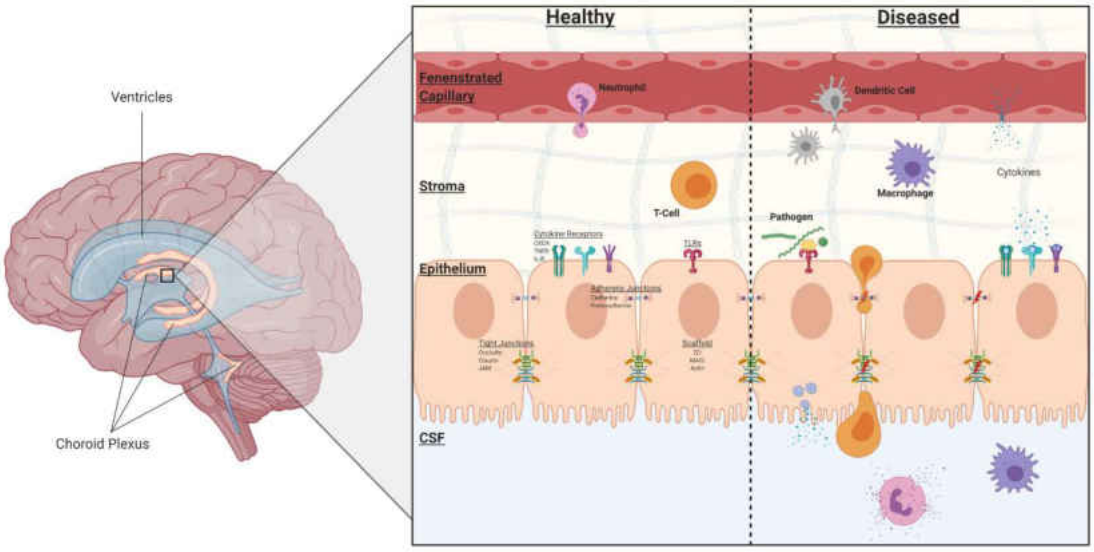

Figure II - 1. Structural features of the choroid plexus.
Under healthy conditions, the choroid plexus maintains peripheral immune cells within the stromal matrix as a form of immunosurveillance. Multiple receptors are present on the epithelium, including cytokine and pattern recognition receptors. The BCSFB is formed by the epithelium through tight junctions, adherens junctions, and desmosomes. During infection or disease states, these junctions may be altered, immune cells may transmigrate across the epithelium, and cytokines from both the epithelial cells and activated immune cells are released. Many of these cytokines induce a pro-inflammatory response and act as chemoattractants for innate and adaptive immune cells. Created with Biorender.com.

bacterial infection and the inflammatory profile of the CSF determines the severity and overall outcome of patients [214–216]; therefore, due to the choroid plexus's anatomical position in separating the periphery and CNS, as well as its secretory, barrier, and immune response roles, the intent of this project was to investigate the effects of *Borrelia burgdorferi* infection on choroid plexus epithelial cells.

The overall aim of this study is to determine the transcriptome profile of primary human choroid plexus epithelial cells (HCPECs) during *B. burgdorferi* infection. Using HCPECs in culture, we demonstrated differential expression of 258 genes following infection with *B. burgdorferi* after 48 hours. Functional and pathway analysis of these transcriptional changes revealed upregulation of host inflammatory and immune responses, related to interferon, chemokine, and cytokine pathways, as well as immune cell trafficking and activation. Although this model does not provide a barrier context, interestingly, functional and cellular components involving cell-cell junctions and tight junctions were seen to be downregulated. Here we present our findings of differential gene expression in HCPECs following infection with *B. burgdorferi*.

Methods

Bacteria Culture

The *Borrelia burgdorferi* strain B31-MI-16 is an infectious clone which was previously sequenced and described [20,217]. Bacteria cultures were grown to approximately 1 x 10^7 bacteria/ml in modified Barbour-Stoenner-Kelly (BSK-II) medium supplemented with 6% rabbit serum at 34°C and used at passage 2.

Cell Culture

HCPECs were obtained from ScienCell Research Laboratories (Carlsbad, CA; catalog #1310). Commercially available human primary cell cultures and protocols used throughout this study followed the University of North Dakota IRB guidelines outlined in form 504 “Categories of Research”, section 2.19 “Commercially Available Human Biological Specimens (45 CFR 46.102, 46.103, and 46.116)” and therefore do not require IRB review. The purity of cells was assessed and confirmed by immunofluorescence, the following primary antibodies and concentrations were used: Rabbit anti-Prealbumin (TTR) conjugated to Alexa Fluor 488 (Abcam, catalog #ab199074; Conc. 1:50), Mouse anti-α-Tubulin (Sigma, catalog #T61999; Conc. 2 ug/ml), Mouse anti-CK18 (Abcam, catalog #ab82254; Conc. 1:50). The secondary antibody, Donkey anti-Mouse conjugated to Alexa Fluor 594 (Jackson Immunoresearch, catalog #715-585-151, Conc. 1:100), was used for anti-CK18 and anti-α-Tubulin antibodies. For immunofluorescence, cells were grown on glass coverslips and fixed with a 4% paraformaldehyde solution for 15 minutes and stored in PBS at 4°C. Permeabilization was performed with a 0.1% Triton-PBS solution for 10 minutes and blocked with a 10% Donkey (Jackson immunoresearch, catalog #017-000-121) or Goat Serum (Jackson Immunoresearch, catalog #005-000-121) in 0.1% Tween-PBS solution for 1 hour. Primary antibodies were incubated overnight at 4°C. Secondary antibodies were incubated for 1 hour at room temperature. DAPI Fluoromount-G (SouthernBiotech, catalog #0100-20) was used for nuclei staining. Western blot analysis was performed on control and infected cell lysates

to determine the presence of TTR and CK18 – previously mentioned primary antibodies were used in conjunction with the secondary antibodies: Donkey anti-rabbit conjugated to peroxidase (Jackson Immunoresearch, catalog #711-035-152, Conc. 1:200,000) and Goat anti-mouse conjugated to peroxidase (Jackson Immunoresearch, catalog #115-035-003, Conc. 1:200,000). Signal was produced by SuperSignal West Femto Maximum Sensitivity Substrate kit from ThermoFisher Scientific (catalog #34094) and imaged on a Licor Odyssey Fc Imaging System.

Cells were maintained in tissue-treated vented cap T-75 flasks (Corning, catalog #430641U) in epithelial cell medium (ScienCell, catalog #4101), containing antibiotics penicillin (100 units/ml) and streptomycin (100 ug/ml) (ScienCell, catalog #0503), 2% fetal bovine serum (ScienCell, catalog #0010), and EpiCGS (ScienCell, catalog #4125). Two groups were used for these experiments – Control, non-infected (n=3) and Infected, 48 hours (n=3); a total of 6 samples. Cells were incubated at 37°C and used at passage 3 at approximately 80% confluence for stimulation by *Bb*. Prior to infection, the cell cultures were washed 3 times with sterile Dulbecco's phosphate buffered saline (DPBS) and the medium replaced with antibiotic-free epithelial cell medium. Cell cultures were stimulated with *B. burgdorferi* at a multiplicity of infection (MOI) of 10:1 (bacteria:cells) for 48 hours. Mean cell count of HCPECs was determined using an automated cell counter (Life Countess II, catalog #AMQAX1000) to determine an appropriate number of bacteria for infection. Control non-treated flasks were prepared identically without infection. Light microscopy was used to

monitor cell morphology and confluency. Additionally, cell proliferation was monitored using an MTS assay (Abcam, catalog #ab197010) and colorimetric plate reader in a 96-well plate under identical conditions. Apoptosis and necrosis were determined by fluorescence microscopy using Apopxin Green Indicator (Apoptosis) and 7-AAD (Necrosis) on cells grown in 24-well plates on glass coverslips under identical conditions (Abcam, catalog #ab176749) and manually counted.

RNA Isolation

RNA was isolated via phenol-chloroform extraction and using the RNeasy Mini kit from Qiagen (catalog #74106) according to the manufacturer's instructions. In short, cell medium was removed from cultures and used for later protein analysis; 1 ml of Trizol was added directly to each flask and a cell scraper was used to fully lyse all cells. Homogenized cells were transferred to RNase-DNase free 1.5 ml Eppendorf tubes, where chloroform was added for 2 minutes and centrifuged at 12,000 x g for 15 minutes at 4°C. The upper aqueous phase was mixed with 70% ethanol and placed in a Qiagen RNeasy Mini column. The flow-through was discarded and the bound RNA fraction remaining on the column membrane was further washed and processed per Qiagen's instructions. Genomic DNA was removed with DNA digestion with RNase-free DNase Set (Qiagen, catalog #79254). RNA quality was assessed with a NanoDrop and integrity assessed by gel electrophoresis on a 2% agarose gel.

Library Construction and RNA Sequencing

Isolated total RNA, as described above, underwent further quality control and purification to obtain mRNA. To assess RNA integrity of total RNA, samples were placed in an Agilent 2100 Bioanalyzer with the RNA 6000 Nano kit (catalog #5067-1511) – all samples passed with an RNA integrity number (RIN) of ≥8.9. To obtain a more accurate concentration, total RNA samples were run on a broad range Qubit 2.0 Fluorometer. mRNA was enriched from total RNA samples using the NEBNext Poly(A) mRNA Magnetic Isolation Module (catalog #E7490S) – in short, oligo d(T) beads are used to bind the poly(A) tail of eukaryotic mRNA. The NEBNext Ultra II RNA-seq library kit (catalog #E7775S) was used for library construction. Libraries were checked for quality and adaptor contamination on the bioanalyzer with the Agilent DNA 1000 kit (catalog #5067-1504). Library concentration was assessed with a BioTek Gen5 Wellplate reader with the Quant-iT PicoGreen dsDNA Assay kit (catalog #P11496). All samples, 3 control and 3 infected, were then pooled and sent to Novogene (https://en.novogene.com) for sequencing. An Illumina HiSeq 4000 was used for 150 bp paired-end sequencing.

RNA Data Analysis

Raw fastq files were received from Novogene and initial quality control was assessed using FastQC version 0.11.2 [218]. All samples passed initial QC following adaptor trimming using Trimmomatic [219]. Reads were aligned to the human (hg19) assembly using Hisat2, version 2.1.0 [220] and indexed by Samtools, version 1.9 [221]. Differential gene expression analysis was performed

using DESeq2, version 1.24.0 [222], with an FDR of 0.05 or lower, and no fold change cut-off. Network mapping and functional analysis was performed with STRING database, version 11.0 [223] and verified with PANTHER, version 14.1 [224]. STRING utilizes Gene Ontology [225,226] to determine functional enrichments within our networks.

Pathway analysis was performed using Signaling Pathway Impact Analysis (SPIA), version 2.36.0 [227,228], which brings fold change and gene function into context. SPIA uses the Kyoto Encyclopedia of Genes and Genomes [229] (KEGG) database to determine impact of DEGs on the respective pathway based on gene enrichment and topology of the pathway. Pathway enrichment is determined from the total number of genes within a specific pathway compared to the Number of Differential Expressed genes (NDE) observed within that pathway; significance of pathway enrichment was set at $pNDE < 0.05$. Furthermore, the topology of a pathway is taken into consideration to determine the impact of DEGs within that pathway. The perturbations (PERT) of a pathway caused by DEGs is determined based on the location of these genes within the pathway; significance was set to $pPERT < 0.05$. Overall global significance (pG) was determined from pNDE and pPERT. Two forms of statistical corrections pG were performed – a Bonferroni correction (pGFWER) and a false discovery rate (FDR) correction (pGFDR). To determine significance of a pathway, $pGFDR < 0.05$ was considered.

Validation of RNA-seq Using RT-qPCR and cDNA Synthesis

Selected individual transcripts were confirmed using PCR primer sets (Qiagen, catalog #330001). cDNA from RNA samples were synthesized using Qiagen's First Strand Kit (catalog #330404). Each reaction was performed following the RT^2 qPCR Primer Assay instructions – each reaction contained 1 ul of the primer mix at 10 uM for each gene of interest, 12.5 ul RT^2 SYBR Green Mastermix, 1 ul cDNA, and 10.5 ul Nuclease-free water, for a total reaction volume of 25 ul. qPCR was initiated with a single 10 min cycle at 95°C for initial denaturing and activation of polymerase. Following this, 40 cycles of 15 seconds at 95°C and 1 minute at 60°C was performed and fluorescent data was collected at the end of each cycle. Melt curve analysis was performed at the end of the reaction using the following conditions: 95°C, 1 min; 65°C, 2 mins; 65°C to 95°C step-wise at 2°C/min. Expression levels of transcripts were compared and normalized to the housekeeping gene *ACTB* (β-actin). Relative gene expression between treated and untreated sample groups were compared using the $2^{-\Delta\Delta CT}$ method. All samples were analyzed in triplicate from three biological replicates.

Supernatant Protein Analysis by Enzyme-linked Immunosorbent Assays

Supernatants from cultures were removed as previously mentioned following treatment. Samples were aliquoted and stored at -20°C until use. ELISAs were performed following manufacturer's instructions (R&D Systems, DuoSet ELISA). Briefly, plates were coated and incubated overnight at room temperature with 100ul of capture antibody. Following aspiration of this antibody and washing, 100 ul of standards and sample were added to each well. Plates

were than incubated at room temperature for 2 hours, aspirated, and then washed. 100 ul of conjugated detection antibody was then added to each well and incubated for 2 hours at room temperature. Colorimetric detection was performed after the addition of a chromogenic substrate and stop solution. Plates were read at a wavelength of 450 nm on a BioTek Epoch plate reader.

Statistical Analysis

Differential gene expression of RNA sequencing data was determined by DESeq2. Briefly, DESeq2 utilizes an empirical Bayes approach and makes the assumption that genes of similar transcript levels will show similar variability. Through this, the package can control for replicate variability at each specific gene by taking into consideration the average variability of similarly expressed genes, and account for sample size. Furthermore, DESeq2 performs a Benjamini-Hochberg adjustment resulting in an adjusted p-value (padj) also called a false discovery rate (FDR). Genes with an FDR < 0.05 were considered significant.

Statistical analysis between control and infected groups for both RT-qPCR and ELISA was performed using an unpaired student's t-test using GraphPad Prism Version 8. Additional post-hoc analysis was performed on RT-qPCR to correct for multiple t-test comparisons. The method of Benjamini, Krieger, and Yekutieli was used to determine the FDR – this method is an updated version of the previously mentioned Benjamini-Hochberg adjustment [230]. Transcripts for RT-qPCR were considered significant if FDR < 0.05 (*). Protein levels from ELISA were considered significant if $p < 0.05$ (*).

Results

Prior to infection, the identity and purity of HCPECs was assessed and confirmed through immunohistochemistry (IHC) with cytokeratin 18 (CK18), an epithelial cell marker, and transthyretin (TTR), a marker for choroid plexus epithelial cells and specific hepatocytes (Figure II-2A and B) – 98% of cells were CK18 and TTR positive [231]. Figure II-2A indicates the colocalization of TTR within CK18 labeled cells; Figure I-2B further illustrates the cytoplasmic localization of TTR by using α-Tubulin to highlight cellular boundaries. Total protein from control and infected groups was isolated to check for the presence of CK18 and TTR (Figure II-2C). The effects of *Bb* infection on HCPEC proliferation, apoptosis, and necrosis was measured through IHC and colorimetric assays - no significant changes were detected between infected and control groups.

Stimulation of Type I/II Interferon Signaling Pathway Following *B. burgdorferi* Infection

B. burgdorferi infection was performed with primary human choroid plexus epithelial cell cultures for 48 hours, and changes in the transcriptome of the human cells were compared to untreated controls (3 biological replicates per group). Supernatant from each replicate was collected and used for protein analysis, and RNA was then isolated. Following RNA isolation, Illumina libraries were made and sequenced on an Illumina HiSeq 4000 as outlined in the Methods section. Differential gene expression analysis was performed using the DESeq2 package in Rstudio. Following count normalization, an MA-plot

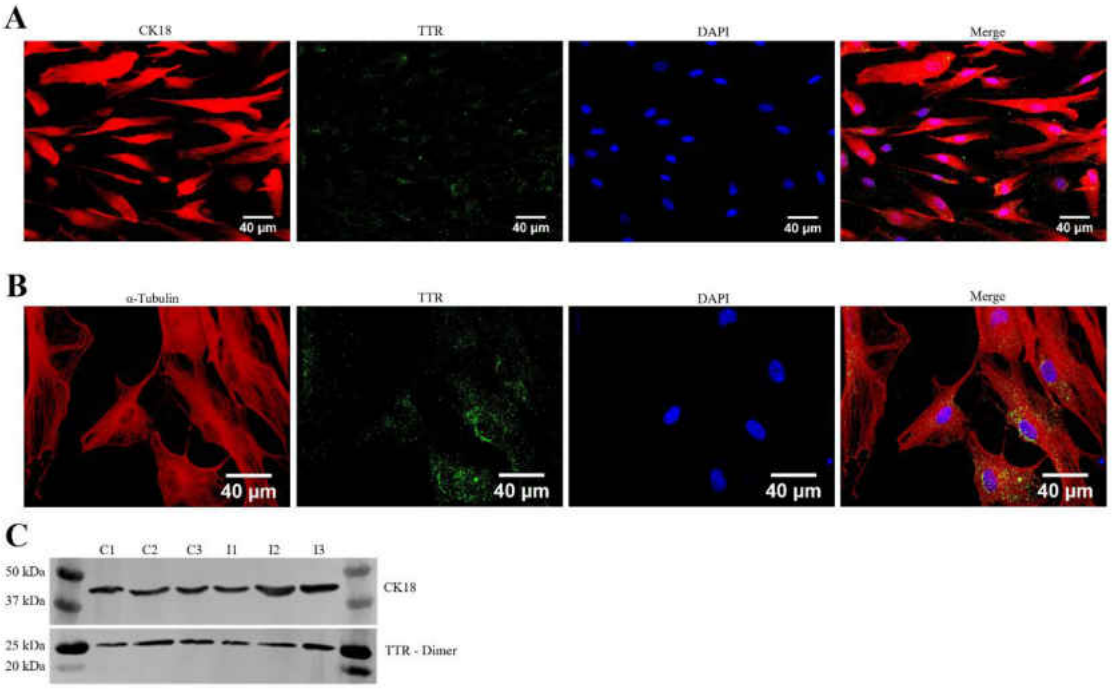

Figure II - 2. Characterization of primary HCPECs.
(A) HCPECs were identified by immunostaining with cytokeratin 18 (CK18 - red), an epithelial cell marker, and transthyretin (TTR – green), a transport protein predominantly expressed by choroid plexus epithelial cells and hepatocytes. Nuclei were stained with DAPI (blue). Magnification: 40x, Scalebar: 40 µm. Further observations of TTR localization within the cytoplasm of HCPECs. **(B)** Colocalization of α-Tubulin (red) and TTR (green); nuclei stained with DAPI (blue). Magnification: 60x, Scalebar: 40 µm. **(C)** Western blot for the presence of CK18 and TTR (dimer). Lanes C1, C2, C3 – Uninfected HCPECs protein; Lanes I1, I2, I3 – Protein from HCPECs infected with *Bb* for 48 hours.

(Figure II-3A) was constructed – this illustrates genome-wide transcriptome expression of the 48-hour *Bb* treated group when compared to the control group. Dots in red represent significant differentially expressed genes (DEGs), plotted as a function of its $\log_2$ fold change versus the mean of normalized counts. Using an adjusted p-value (false discovery rate) less than or equal to 0.05, and no fold change threshold, a total of 258 genes were shown to have significant differential expression. A full list of these differentially expressed genes can be found in Appendix A. Of these 258 DEGs, 160 were upregulated and 98 downregulated. Hierarchical clustering of replicates based on treatment is further illustrated in the heatmap analysis (Figure 2-3B) of the 258 DEGs for each replicate.

In order to validate our RNA-seq findings, RT-qPCR was performed on a set of select genes (Figure II-4A). The upregulated genes *cxcl3*, *cxcl6*, *ccl5*, *ifit1*, and *ifitm1* were found to be significantly upregulated by RT-qPCR when comparing 48-hour infected group to the untreated group. Although *cxcl5* and *irf7* transcripts were not significantly increased, an increasing trend was observed that correlates with the RNA-seq data. Additionally, the downregulated genes *cdh2*, *flt1*, and *anxa1* showed a non-significant downward trend that corresponds with our previous data. In order to determine if transcriptional changes observed in response to *Bb* resulted in protein production and secretion from the choroid plexus epithelial cells, we measured the cytokine levels in cell culture supernatants by ELISA (Figure 2-4B-E). Following 48-hours post *B. burgdorferi* stimulation, Cxcl1, Cxcl2, Cxcl5, and Cxcl6 supernatant concentrations were

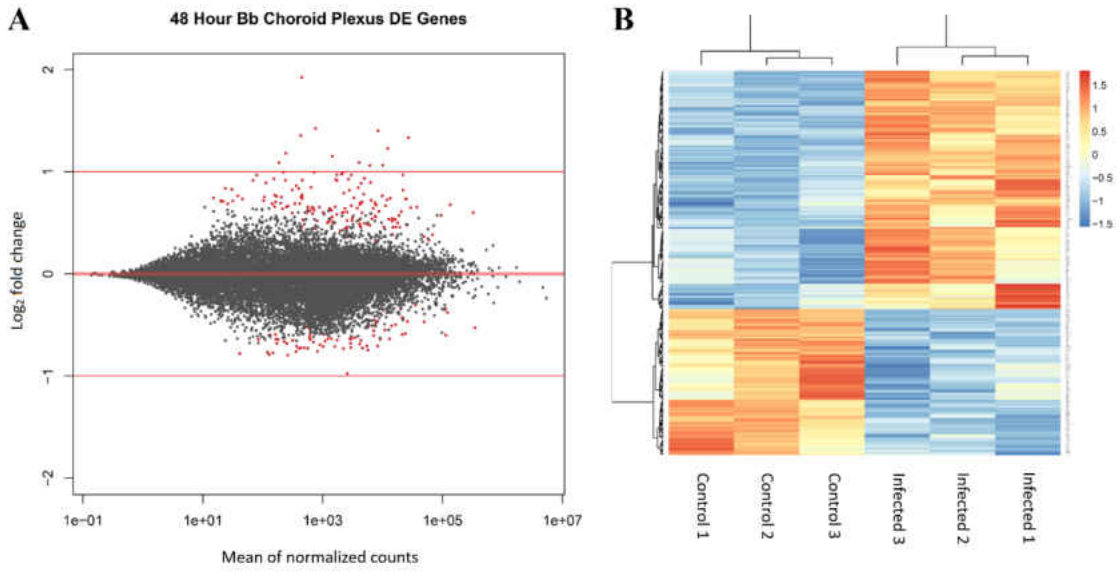

Figure II - 3. RNA-seq was performed on HCPECs that were infected by *B. burgdorferi* for 48 hours and from uninfected controls. **(A)** MA-plot representing gene expression patterns of infected group compared to control (n=3). Red dots indicate significant differentially expressed genes (DEGs; FDR <0.05). A total of 258 genes were differentially expressed. **(B)** A heatmap of the 258 DEGs showing clustering patterns between each biological replicate.

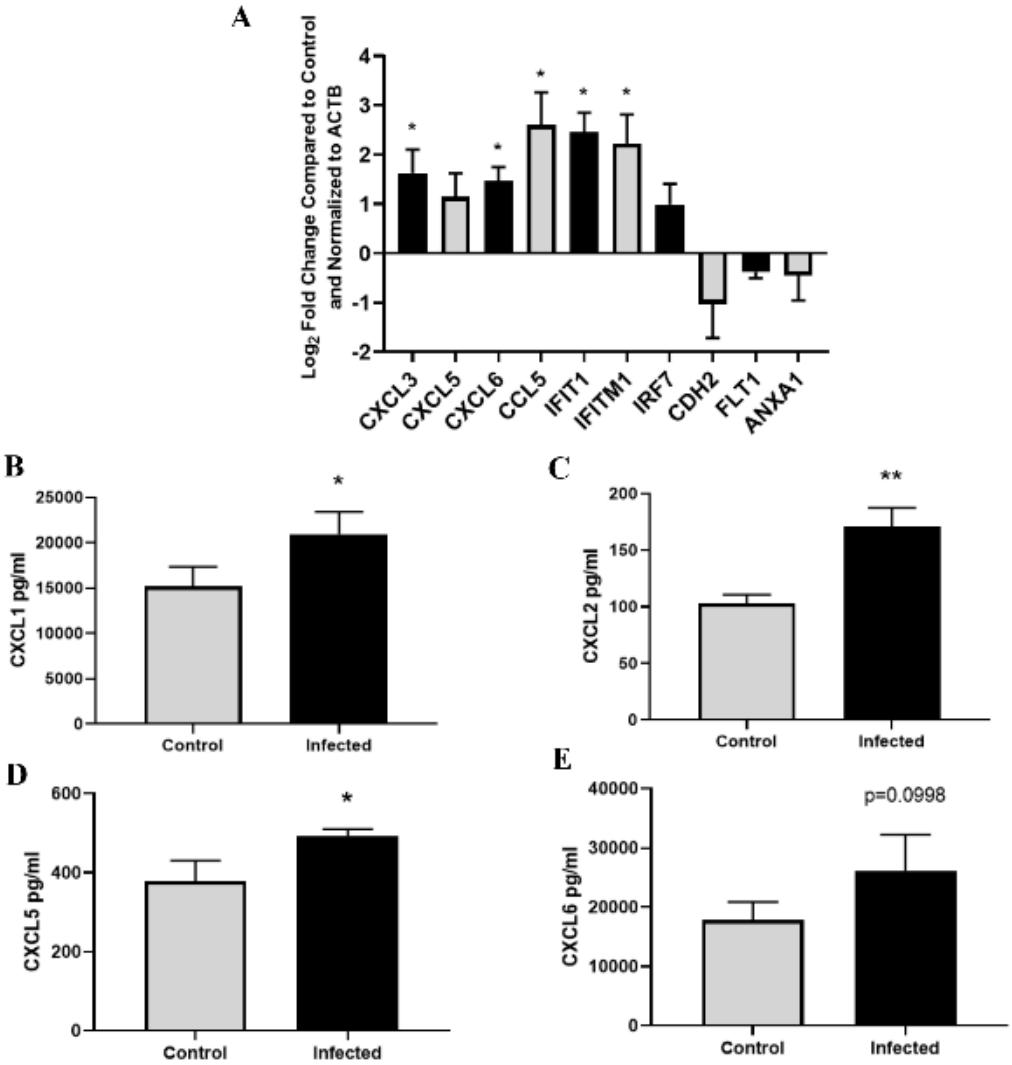

Figure II - 4. Validation of RNA-seq gene expression data.
(A) Select differentially expressed genes following 48-hour *B. burgdorferi* treatment were validated by RT-qPCR. Primers specific to *cxcl3*, *cxcl5*, *cxcl6*, *ccl5*, *ifit1*, *ifitm1*, *irf7*, *cdh2*, *flt1*, *anxa1*, and *actb* were used for amplification. The relative gene expression between 48-hour *B. burgdorferi* treated and untreated control groups are expressed as Log2FC and normalized to the housekeeping gene ACTB. Significance was calculated by Student's t-test (* $p<0.05$, n=3). **(B-E)** Supernatant from infected and untreated groups were collected and analyzed by ELISA. Concentrations of these secreted cytokines are shown as the mean and standard deviation. Significance was calculated by Student's t-test followed by Benjamini, Krieger, Yekutieli correction (* FDR < 0.05, n=3).

assessed. Cxcl1, Cxcl2, and Cxcl5 were induced and secreted at significantly higher levels in the infected samples compared to untreated controls. Though Cxcl6 did not show significant elevation, a similar increase in protein levels was observed. These data agree with our RNA-seq findings.

Both subsets of upregulated and downregulated genes were analyzed for known interactions of their associated proteins using the STRING (Search Tool for the Retrieval of Interacting Genes/Proteins - https://string-db.org/) database (Figure II-5 and II-6) [223]. STRING analysis provides insight into the protein-protein interactions of each gene – each node represents one of the DEGs; lines between nodes correspond to known interactions that were experimentally determined or curated from databases utilized by STRING. STRING also provides information on functional and pathway analysis through the use of Gene Ontology (GO) [225,226] and KEGG [229]. Upregulated DEGs (Figure 2-5A) show two distinct clusters within the network. The first cluster, shown in the top left, is predominantly comprised of chemokines and cytokines – the red nodes denote genes within the chemokine-mediated signaling pathway (GO:0070098, FDR 8.23E-08). Additionally, the second highly clustered nodes situated within the center indicates genes associated with type I (blue) and type II (green) interferon pathways (GO:0060337, FDR 2.71E-23; GO:0034341, FDR 9.58E-15, respectively). The biological processes that were enriched predominantly involved inflammatory/immune response pathways and cell-cell communication (Figure 2-5B). A large subset of the upregulated genes was found to be interferon pathway genes (Table II-1). Of note, the interferon-induced protein

A

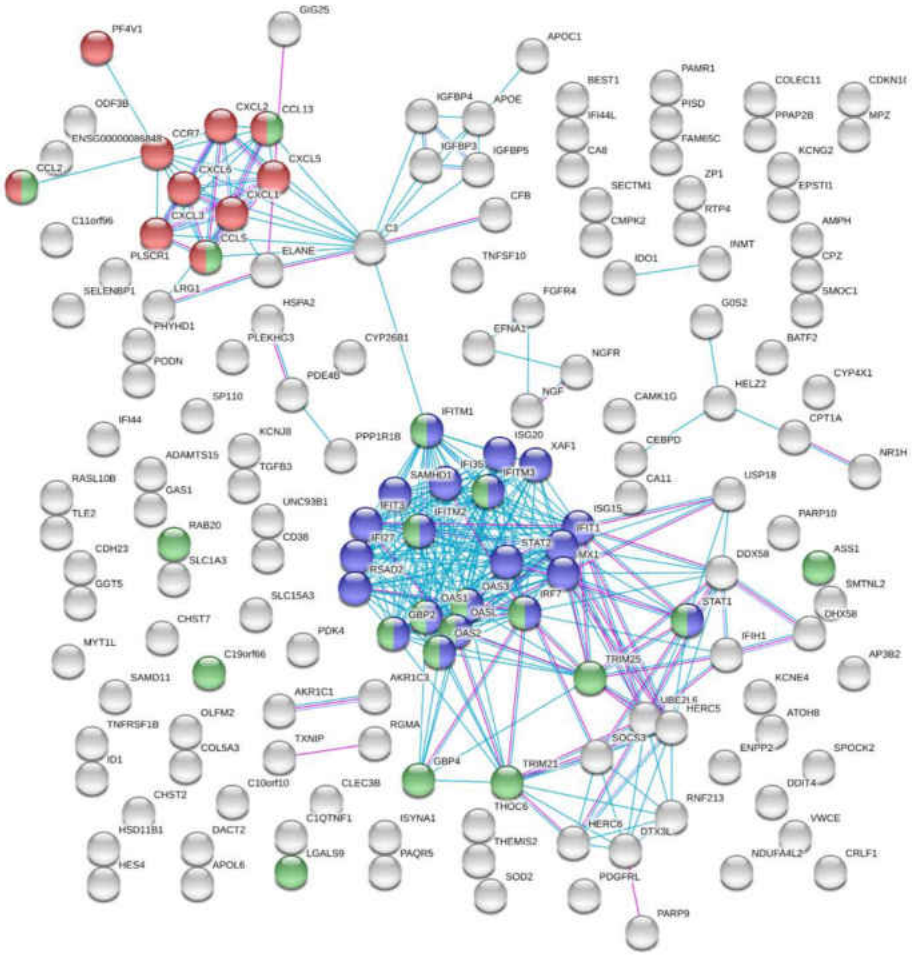

B

GO Enrichment	FDR	GO Term
Response to type I interferon	3.75E-24	GO:0034340
Type I interferon signaling pathway	2.71E-23	GO:0060337
Innate immune response	1.61E-21	GO:0045087
Cytokine-mediated signaling pathway	4.29E-21	GO:0019221
Immune response	4.67E-20	GO:0006955
Response to interferon-gamma	9.58E-15	GO:0034341
Inflammatory response	1.67E-10	GO:0006954
Chemokine-mediated signaling pathway	8.23E-08	GO:0070098
Regulation of leukocyte chemotaxis	2.31E-06	GO:0002688
Positive regulation of neutrophil chemotaxis	7.71E-07	GO:0090023

Figure II - 5. Network and functional analysis of upregulated DEGs by STRING analysis.
(A) STRING network – Each node represents a DEG; lines between nodes indicate known protein-protein interactions. Nodes in blue and green correspond to type I or type II interferon pathways, respectively; Red corresponds to chemokine-mediated signaling pathway. **(B)** Table of select GO enrichments.

A

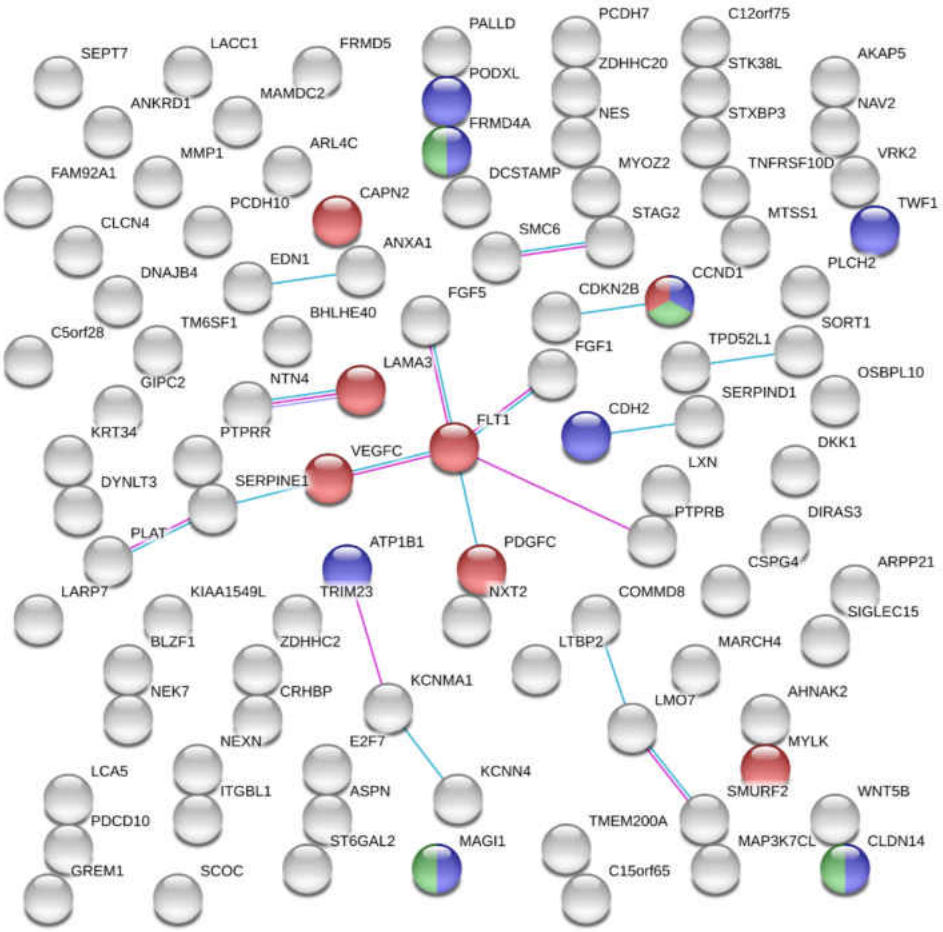

B

GO Enrichment	FDR	Go Term
Regulation of cell migration	0.00047	GO:0030334
Blood vessel morphogenesis	0.0006	GO:0048514
Angiogenesis	0.00082	GO:0001525
Epithelium development	0.0127	GO:0060429
Cell-cell junction	0.0244	GO:0005911
Bicellular tight junction	0.0492	GO:0005923

Figure II - 6. Network and functional analysis of downregulated DEGs by STRING analysis.
(A) String network – Nodes in blue and green represent cell-cell junctions (GO:0005911) and bicellular tight junctions (GO:0005923), respectively. Nodes in red indicate genes within the focal adhesion pathway from KEGG pathway analysis (hsa04510). **(B)** Table of selected GO enrichments.

Table II - 1. Select inflammatory and immune response genes

	Gene Symbol	Log_2 Fold Change	p-value (adjusted)	Function (Uniprot ID)
Interferon Related	OASL	1.923812	7.63E-18	Type I/II interferon signaling pathway – RNA binding (Q15646)
	IFITM1	1.336366	1.99E-13	Type I/II interferon signaling pathway – Inhibits entry of virus (P13164)
	IFIT3	1.228324	6.81E-11	Type I/II interferon signaling pathway – Inhibits viral processes (O14879)
	IFIT1	1.4001	1.51E-10	Type I interferon signaling pathway – RNA binding (P09914)
	RSAD2	1.424712	7.87E-09	Type I interferon signaling pathway – CD4+ T-cell activation (Q8WXG1)
	OAS2	1.064886	3.93E-06	Type I/II interferon signaling pathway – Innate antiviral response (P29728)
	OAS1	1.061772	1.35E-05	Type I/II interferon signaling pathway – Innate antiviral response (P00973)
	IFITM3	0.677765	2.45E-05	Type I/II interferon signaling pathway – Inhibits entry of virus (Q01628)
	IFI27	0.865445	0.000102	Type I interferon signaling pathway – Innate immune response (P40305)
	IFITM2	0.57169	0.000815	Type I/II interferon signaling pathway – Inhibits entry of virus (Q01629)
	IRF7	0.764681	0.004436	Type I/II interferon signaling pathway – Key transcriptional regulator (Q92985)
	OAS3	0.72591	0.008201	Type I/II interferon signaling pathway – Innate antiviral response (Q9Y6K5)
	IFI35	0.759788	0.012529	Type I interferon signaling pathway (P80217)
	GBP2	0.400131	0.049661	Type I/II interferon signaling pathway – anti-pathogen activity (P32456)
	STAT1	0.734634	1.89E-05	Signal transducer – Mediates interferon response (P42224)
	STAT2	0.45657	0.026725	Signal transducer – Mediates interferon response (P52630)
Chemokine/cytokine Related	CCL5	1.355304	4.67E-09	Chemotaxis – Monocytes, T-helper cells, eosinophils, neutrophils (P13501)
	CXCL2	0.927644	3.00E-07	Chemotaxis – Leukocytes, neutrophils (P19875)
	CXCL1	0.734937	1.35E-05	Chemotaxis – Neutrophils (P09341)
	CXCL6	0.654966	2.30E-05	Chemotaxis – Neutrophils, leukocytes (P80162)
	CCL2	0.479371	0.002206	Chemotaxis – Monocytes, basophils (P13500)
	CXCL3	0.837774	0.005424	Chemotaxis – Leukocytes, neutrophils (P19876)
	ELANE	0.819051	0.007334	Modulates natural killer cells, monocytes, granulocytes, neutrophils (P08246)
	CXCL5	0.652521	0.009551	Chemotaxis – Neutrophils, leukocytes (P42830)
	CCR7	0.659729	0.009835	Chemokine receptor – mediates immune cell chemotaxis (P32248)
	CCL13	0.714727	0.032672	Chemotaxis – Monocytes, lymphocytes, basophils, eosinophils (Q99616)
	C3	0.68928	0.037701	Complement system (P01024)

family of genes, *ifit1*, *ifit3*, *ifitm1*, *ifitm2*, *ifitm3*, and others, were shown to be significantly upregulated. Type I and II interferon related genes, such as *gbp2*, *ifit1*, and *oasl*, have been previously reported as being significantly elevated as a consequence of *B. burgdorferi* infection [197,232]. Furthermore, major transcription factors that were observed to be upregulated including *irf7*, *stat1*, and *stat2*, have been shown to play important roles in regulating the *Bb*-induced interferon response [233–235]. Interferon related genes have traditionally been associated with viral, not bacterial, infections, and this is reflected in regard to the labeling of gene function and pathway analysis within these data. However, it is well documented that such genes are often observed to play key roles during bacterial infections, including Lyme disease [236–239]. Signaling Pathway Impact Analysis (SPIA) was performed to determine pathway enrichment based on an increase in gene enrichment and position of genes within a pathway. A total of 14 pathways were identified as being significantly enriched (Figure II-7). The top activated pathways involve the activation of viral pathways, including Influenza A, Measles, and Herpes simplex infection. As stated before, these viral pathways involve the interferon related response as observed in our data. These data imply that infection with *B. burgdorferi* produces a significant immune response that encapsulates major interferon-signaling pathways within HCPECs.

B. burgdorferi Infection Induces a Chemokine Profile in HCPECs Conducive to the Chemotaxis of Immune Cells

Many of the transcripts that were upregulated were categorized into pro-inflammatory cytokines and chemokines (Table 2-1) - these involved the C-X-C

Figure II - 7. Signaling Pathway Impact Analysis.
SPIA of all DEGs based on pathway gene enrichment (pNDE) and pathway perturbations (pPERT) that take into account gene placement and topology within the pathway. Both pNDE and pPERT are used to determine global significance, pG. **(A)** SPIA two-way evidence plot. Each dot represents a pathway that contains at least one DEG. The impact analysis plots each pathway based on pNDE and pPERT. Pathways above the solid blue line are significant following FDR correction (pGFDR < 0.05). Pathways above the solid red line are significant following Bonferroni correction (pGFWER < 0.05). **(B)** A table of all significant pathways (PGFDR <0.05) and their respective status is shown.

A

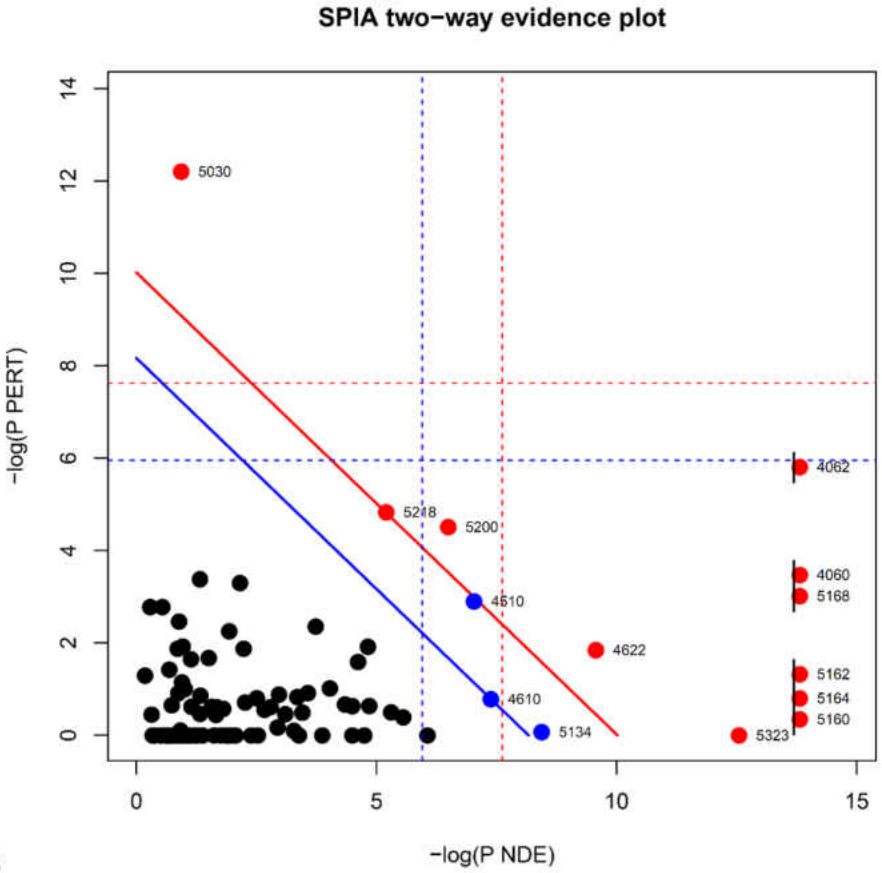

B

Pathway ID	Pathway	pGFdr	Status
5164	Influenza A	2.33E-10	Activated
4060	Cytokine-cytokine receptor interaction	7.84E-09	Activated
5162	Measles	1.75E-07	Activated
4062	Chemokine signaling pathway	6.71E-07	Activated
5168	Herpes simplex infection	7.51E-07	Activated
5160	Hepatitis C	1.76E-05	Inhibited
5030	Cocaine addiction	0.000405	Inhibited
5323	Rheumatoid arthritis	0.000612	Inhibited
4622	RIG-I-like receptor signaling pathway	0.00155	Activated
5200	Pathways in cancer	0.002034	Inhibited
5218	Melanoma	0.004492	Inhibited
4510	Focal adhesion	0.004505	Inhibited
5134	Legionellosis	0.014968	Inhibited
4610	Complement and coagulation cascades	0.018952	Activated

and C-C motif family of chemokines. *cxcl1*, *cxcl2*, *cxcl3*, *cxcl5*, and *cxcl6* showed elevated levels in response to *B. burgdorferi* infection. In addition to their role in modulating immune cell activation and inflammation, these chemokines provide a mechanism for the chemotaxis of immune cells. Predominantly, the C-X-C family possesses chemoattractant properties for leukocytes, such as neutrophils [124–126]. In fact, Cxcl1 mediates the recruitment of neutrophils and subsequent swelling in Lyme arthritis and carditis [127]. In contrast, the C-C family induces the migration of PBMCs, including lymphocytes and monocytes [240]. In our experiments, *ccl2*, *ccl5*, *ccl13*, and the receptor, *ccr7*, were found to be upregulated. This is corroborated in a study that previously showed *ccl2* (*mcp-1*) and *ccl5* (*rantes*) were elevated in human monocytes in response to *B. burgdorferi* [241]. Ccr7, a receptor for Ccl19 and Ccl21, is constitutively expressed in intestinal and gastric epithelial cells and has been shown to be upregulated in response to *Helicobacter pylori* infection [242,243]. Biological process analysis performed by GO, via STRING, indicates cytokine and chemokine-mediated signaling pathways to be significantly enriched. Moreover, processes involving the regulation of leukocyte and neutrophil chemotaxis were shown to be enriched as well (Figure 2-5B). These observations are further strengthened by SPIA, where the pathways cytokine-cytokine receptor interaction and chemokine signaling pathways were found to be significantly enriched and activated (Figure 2-7). Further evidence that may imply the immune trafficking role of HCPECs comes from the secretion of these proteins at elevated levels within the culture media, as previously stated (Figure 2-3B-E).

B. burgdorferi Effects on Cellular Components Involved in Cell-Cell Junctions and Adhesion

Although HCPECs were grown in a non-barrier monolayer culture, it was found that a number of genes related to cellular junctions and adhesion were modestly downregulated (Table II-2). The integrity of the BCSFB at choroid plexus epithelium is contingent on the presence of several tight and adherens junctions. Adherens junctions, found more basal than tight junctions (Figure II-1), mainly involve cadherin proteins, for example E-cadherin, VE-cadherin, and N-cadherin [244]. The presence of CDH2 (N-cadherin) has been observed on the basolateral side of the choroid plexus epithelium in mice [245]. Three genes within the cadherin superfamily were found to be downregulated – *cdh2*, *pcdh7*, and *pcdh10*. Likewise, genes that code for tight junction components showed lowered expression – *cldn14* and *magi1*. Genes within regulatory pathways that promote the formation of these junctions or other cellular adhesins were also found to have decreased expression – *mtss1*, *atp1b1*, and *frmd4a*. Network analysis showed minimal clustering of genes involved in cellular adhesion regarding protein-protein interactions (Figure 2-6A). Additionally, genes involved in the modulation of surrounding extracellular matrix and vasculature were observed to be downregulated, some of which shared overlapping function with cellular adhesion – *mmp1*, *flt1*, *vegfc*, and *serpine1*. GO enrichment indicated enriched cellular components that involve cell-cell junction and bicellular tight junctions, as well as angiogenesis and epithelium development processes.

Table II - 2. Select genes involved in cell-cell junctions, tight junctions, and adherens junctions.

	Gene Symbol	Log_2 Fold Change	p-value (adjusted)	Function (Uniprot ID)
Functional component	CLDN14	-0.77849	0.014354	Tight junction protein; Cell adhesion (O95500)
	PCDH10	-0.70536	0.000243	Protocadherin; cell-cell adhesion (Q9P2E7)
	CDH2	-0.65003	3.70E-07	Adherens junction protein; Cell adhesion (P19022)
	MAGI1	-0.42719	0.03935	Scaffolding/Tight Junction Protein; Cell adhesion (Q96QZ7)
	PCDH7	-0.39693	0.011885	Protocadherin; cell-cell adhesion (O60245)
Regulatory component	PODXL	-0.97617	6.91E-07	Positive/negative regulation of cell adhesion (O00592)
	TWF1	-0.67896	0.038453	Actin binding; Cadherin binding; Focal adhesion (Q12792)
	NEXN	-0.63395	0.015809	Actin binding protein; Cell adhesion (Q0ZGT2)
	MTSS1	-0.53155	0.000231	Actin binding protein; Positive regulation of cell-cell junctions, adhesion (O43312)
	FLT1	-0.50364	0.01255	VEGF receptor; Endothelial proliferation, survival, cell adhesion (P17948)
	ATP1B1	-0.47766	0.034878	ATPase non-catalytic beta subunit; Cell adhesion; Epithelial cell polarity (PO5026)
	MYLK	-0.43527	0.014211	Regulates tight junctions; Regulates epithelial cell survival, wound healing (Q15746)
	CCND1	-0.37679	0.008102	Regulates cell cycle; Interactions with tight junction proteins (P24385)
	FRMD4A	-0.3571	0.017093	Scaffolding Protein – Regulates epithelial cell polarity, adherens junctions (Q9P2Q2)
	CAPN2	-0.33762	0.047708	Protease; Negative regulation of junction and adhesive pathways (P17655)
	PALLD	-0.30542	0.041217	Scaffolding/Cytoskeletal protein; Cell adhesion (Q8WX93)

Pathway analysis indicates an inhibition of the focal adhesion pathway (Figure II-7). The functional and structural impact of these downregulated genes in response to *B. burgdorferi* infection is yet to be determined in an animal model.

Discussion

The neurological symptoms associated with Lyme disease are largely attributed to the dissemination of *Borrelia burgdorferi* into the CNS and the resulting host immune response. While previous studies have investigated the effects of this bacteria on endothelial models of the BBB, little is known about its impact on the epithelium of the choroid plexus which comprises the BCSFB. The CP epithelium is situated at a key interface that separates the blood from the CSF and has repeatedly been shown to play an important role in modulating the immune response between the periphery and CNS during infection. The importance of the composition of the CSF in regards to cytokines and infiltrating immune cells in Lyme disease patients has been previously reported [76,84,246–248]. However, in the context of Lyme disease, the choroid plexus has been greatly understudied, and given its role as the major producer of CSF, as well as its ability to regulate its composition, it constitutes a major gap in knowledge for the pathophysiology of the disease [249]. To the best of our knowledge, this is the first study to directly investigate the impact of *Borrelia burgdorferi sensu lato* on choroid plexus epithelium.

This study demonstrates a robust change in gene expression in HCPECs induced by *B. burgdorferi* infection. The most prevalent outcome was the upregulation in immune and inflammatory response genes that were primarily

categorized within the chemokine/cytokine mediated pathways and type I and II interferon pathways. Consistent with our report, previous studies have observed similar results regarding the inflammatory and immune response within monocytes, macrophages, and dendritic cells, showing an increase in cytokines such as *cxcl1*, *cxcl2*, *ccl2*, and *ccl5* [250,251]. Likewise, interferon-stimulated genes within a murine model were reported to be upregulated, involving the transcripts *Ifit1*, *Ifit3*, and *Irf7* [234]. Irf7 has been shown to be a master regulator of interferon stimulated genes, and in conjunction with the upregulation of *ddx58* (*rig-I*), *ifih1* (*mda4*), and *trim25*, may provide insight into the activation of the interferon pathway being observed. Additionally, the induction of inflammatory cytokines including type I and type III interferons were reported when human PBMCs were infected with *B. burgdorferi* [252]. Furthermore, when characterizing the immunophenotypes of infiltrating immune cells and cytokines within the erythema migrans (EM) lesions of patients, T cells, monocytes, macrophages, and dendritic cells were found to be enriched in addition to inflammatory cytokines [169].

While this study shows overlapping features common in other cell types or animal models infected with *Bb,* the importance of the choroid plexus's role in immune cell trafficking is further highlighted in other models of infection and disease. The concept of the immunosurveillance activity within the choroid plexus is not new, and the abundance of immune cells found within the choroid plexus and subsequent transmigration following infection or insult has been widely reported [208,211,213,253,254]. Functional and pathway analysis indicates that

many of these genes are involved in chemotaxis of immune cells [124,125,255–258]. In fact, *Cxcl1* (previously known as *Kc*) and *Ccl2* (previously known as *Mcp-1*) have been shown to mediate the recruitment of neutrophils into the joints of mice infected with *B. burgdorferi,* and are required for the development of Lyme arthritis [259]. The upregulation of *cxcl1*, *cxcl2*, *cxcl3*, *ccl2*, and *ccl5*, potent chemoattractants for immune cells including neutrophils, monocytes, and T cells, among others, have also been consistently reported to be elevated in other bacterial infections of the CP. In a barrier model of the choroid plexus involving infection with *Neisseria meningitidis,* in addition to an increase in these chemoattractants, the recruitment and subsequent transmigration of polymorphonuclear neutrophils and monocytes was observed [260,261]. Similar results are also seen in response to *Streptococcus suis,* a gram-positive bacterium that can be transmitted to humans from pigs, leading to symptoms such as meningitis [262]. In a BCSFB model using human choroid plexus papilloma cells, a viral infection with Echovirus 30 showed an enhanced secretion of Cxcl1, Cxcl2, Cxcl3, and Ccl5 [263]. Indeed, when investigating the composition of the CSF from individuals with *B. burgdorferi* induced meningoradiculitis, an increase in inflammatory cytokines and a large number of B cells and plasma cells are observed [264]. Collectively, the choroid plexus has been shown to contribute significantly to the pathogenesis of many diseases and in regards to Lyme disease, our data implies that the choroid plexus may play an important role in the abundance of immune cell invasion of the CSF and the exacerbation of CNS inflammation that is seen in patients [265,266].

In our current model, our transcriptome analysis indicates a downregulation of key tight junction and adherens junction genes, as well as regulatory cell adhesion genes. *cldn14*, a tight junction protein associated with the choroid plexus, as well as *cdh2*, an adherens junction protein, were found to be downregulated [267,268]. The injection of LPS in mice to stimulate a peripheral inflammatory response showed a similar gene expression pattern, where the majority of upregulated genes within the choroid plexus involved immune-mediated pathways, while downregulated genes participated in barrier function, including claudins and protocadherins [269]. Though the functions of protocadherins are still being fully elucidated, they have been found to play a key role in cellular adhesion and barrier integrity [270,271]. In addition, the sodium/potassium transporter beta subunit, *atp1b1*, was found to be downregulated, yet, seems to be an unlikely participant in the formation of cell-cell junctions; however, it has been shown to play an integral part in cell adhesion and in both the formation and maintenance of tight junctions in epithelial cells [272–275]. The downregulation of a number of these components, as well as scaffolding and other regulatory genes such as *magi1* and *mtss1*, would indicate a potential dysregulation of the choroid plexus barrier. This may lead to the possibility of immune cell invasion as well as an entry site for *Borrelia burgdorferi* into the CSF. In fact, the choroid plexus has already been implicated as a possible site of entry for both *N. meningitidis* and *S. suis,* specifically from the basolateral side [276]. By using two *in vitro* barrier models constructed by human brain microvascular endothelial cells (BMEC) and umbilical vein

endothelial cells (HUVEC), *Bb* was found to differentially transverse these barrier systems [89,277,278]. While *B. burgdorferi* was capable of crossing the HUVEC monolayer, the traversal of the bacteria across the BMEC barrier required the addition of plasminogen and was found to induce the expression of plasminogen activators, receptors, and matrix metalloproteinases – supporting the concept that the bacteria is able to utilize the fibrinolytic system which may promote its dissemination through the degradation of the extracellular matrix and cell-to-cell junctions [89,277,278]. However, in our experiments, we found conflicting results – tissue plasminogen activator, tPA (*plat*), as well as its inhibitor, *serpine1*, were both found to be downregulated. Furthermore, the metalloproteinases, *mmp1*, and *adamts15*, were found to be downregulated and upregulated, respectively. Though our system does not represent a barrier model, the observed outcome lends credibility for our future studies involving *B. burgdorferi* infection in an *in vivo* model to explore the impact of systemic infection on the BCSFB.

Conclusion

Following infection of HCPECs with *Borrelia burgdorferi*, we identified a gene expression pattern that is marked by a robust increase in immune and inflammatory genes within the cytokine/chemokine pathways and type I and II interferon pathways. Protein analysis showed an enhanced secretion of these inflammatory and chemotactic cytokines. Additionally, the downregulation of genes involved in cell-cell adhesion, adherens junctions, and tight junctions was observed. Overall, our data indicates that the choroid plexus, like in many other infectious diseases, may play a key role in the pathogenesis of Lyme

neuroborreliosis through the induction of inflammatory factors, the promotion of immune cell migration, and potentially through the dysregulation of the BCSFB. Our future studies will aim to elucidate the impact of *B. burgdorferi* infection on the BCSFB integrity within an *in vivo* model. By understanding how the inflammatory and immune response is modulated within the CNS, as well as mechanisms by which *Borrelia burgdorferi* is able to traverse into the CNS, new treatments for Lyme disease can be developed.

CHAPTER III

DIFFERENTIAL METHYLATION IN HUMAN ASTROCYTES IN RESPONSE TO *BORRELIA BURGDORFERI* SENSU STRICTO STRAINS

Introduction

The pathophysiology of Post-Treatment Lyme Disease Syndrome (PTLDS) is currently unknown and many avenues remain to be explored. Following treatment, 10-20% of individuals develop or experience a continuation of symptoms that commonly include neurological involvement such as fatigue, sleep disturbances, and cognitive difficulties. As some evidence has shown, the peripheral immune response may indirectly lead to a deleterious state within the CNS through the diffusion of inflammatory factors or migration of peripheral immune cells across the blood-brain barrier and blood-CSF barrier. Additionally, the direct involvement of resident immunity may lead to the exacerbation of symptoms seen in patients, as *B. burgdorferi* has been shown to elicit a strong inflammatory response within the CNS. Multiple studies have shown that both live and heat or sonicated killed *B. burgdorferi* are capable of eliciting an immune response in a wide variety of tissues, with spirochetal antigens being found in the synovium of Lyme arthritis patients and in the CSF of neuroborreliosis patients [76,279–282]. In fact, microglia and astrocytes, both resident glial cells of the brain, produce an inflammatory response induced by *B. burgdorferi* [109,198]. Furthermore, the release of these inflammatory mediators has been implicated in

neuronal apoptosis [80,151,283]. A more recent study in 2018 by researchers at Johns Hopkins corroborated this role of glial activation in individuals with PTLDS. By measuring the expression of the 18 kDa translocator protein (TSPO), a mitochondrial protein that is greatly increased in activated microglia and reactive astrocytes, through the use of a radiotracer ([^{11}C]DPA-713) and positron emission tomography (PET), the researchers were able to identify an increase of this inflammatory marker in PTLDS patients [284]. Many of the symptoms experienced by PTLDS patients are difficult to assess and are highly subjective, however, these patients exhibit clinically significant levels of pain, sleep disturbances, depression, and overall poorer quality of life [101]. As there are few quantifiable abnormalities that can be measured in PTLDS, studies aimed at investigating objective variables of the syndrome become even more important for accurate diagnosis and clinical care that patients receive. Astrocytes are the most abundant cell type in the brain, and due to their diverse roles and implication to neuroborreliosis and PTLDS, they are the focus of the next two chapters [199].

Astrocytes

Astrocytes, receiving their name from their star-like appearance, are highly heterogeneous in their function and morphology. Through their numerous processes, they form extensive intercellular networks that allow them to communicate with each other through the formation of gap-junction channels [285]. These networks extend to form neuro-glial connections that provide nutritional support to neurons and, through the trafficking of metabolic substrates

such as lactate, aid in sustaining neuronal activity during energy deprivation [286,287]. Their relationship with neurons continues through their alterations of neuronal synapses, by controlling their formation, removal, and the modulation of neurotransmitters [288–292]. Additionally, with their specialized endfeet, astrocytes are able to make physical contact with the endothelial cells of brain vasculature, enveloping the CNS capillaries to aid in the formation, maintenance, and function of the blood-brain barrier [293,294].

During neurological stress such as traumatic injury or disease, astrocytes undergo a reactive state termed astrogliosis. This reactive state is marked by an increase in proliferation, an increase in the length and number of processes, and hypertrophy [295,296]. Intermediate filaments, which are prominent components of the cytoskeletal system, are necessary for the morphological changes that occur during astrogliosis [297]. Glial fibrillary acidic protein (GFAP), an intermediate filament, is a standard marker for astrocytes, and the upregulation of GFAP is a hallmark of astrocyte activation [298]. While the roles of astrocytes during a healthy state are varied, the functions that follow astrogliosis are highly diverse and context dependent. This is emphasized to such a degree that reactive astrocytes may provide beneficial and protective roles in one scenario, while becoming deleterious and cytotoxic in another [299–301]. In the context of infection, reactive astrocytes become involved in the immune response by modulating the inflammatory response in the brain [302]. Class II major histocompatibility complex (MHC) are molecules that play an important role in the immune response through the presentation of antigens and, the expression of

MHC II is normally seen on professional antigen-presenting cells such as macrophages, dendritic cells, and B cells. However, the expression of MHC II on astrocytes has been shown to be induced by immune factors such as IFN-γ and enhanced by TNF-α, and in fact, astrocytes were the first CNS cell type to be shown to express MHC II upon IFN-γ stimulation [303,304]. In addition to their antigen-presenting roles, in the context of diseases or infections, astrocytes are able to secrete inflammatory cytokines and express chemokine receptors. These can function as anti-inflammatory factors such as IL6 or IL10, or promote inflammation such as CCL2, CCL5, CXCL1, and CXCL10 which lead to the recruitment and activation of peripheral immune cells [305]. During infection, astrocytes may encounter pathogen associated molecular patterns (PAMPS) that are recognized by several receptors such as Toll-like receptors (TLRs). Activation of TLRs results in a robust cytokine response that leads to a hostile environment for resident cells [306]. This inflammatory state can disrupt the homeostatic environment and lead to cytotoxicity [306–308]. As stated previously, patients with PTLDS show an increased amount of glial inflammation within the brain, and evidence has shown that astrocytes may contribute to behavioral disturbances that are associated with inflammation, including regulation of sleep, pain, and depression [284,309–312]. This is not surprising when considering the broad functionality of astrocytes that allow them to regulate the immune and inflammatory response, provide structural and nutritional support including the blood-brain barrier, and modulate neuronal synapses.

A previous study by our laboratory investigated the effects of *B. burgdorferi* on primary human astrocytes *in vitro* and found differentially expressed genes that were involved in the immune response, structural and cellular development, cell adhesion, and chromatin assembly [198]. As inflammation is an important factor in the development of persistent symptoms of PTLDS patients, and astrocytes have been shown to play an important role in modulating this response in multiple diseases including Lyme disease, we sought to investigate an alternative mechanism for the pathogenesis of PTLDS. Therefore, we hypothesized that during infection, *B. burgdorferi* induces epigenetic modifications in host cells that are conducive to a persistent inflammatory state. The two epigenetic alterations that we have explored are DNA methylation and chromatin accessibility, the former being the subject of this chapter.

DNA Methylation

DNA methylation and its equally important counterpart, demethylation, is the process in which methyl groups are added, or removed, to genomic DNA (Figure III-1) [313]. In mammalian cells, DNA methylation occurs on cytosines at position C5 and is predominately found in CpG dinucleotides [314,315]. DNA methylation plays an important role in gene expression. When it occurs within promoter or enhancer regions, it is typically associated with the silencing of gene expression; however, current evidence suggests that the opposite may be true when it occurs within the gene body, that methylation within the gene body is positively correlated to transcription [316–319]. As such, DNA methylation is

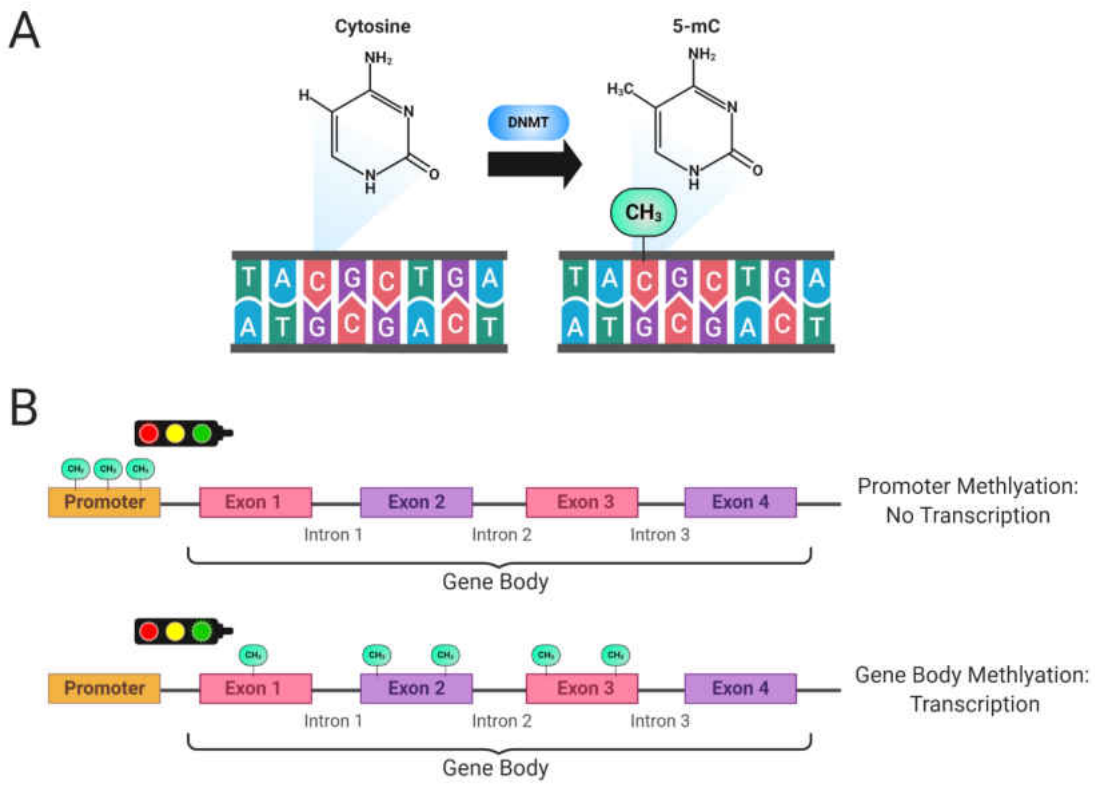

Figure III - 1. DNA methylation and its effects on gene transcription. **(A)** Schematic of DNA methylation depicting the process whereby a methyl group is transferred to cytosine by a DNA methyl transferase (DNMT1, DNMT3A, DNMT3B). **(B)** The effects of DNA methylation on gene expression is an on-going project. Methylation within the promoter region leads to a silencing of that gene. While methylation within the gene body seems to promote gene transcription.

fundamental to several important processes including normal development, genomic imprinting, X chromosome inactivation, and cell differentiation [315,320–324]. DNA methyltransferases (DNMTs) are enzymes that catalyze the transfer of a methyl group to cytosine. The main function of DNMT1 is methylation maintenance, and it has been shown to preferentially act upon hemimethylated CpGs, typically during DNA replication [325]. During DNA replication, DNMT1 copies the methylation pattern to the newly synthesized strand [326,327]. In contrast, DNMT3A and DNMT3B function in *de novo* methylation and act upon unmethylated DNA, though this function may also aid in the maintenance of methylation patterns that were not established by DNMT1 [322,328–330]. Following fertilization, parental genomes of the zygote undergo dramatic demethylation, and in fact, the paternal genome in mice undergoes significant active demethylation within 6-8 hours of fertilization, while maternal genome demethylation occurs after several cleavage divisions [323]. *De novo* methylation by DNMT3A and DNMT3B re-establishes the DNA methylation pattern following this demethylation stage and is in part responsible for cellular-specific differentiation [331,332].

Upon microbial invasion, host cells undergo large transcriptional changes that involve genes associated with immunity, inflammation, cellular protection/apoptosis, adhesion, and motility. It is therefore not surprising that such changes in gene expression are not only dependent on transcription factors but epigenetic alterations that provide transcriptional regulation through chromatin accessibility and DNA methylation. Bacterium-induced epigenetic

modifications have gained attention in recent years as mechanisms that underlie the host defense response [333]. DNA methylation alterations in response to a pathogen have been best documented in *H. pylori* infections. *H. pylori*, best known to cause gastric ulcers, as well as gastric cancer, has been shown to cause aberrant DNA methylation in human gastric mucosa. Notably, this occurred at the promoters of genes that were previously found to be methylated in gastric cancer cells, such as hypermethylation of tumor-suppressor genes (e.g. *USF1/2*) and DNA repair genes (e.g. *MLH1*) [334–338]. Furthermore, epigenetic regulation of the inflammatory response in infection and chronic inflammatory diseases has garnered greater attention in recent years [333,339]. These alterations to the epigenetic landscape may have lasting effects and lead to epigenetic memory or “imprinting” on the genome. Evidence of this epigenetic imprinting is found following the removal of *H. pylori* infection in human patients, in which a decrease but not a return to basal levels of methylation is seen in the promoter regions of genes associated with the risk of gastric cancer [340].

As epigenetic alterations are continuing to be researched in association with bacterial infections, we sought to investigate the role of *B. burgdorferi* as an epimutagen, which could be further investigated as a potential mechanism for the persistent symptoms seen in PTLDS patients. To this end, we utilized primary human astrocytes grown in culture, which were then subjected to *B. burgdorferi* infection. The methylome was then profiled through the Illumina beadchip array.

Materials and Methods

Bacteria culture

Three strains of *B. burgdorferi sensu stricto* were used throughout the experiments based on infectivity: B31-e2, a high-passage-number noninfectious clone of B31 tick isolate; B31-MI-16, an infectious clone of B31; and 297, an infectious and suspected neurotropic isolate from the CSF of a Lyme disease patient [19,20,85,217,341,342]. All strains were grown and utilized in an identical manner. Bacteria cultures were grown in modified Barbour-Stoenner-Kelly (BSK-II) medium supplemented with 6% rabbit serum at 34°C to approximately 1 x 10^7 bacteria/ml and used at passage 2 [343,344].

Cell culture

Primary human astrocytes were obtained from ScienCell Research Laboratories (catalog # 1800). Cultures were maintained in tissue-treated vented cap T-75 flasks (Corning, catalog #430641U) in astrocyte cell medium (ScienCell, Catalog #1801) that was supplemented with 1% astrocyte growth supplement (ScienCell, Catalog #1852), 2% fetal bovine serum (ScienCell, Catalog #0010), and antibiotics penicillin and streptomycin at a final concentration of 100 units/ml and 100 ug/ml, respectively (ScienCell, catalog #0503). Cells were incubated at 37°C and used at passage 3 at approximately 80% confluency for *B. burgdorferi* infection. Prior to the addition of *B. burgdorferi*, cell cultures were washed 3 times with sterile Dulbecco's phosphate buffered saline (DPBS) and new antibiotic-free astrocyte medium was added to the

cultures. Light microscopy was used to monitor cell morphology and confluency before and after infections.

Infection

Cell cultures were stimulated with either *B. burgdorferi* B31-e2, B31-MI-16, or 297 at a multiplicity of infection (MOI) of 10:1 (bacteria:cells) for 24, 48, 72, and 92 hours. Global methylation arrays were performed on astrocytes infected with B31-e2 and B31-MI-16. To achieve an appropriate MOI, the mean cell count of astrocytes was determined using an automated cell counter (Life Countess II, catalog #AMQAX1000). The control group was prepared identically without *B. burgdorferi* infection.

DNA Isolation and Differential Methylation

For both the global DNA methylation assays and the Illumina Infinium MethylationEPIC beadchip array, DNA was isolated from samples using DNeasy Blood and Tissue kit from Qiagen (Qiagen, catalog #69506) according to the manufacturer's instructions. Briefly, culture supernatant was removed to be used for protein analysis, and cultures were washed 3 times with DPBS. Following washes, cells were collected using Trypsin (ThermoFisher, catalog #15050065), centrifuged for 5 min at 300 x g at 4°C, and supernatant was aspirated from the cell pellet. The pellet was then resuspended in PBS, and proteinase K and RNase A were added. Cells were then fully lysed, and the resulting mixture was added to the DNeasy spin columns. Following subsequent washes, RNA-free genomic DNA was eluted in 100 ul of nuclease-free water. Initial DNA concentration and quality was assessed by NanoDrop.

Samples were submitted to the University of Minnesota Genomics Center for differential methylation analysis using the Illumina Infinium MethylationEPIC BeadChip array. The array queries 850,000 individual CpG sites in the human genome. Prior to this, samples underwent further QC which included PicoGreen DNA quantification and QC1 assay, a q-PCR based assay to assess impurities. All samples passed quality control. Samples were then subjected to DNA bisulfite conversion, in which unmethylated cytosines are converted to uracil and methylated cytosines remain. Through this method, single-nucleotide resolution of CpG methylation can be obtained via the Illumina Infinium MethylationEPIC BeadChip. Data analysis was performed by the University of North Dakota Genomics Core at the School of Medicine and Health Sciences.

Global Methylation was assessed using the MethylFlash Global DNA Methylation (5-mC) ELISA Easy Kit (Colorimetric) (EpiGentek, Catalog #P-030-48), according to manufacturer's instructions. In short, this assay provided a one-step ELISA-like reaction in which the DNA is bound to a 96 well-plate, capture and detection antibodies for methylated DNA were added, and the resulting signal was quantified colorimetrically using a BioTek Epoch plate reader. Infected groups at each time point were compared to uninfected control groups by a Student's t-test. Significance was determined if $p < 0.05$.

Protein Analysis of Supernatant by ELISA

Supernatants from cultures were removed as previously mentioned following treatment. ELISAs were performed following manufacturer's instructions (R&D Systems, DuoSet ELISA). In short, 96 well plates were coated with capture

antibody and incubated overnight at room temperature. The antibody was then aspirated, and wells were washed, followed by the addition of 100 ul of standard or sample to each well. Following incubation at room temperature for 2 hours and subsequent aspiration of samples, a conjugated detection antibody was added. The addition of a chromogenic substrate and stop solution allowed for colorimetric detection on a BioTek Epoch plate reader.

Results

Global Methylation

Our initial investigation into differential methylation caused by *B. burdorferi* involved assessing changes in global DNA methylation by using the Epigentek global methylation assays. Primary human astrocytes were cultured and infected with either B31-e2 or B31-MI-16 for 24, 48, 72, and 96 hours (n=3 for each group). As B31-e2 is a non-infectious strain, it was used to determine changes in global methylation that were associated with infectivity when compared to B31-MI-16. No significant changes in global methylation were found at any time points for astrocytes infected with B31-e2 when compared to control groups and no morphological changes were observed under light microscopy (Figure III-2A). For infection with B31-MI-16, no significant changes in global methylation were found in 24, 48, and 72-hour time points and no morphological changes were apparent. However, a significant increase in global methylation was observed at 96 hours, resulting in approximately a 0.6% increase in methylation (Figure 3-2B). An overall increasing trend in global methylation can be seen in astrocytes infected

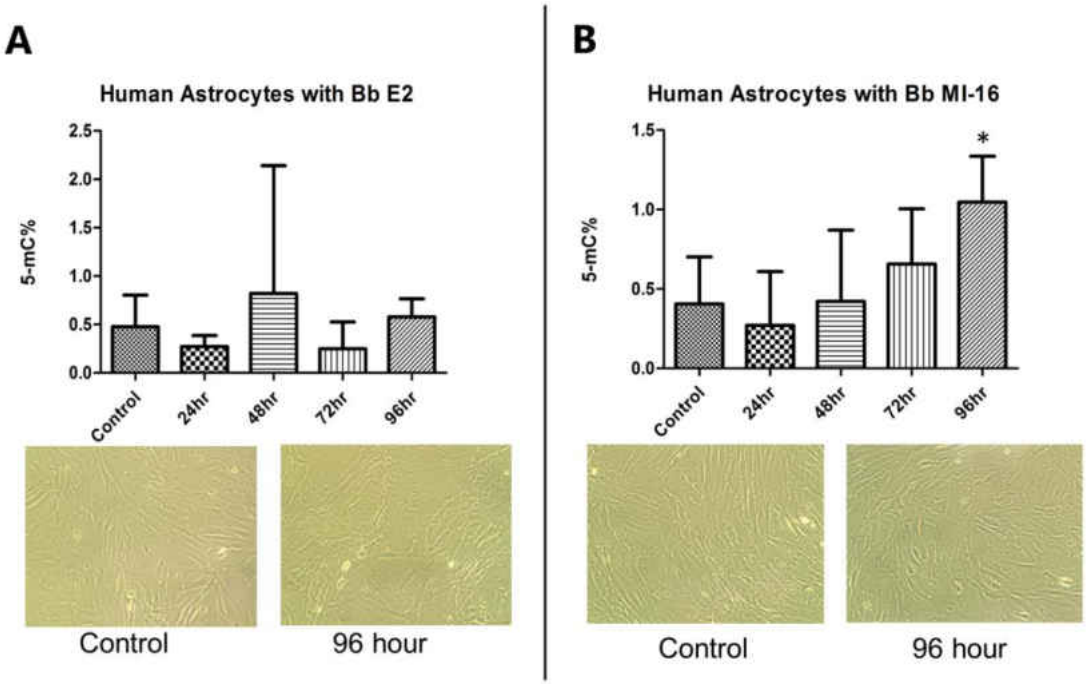

Figure III - 2. Changes in global DNA methylation in astrocytes in response to infection.
Astrocytes were infected with either *B. burgdorferi* strain B31-e2 or B31-MI-16 for 24, 48, 72, and 96 hours. **(A)** Infection with e2 showed no significant changes in global DNA methylation in astrocytes. **(B)** Infection with MI-16 showed a general increase in global DNA methylation, and a significant increase at 96 hours compared to control. No morphological changes in astrocytes were observed in either infection, based on light microscopy. Statistical testing was done by Student's t-test, and significance was set at $p < 0.05$.

with B31-MI-16, however, this trend is not observed in cells infected with B31-e2, as changes in methylation seemed more sporadic.

The data obtained from these sets of experiments were limited by the high variance between biological replicates, as observed in the plotted error bars of the standard deviation. This variability was exacerbated by the low replicate number and could be ameliorated by an increase in replicates. At this point in the experimentation, we evaluated the cost-benefit of these set of experiments in regard to the relevance and importance in further investigating global methylation. Though we were able to detect a significant change in global methylation in the 96-hour time point of B31-MI-16 infected group, and no change in the B31-e2 groups, this data provided little insight. As these assays assessed the global methylation status within astrocytes, it provided no specificity in the regions or genes that were altered. Furthermore, and of greater importance, changes in global methylation or lack thereof, cannot be determined as biologically relevant. In other words, the lack of global methylation changes that were seen in all but one group does not negate the possibility that region specific methylation changes are occurring, e.g. if one gene becomes hypermethylated, while another gene becomes hypomethylated, this may be correlated to a drastic transcriptional change, but global methylation is not altered overall. Due to this, we felt pursuing genome-wide CpG specific analysis would provide a greater outcome.

Microarray Methylation Profiling

Similar to our global methylation experiments, we assessed the alterations to specific CpG's in astrocytes infected with either B31-e2, B31-MI-16, and 297 for 24, 48, 72, and 96 hours. A total of 9 biological replicates were used for each group except for 297 which contained 3 replicates as it was a late addition to the experiments. These biological replicates came from 3 separate primary samples (e.g. samples taken from 3 different individuals), except for 297 which came from a single primary sample. Following these infection time points, the supernatant was collected for protein analysis and DNA was isolated from cells. To determine if astrocytes responded to infection as expected, protein analysis of the supernatant was first assessed by ELISA for the following factors: Serpin G1, IL-6, CCL20, CXCL1, and CXCL8 (Figure III-3). These proteins were chosen for their function in immunity and their differential regulation that was observed in the previous study performed in our laboratory regarding astrocytes [198]. SerpinG1, also known as C1-inhibitor, functions to inhibit the complement system – no significant changes were seen across time points and strains when compared to control. Similarly, IL-6, an interleukin that can act as both pro- or anti-inflammatory, and CCL20, a chemotactic for peripheral immune cells, were not seen to be significantly altered. CXCL1 and CXCL8, neutrophil activator and attractant, respectively, were found to be significantly upregulated in a number of groups. Astrocytes infected with either MI-16 and 297 saw a significant increase in these factors at later time points, 72 and 96 hours, while 297 also elicited a significant response at 48 hours. Infection with e2 seemed to stay at basal levels

Figure III - 3. Analysis of cytokine production by astrocytes infected with *B. burgdorferi.*
The supernatant from cell cultures was collected following infection with either *B. burgdorferi* strain B31-e2, B31-MI-16, or 297 for 24, 48, 72, and 96 hours, and were analyzed by ELISA. Serpin G1, IL-6, CCL20, CXCL1, and CXCL8 were analyzed and were chosen for their role in the immune response. Strain specific and time effects were as expected. In general, e2 remained at similar levels as control. MI-16 and 297 produced similar effects at slightly different magnitudes. Serpin G1, IL-6, and CCL20 showed no significant changes. Infection with MI-6 and 297 produced a significant increase in CXCL1 and CXCL8 at 72 and 96 hours, while 297 also induced an increase in CXCL8 at 48 hours.

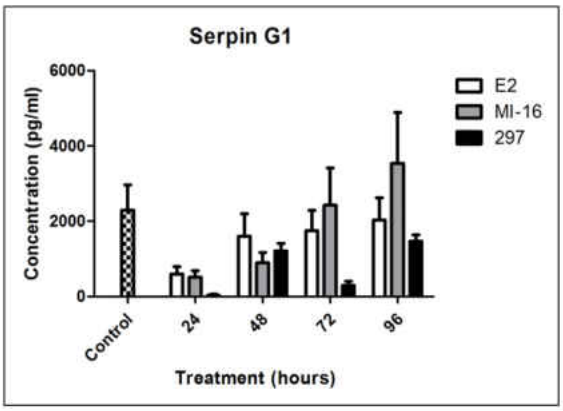
Serpin G1
Concentration (pg/ml)
6000
4000
2000
0
E2
MI-16
297
Control
24
48
72
96
Treatment (hours)

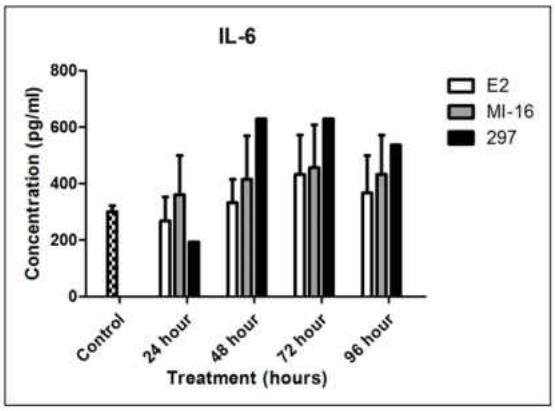
IL-6
Concentration (pg/ml)
800
600
400
200
0
E2
MI-16
297
Control
24 hour
48 hour
72 hour
96 hour
Treatment (hours)

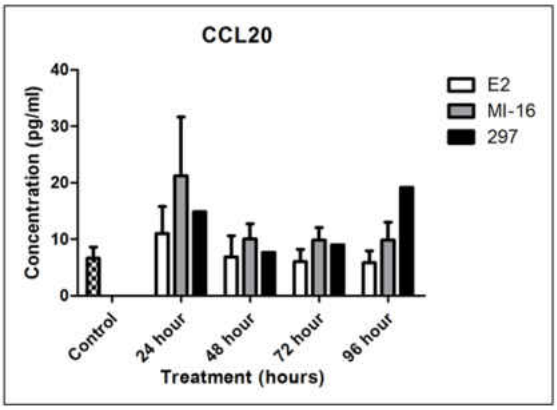
CCL20
Concentration (pg/ml)
40
30
20
10
0
E2
MI-16
297
Control
24 hour
48 hour
72 hour
96 hour
Treatment (hours)

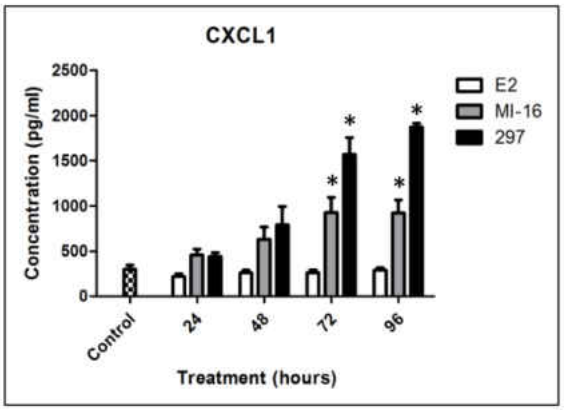
CXCL1
Concentration (pg/ml)
2500
2000
1500
1000
500
0
E2
MI-16
297
*
*
*
Control
24
48
72
96
Treatment (hours)

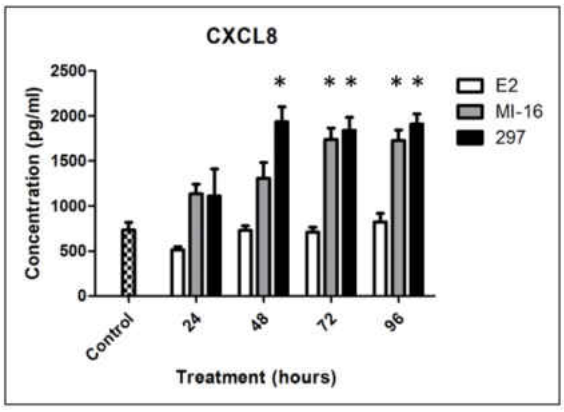
CXCL8
Concentration (pg/ml)
2500
2000
1500
1000
500
0
E2
MI-16
297
*
* *
* *
Control
24
48
72
96
Treatment (hours)

relative to the control. Interestingly, 297, a potentially more neurotropic strain, showed a generally larger response than MI-16. These data, specifically regarding CXCL1/8 indicated that our infections led to an expected immune response from astrocyte cultures.

Following these experiments, DNA samples were pooled according to strain and time point, but primary samples remained separate, to be sent for methylation profiling – this was necessary to reduce cost but still maintain an appropriate replicate number. Table III-1 indicates the samples that were submitted. Data analysis was performed by the University of North Dakota Genomics Core – differential methylation was considered significant with an FDR < 0.05. Surprisingly, there were no significant differentially methylated regions across any time points or strains compared to control which immediately raised concerns. DNA samples were isolated from the same samples that the supernatant was collected from, which showed a general response to infection with *B. burgdorferi*, as well as being strain specific. Additionally, all DNA samples passed QC within our laboratory, QC within the UND genomics core, and QC within the University of Minnesota Genomics Center. Figure III-4A depicts selected histograms of the adjusted p-values of infected groups compared to control. All reads were greater than the significance threshold of FDR < 0.05. A multidimensional scaling plot (MDS plot) is a method to visualize the similarity of all samples with each other. Through this we can visualize how each treatment clusters together e.g. do samples infected with 297 cluster more closely to samples infected with MI-16 than with e2 infected groups? When an MDS plot

Table III - 1. Sample submission

Sample ID	Primary Biological Replicate	*B. burgdorferi* Strain	Time Point
17-060-001	1	e2	24 hr
17-060-002	1	e2	48 hr
17-060-003	1	e2	72 hr
17-060-004	1	e2	96 hr
17-060-005	1	MI-16	24 hr
17-060-006	1	MI-16	48 hr
17-060-007	1	MI-16	72 hr
17-060-008	1	MI-16	96 hr
17-060-009	1	Control	Control
17-060-010	2	e2	24 hr
17-060-011	2	e2	48 hr
17-060-012	2	e2	72 hr
17-060-013	2	e2	96 hr
17-060-014	2	MI-16	24 hr
17-060-015	2	MI-16	48 hr
17-060-016	2	MI-16	72 hr
17-060-017	2	MI-16	96 hr
17-060-018	2	297	24 hr
17-060-019	2	297	48 hr
17-060-020	2	297	72 hr
17-060-021	2	297	96 hr
17-060-022	2	Control	Control
17-060-023	3	e2	24 hr
17-060-024	3	e2	48 hr
17-060-025	3	e2	72 hr
17-060-026	3	e2	96 hr
17-060-027	3	MI-16	24 hr
17-060-028	3	MI-16	48 hr
17-060-029	3	MI-16	72 hr
17-060-030	3	MI-16	96 hr
17-060-031	3	Control	Control

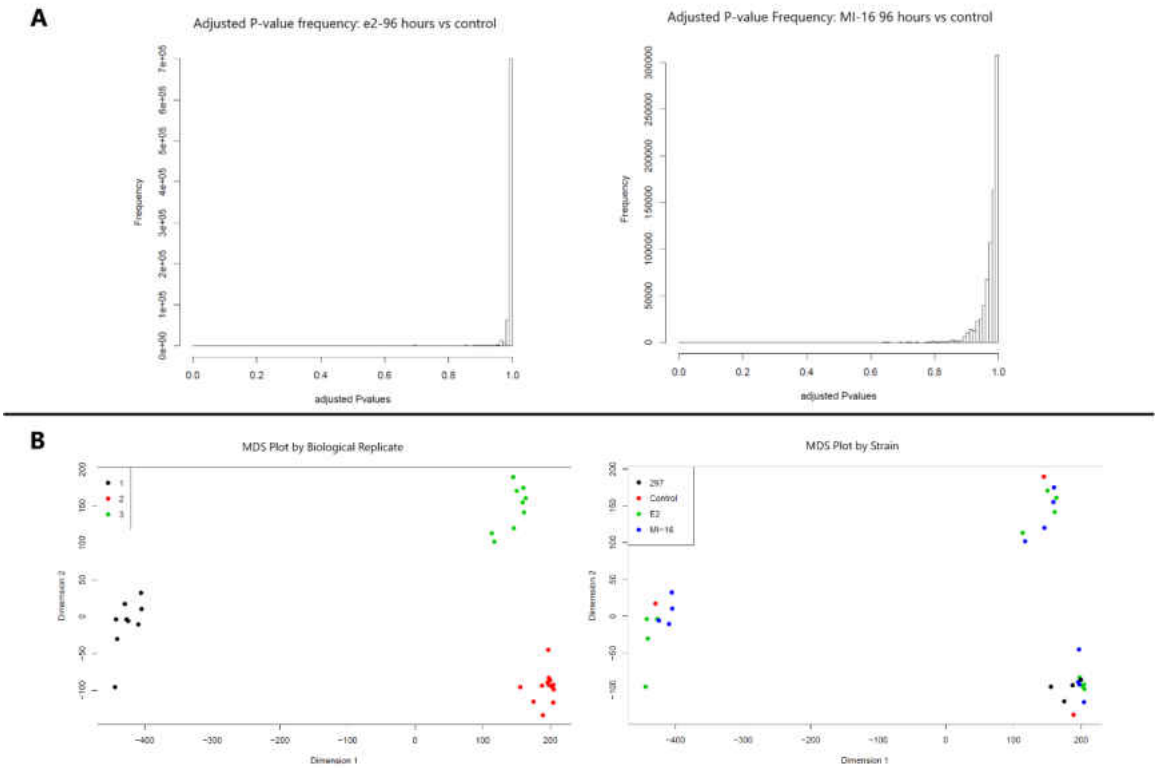

Figure III - 4. A representative overview of DNA methylation profiling results. Following infection, astrocyte DNA was isolated and DNA methylation profile of each sample was analyzed by Illumina MethylationEPIC array. **(A)** Histograms indicating adjusted p-value frequency at e2 96 hours and MI-16 96 hours, representative of all other groups. No significant changes in DNA methylation were observed in any strain or time group. Maximum frequency of p-values neared a p-value of 1.0.
(B) Multidimension scaling plot (MDS) by biological replicate and *B. burgdorferi* strain. As no significant results were found, an explanation was sought. The MDS plot by biological replicate explains a major reason for this – large variability between replicates exist due to biological replicates being obtained from three different primary samples. The MDS plot by strain indicates that greater similarity exists between strain and time point than between biological replicates.

was generated for our samples, we expected similarities to occur based on infectivity of the strain and/or time points. However, as seen in Figure 3-4B, all samples densely clustered according to their biological replicate. This was a clear indication that the variability between primary samples was far greater than anticipated and was to such an extent that the effects of *B. burgdorferi* strain and duration of infection had no significant impact on DNA methylation when compared to controls. Additionally, biological replicate 1 was male, while replicates 2 and 3 were female and seemed to cluster slightly closer together.

In order to control for the variability between biological replicates, biological replicate 1 was removed and a number of comparisons were made. A summary of these comparisons and results are seen in Table III-2. Removal of the first biological replicate provided minimal number of differential methylation CpGs. Many of the differentially methylated regions were not associated with any gene, let alone within the gene itself. A gene that commonly came up across multiple comparisons that was associated with was C4orf22, also known as cilia- and flagella-associated protein 299 (CFAP299), which has no well-known function but is predicted to play a role in spermatogenesis [345].

Pooling MI-16 and e2 groups together provided the most robust change in methylation that was seen at 24 hours. It is uncertain the biological relevance of this change, as the pooling of the non-infectious strain B31-e2, which previously did not induce a response in astrocytes at the protein and methylation level, would not be expected to have any significance. Nevertheless, a total of 91 differentially methylated CpGs were observed, with 78 being methylated and

Table III - 2. Summary of differential methylation comparisons

Sample Comparison		Total Differential Methylation	Methylated	Unmethylated
E2.24	Control	0	0	0
E2.48	Control	1	1	0
E2.72	Control	0	0	0
E2.96	Control	0	0	0
MI16.24	Control	3	3	0
MI16.48	Control	5	5	0
MI16.72	Control	0	0	0
MI16.96	Control	0	0	0
MI16.24	E2.24	0	0	0
MI16.48	E2.48	0	0	0
MI16.72	E2.72	0	0	0
MI16.96	E2.96	1	0	1
MI-16 + e2 – 24 hour	Control	91	78	13
MI-16 + e2 – 48 hour	Control	2	1	1
MI-16 + e2 – 72 hour	Control	0	0	0
MI-16 + e2 – 96 hour	Control	1	0	1
297 + MI-16 – 24 hour	Control	1	1	0
297 + MI-16 – 48 hour	Control	3	2	1
297 + MI-16 – 72 hour	Control	0	0	0
297 + MI-16 – 96 hour	Control	0	0	0

13 unmethylated. Table III-3 displays genes of interest that contained a differentially methylated CpG. Neuronal growth regulator 1 (NEGR1) shown to be differentially methylated within the body of the gene – suggesting an upregulation to gene transcription. NEGR1 is associated with neurogenesis as well as behavior disorders, intellectual disability, and depression [346–348]. Another gene associated with an increased CpG methylation was Myosin-9 (MYH9), which encodes the heavy chain of non-muscle myosin of class II, isoform A protein (NM IIA). NM IIA is found in most cell types and participates in a number of functions that include cytokenisis/proliferation, cell migration and motility, maintenance of cell shape and polarization, and adhesion [349,350]. However, the methylation occurred within the 5' untranslated region (UTR) of the gene, which may lead to an increase in gene transcription but has also shown conflicting correlation to gene expression; it may also play a role in translation [351–353]. Additionally, STX8, SNX33, and DYM are genes that have functions in cytoskeletal restructuring, endocytosis, cellular vesicle trafficking, and secretory pathways [354–360]. All methylated regions predict an upregulation in gene expression.

Two main functions of astrocytes may be altered in response to infection within this same comparison group: neurotransmitter uptake, specifically glutamate, and the regulation of the immune response. An increase in methylation was found within three genes within the solute carrier family: SLC1A3, SLC20A2, and SLC22A23. SLC1A3 and SLC22A23 contained a methylated CpG within the body of the gene, associated with an increase in gene

Table III - 3. Selected methylation sites

Gene Symbol	CpG	logFC	Methylation Status	Location relative to gene	Predicted Transcription
NEGR1	cg00977511	2.449765355	Methylated	Body	Upregulated
NFKBIA	cg05876984	0.697056168	Methylated	Body	Upregulated
STX8	cg16912386	1.271511984	Methylated	Body	Upregulated
MYH9	cg17970221	2.214659635	Methylated	5' UTR	Uncertain
SLC1A3	cg16963869	2.165907577	Methylated	1st Exon	Upregulated
SLC20A2	cg23724878	1.025452981	Methylated	5' UTR	Uncertain
SLC22A23	cg15717840	0.736275325	Methylated	Body	Upregulated
STX8	cg16912386	1.271511984	Methylated	Body	Upregulated
SNX33	cg01227133	1.162017636	Methylated	3' UTR	Upregulated
DYM	cg23277314	1.209629049	Methylated	Body	Upregulated
PDE7A	cg00957886	-6.23578645	Unmethylated	Body	Downregulated

expression; transcription of SLC20A2 is less known as methylation occurred with the 5' UTR. The solute carrier family is a family of transmembrane proteins that function as transporters across cell membranes. Of interest is SLC1A3 as it encodes for the protein excitatory amino acid transporter 1 (EAAT1), which is also commonly called glutamate aspartate transporter 1 (GLAST-1). It is found throughout the CNS and is highly expressed in astrocytes [361–363]. GLAST-1 is a glutamate transporter that functions to maintain the extracellular glutamate concentrations, an important function that aids in regulating neuronal function as glutamate is a major neurotransmitter [362]. Through these functions, astrocytes are the key players in glutamate regulation and thus are able to modulate synapse function and protect from excitotoxicity of neurons that may occur if extracellular glutamate concentrations are too high [364–366]. Dysregulation in glutamate concentrations is associated with a number of deleterious outcomes. Glutamate-induced excitotoxicity can lead to a decrease in neuronal regeneration and dendritic branching, as well as behavioral alterations that follow [367–369]. This potential upregulation of SLC1A3 through the methylation of the gene body would suggest a neuroprotective effect following *B. burgdorferi* infection. This "protective effect" also extends to the methylation within the gene body of NF-κB inhibitor alpha (NFKBIA, also known as IκBα), which would have a predicted upregulation in gene expression. The protein functions as an inhibitor to the well-known transcription factor NF-κB, which itself is a major player in the pro-inflammatory signaling pathway [370]. However, the NF-κB pathway has been shown to play many different roles that are context dependent, and as there is a

major dichotomy in CNS inflammation as being beneficial or deleterious, it is difficult to label such an effect as being “protective”. Interestingly, another role of NF-κB appears to be the downregulation of GLAST1 expression, through the ERK/PI3K/NF-κB signaling pathway, induced by tumor necrosis factor-α (TNF-α) [364,371,372]. Therefore, NFKBIA may provide a pathway for the upregulation of GLAST1 (SLC1A3). Finally, phosphodiesterase 7A (PDE7A) has been associated with immunity and inflammation and may be required for T cell activation, though this requirement may be overstated [373–376]. Regardless, demethylation was found in the gene body of PDE7A, associated with downregulation of the gene. Unfortunately, no other comparisons that were made provided a substantial or relevant change in methylation.

Discussion

Minimal changes were noted across comparisons of *B. burgdorferi* strains and time points. However, through the removal of replicate 1 that showed the most dissimilarity compared to the other two replicates, additional insight was gained. Increasing statistical power through the pooling of MI-16 and e2 infected groups provided the most robust change when compared to control at 24 hours. Taking into consideration the effects of methylation on gene transcription, astrocytes seemed to respond to infection in several ways. Genes associated with cytoskeletal restructuring and cellular trafficking are predicted to be upregulated and may be associated with changes in morphology, secretion, and cell proliferation, suggesting that astrocytes may be undergoing astrogliosis. One of the major functions of astrocytes is the structural and trophic support of

neurons, specifically the modulation of the neurotransmitter glutamate. Three members of the solute carrier family were found to be affected. SLC1A3 encodes for a major glutamate transporter, GLAST1 and is responsible for maintaining a homeostatic environment of extracellular glutamate. This is important to prevent the excitotoxicity of neurons that have been associated with a number of neurological disorders. Additionally, there seem to be conflicting results regarding immunity and inflammation, with the predicted upregulation of NF-κBIA and PDE7A. The CNS is a tightly regulated system that requires strict control of the resident immune response in order to maintain functionality. This is compounded by the dual nature of inflammation – during infection, an inflammatory response aids in the destruction and clearing of a pathogen; however, as seen in Lyme disease, specifically PTLDS, prolonged inflammation plays a major role in the pathogenesis of these symptoms. Determination of gene expression is uncertain and furthermore, the phenotypic outcome is difficult to predict. However, taken together, a generous assumption would state that it does seem that infection with *B. burgdorferi* may cause alterations to DNA methylation that could lead to phenotypic characteristics associated with PTLDS, but due to many limitations of the data, these results must be understated.

As highlighted previously, the major issue in the generation of relevant data lies in the variability of our biological replicates which came from three different primary samples. In hindsight, this can be seen in the large error bars of our ELISA experiments. In order to overcome this, we have changed our methodology for future experiments utilizing primary samples, such that

biological replicates stem from the same primary sample i.e. obtained from a single individual. With that said, other methods of data analysis within our current data set could provide additional information. Two methods could be adopted. As each biological replicate clusters within itself, analysis of each replicate individually could be done. The obvious limitation to this would be that each data set would only have an N of 1, so the lack of statistical power would limit statistically significant results. However, data obtained through this method could provide understanding into the variability of symptoms of Lyme disease patients, and why some individuals have a poor prognosis while others seemingly recover without ill-effects.

The second method to reevaluate our data set can be applied to both circumstances. As seen in our dataset, methylation occurs at single CpGs, and no gene showed multiple CpG differential methylation. This is another factor that should be taken into consideration when discussing the biological significance of our results. While the methylation of gene regions can be associated strongly with either up or down gene expression (e.g. promoter methylation results in down-regulation), it is not clear what a change in methylation of a single CpG would result in. One method to ameliorate this would be to bin the genome into specific regions. For example, the methylation of the entire promoter region of a gene would be compared between treatment groups. This would potentially provide a larger number of statistically significant differentially methylated regions and provide the much-needed context in relation to gene transcription.

Though our experiments were not as fruitful as we had anticipated, the importance of research into the epigenetics of infections continues to grow. With the advent of newer sequencing technologies, the price of performing these experiments are being rapidly reduced. Thus it is hopeful that this topic can be reexamined in the context of Lyme disease, and as new therapeutics are being developed to target epigenetic markers, such work will become even more significant [377–380].

CHAPTER IV

INVESTIGATING THE CHROMATIN STRUCTURE OF HUMAN ASTROCYTES IN RESPONSE TO *BORRELIA BURGDORFERI* SENSU STRICTO STRAINS

Introduction

The human genome consists of approximately 6 billion base pairs, and the genome of a single cell would span roughly two meters. To cope with the physical size needed to fit within the nucleus, DNA is orderly packaged and condensed into chromatin, a complex of DNA and protein. This organization of the genome facilitates cell division and aids in regulating gene expression and DNA replication. At its core, the main protein component of chromatin are histones that condense DNA into a basic structural unit called nucleosomes. Nucleosomes consist of ~147 bp of DNA wrapped around a histone octamer core, which consists of two copies of each of the four histone proteins, H2A, H2B, H3, and H4 [381,382]. This tightly condensed chromatin, also called heterochromatin, is poorly conducive to gene transcription; however, chromatin is a highly dynamic structure that can be regulated to allow for more optimal accessibility to transcription factors and thus gene transcription. This lightly packed and more accessible structure, also called euchromatin, resembles beads on a string and allows for the binding of regulatory proteins and RNA polymerase to DNA.

A predominant mechanism that allows for the regulation of chromatin structure is the post-translation modification of histones. These modifications typically occur on the N-terminal tails of the histones. There is a wide range of modifications that can occur, including citrullination, phosphorylation, SUMOylation, and ubiquitination. However, some of the most well-studied modifications and those that are of interest to this study are methylation and acetylation [383,384]. Through these modifications, the interactions between histones and DNA can be altered, thus leading to chromatin restructuring and modulation of gene transcription [385]. Many modifications and their impact on chromatin structure have been investigated, making up a so-called “histone code” through the combinatorial effects of these modifications [386,387]. Some of these modifications and their subsequent impact of chromatin include – H3K4me1: Activation, H3K4ac: Activation, H3K9me1: Activation, H3K9me3: Repression, H3K27me3: Repression, and H3K27ac: Activation [387–391]. As this is such a significant and global system for regulation of gene transcription, it has spanned across all fields of research including infection. Many studies have shown that bacterial products such as LPS or host secreted factors such as IFN-γ can induce histone modifications and therefore chromatin restructuring. This is true for *Helicobacter pylori* and its secreted factor HP0175 which activates TLR4 and induces NF-κB, ERK, and p38 MAPK activation leading to subsequent histone acetylation and IL-6 production [392,393]. Similarly, *Listeria monocytogenes* has been shown to induce similar pathways leading to alterations in the phosphorylation of H3S10 and H4 acetylation [394,395]. Of

further relevance to the data presented in this chapter, many of these effects occur through the activation of TLRs and associated transcription factors within the AP-1 complex including JUN and ATF [333,392,396–398].

We sought to investigate the astrocytic response to *B. burgdorferi* and its impact on chromatin structure and histone modifications. As such, we hypothesize that infection with *B. burgdorferi* leads to chromatin remodeling that is conducive to a deleterious inflammatory response and dysregulation of normal astrocytic functions. Our experimental design utilized primary human astrocytes in culture and infected with *B. burgdorferi* for four time points: 24, 48, 72, and 96-hours. Through these time points, we aimed to determine temporal and therefore dynamic alterations in chromatin accessibility. By using the Assay for Transposase-Accessible Chromatin (ATAC) sequencing, we aimed to achieve a global profile of these changes. Furthermore, we had simultaneously performed identical experiments to provide material for further correlation to gene expression and histone modifications by RNA-seq and ChIP-PCR/Seq, respectively. Unfortunately, due to technical shortcomings, we had only achieved minimal coverage via ATAC-seq and therefore we did not continue further investigation. The data presented in this chapter covers our findings of our ATAC-seq, highlighting these dynamic changes in the chromatin accessibility and the potential impact of gene expression.

Materials and Methods

Bacteria Culture

Borrelia burgdorferi strain B31-MI-16 was used for infection. Cultures were grown in modified Barbour-Stoenner-Kelly (BSK-II) medium supplemented with 6% rabbit serum at 34°C to approximately 1 x 10^7 bacteria/ml and used at passage 2 [343,344].

Cell Culture

Primary human astrocytes were obtained from ScienCell Research Laboratories (catalog # 1800). Cultures were maintained in tissue-treated vented cap T-75 flasks (Corning, catalog #430641U) in astrocyte cell medium (ScienCell, Catalog #1801) that was supplemented with 1% astrocyte growth supplement (ScienCell, Catalog #1852), 2% fetal bovine serum (ScienCell, Catalog #0010), and antibiotics penicillin and streptomycin at a final concentration of 100 units/ml and 100 ug/ml, respectively (ScienCell, catalog #0503). Cells were incubated at 37°C and used at passage 3 at approximately 80% confluency for *B. burgdorferi* infection. Prior to the addition of *B. burgdorferi*, cell cultures were washed 3 times with sterile Dulbecco's phosphate buffered saline (DPBS) and new antibiotic-free astrocyte medium was added to the cultures. Light microscopy was used to monitor cell morphology and confluency before and after infections.

Infection

Cell cultures were infected with either *B. burgdorferi* B31-MI-16 at a multiplicity of infection (MOI) of 10:1 (bacteria:cells) for 24, 48, 72, and 92 hours.

To achieve an appropriate MOI, the mean cell count of astrocytes was determined using an automated cell counter (Life Countess II, catalog #AMQAX1000). Bacterial cultures were manually counted using a Petroff-Hausser Counting Chamber (Hausser Scientific, catalog #3900) and dark field microscopy. The control group was prepared identically without *B. burgdorferi* infection. N=3 for all groups.

ATAC-seq

ATAC-seq was performed as previously described [399]. Following infection, cultures were washed with DBPS and harvested by trypsinization. Cell viability and cell number were determined to be >95% by trypan blue staining and automated counting. A fundamental aspect of ATAC is the need for only a small number of cells – following viability and counting, 50,000 cells were isolated and centrifuged. Cells were centrifuged at 500g at 4°C for 5 minutes. The supernatant was aspirated and 25 ul of CSK lysis buffer (10 mM PIPES, pH 6.8; 100 mM NaCl; 300 mM sucrose; 3 mM $MgCl_2$; 0.1% Triton X-100) was added to the cell pellet for nuclei isolation and placed on ice for 5 minutes. The presence of isolated nuclei was checked using trypan blue and light microscopy. Prior to this, optimization of lysis buffer was determined – astrocytes were subjected to either Greenleaf lysis buffer (10 mM Tris-HCl, pH 7.4; 10 mM NaCl; 3 mM $MgCl_2$; 0.1% (v/v) Igepal CA-630) or CSK; using trypan blue and light microscopy, it was determined that CSK was a more efficient buffer for nuclear isolation, as a greater percentage of nuclei were observed. Following lysis, nuclei were pelleted

at 500g at 4°C for 10 minutes, supernatant was aspirated, and the resulting pellet was placed on ice.

For the transposition step of ATAC, the Nextera DNA library preparation kit was used (Illumina, catalog #FC-121-1030). 50 ul of the transposition mix (25 µl TD 2x reaction buffer, 2.5 µl TDE1 Tn5 Transposase, and 22.5 µl nuclease-free water) was added to the nuclei pellet and resuspended. The transposition reaction was incubated at 37°C for 30 minutes. The reaction was then purified using Qiagen MinElute PCR Purification Kit according to the manufacturer's instructions (Qiagen, catalog #28004) and DNA was eluted using Buffer EB (10 mM Tris-Cl, pH 8.5). Transposed DNA was then amplified by PCR. In short, primers from the Nextera Index Kit (Illumina, catalog #FC-121-1011) were selected to provide unique indexing of each sample during PCR amplification, and PCR master mix from NEB (NEB, catalog #M0541S) was used. Thermal cycle settings were followed according to Buenrostro et al [399]. The amplified library was purified again using the Qiagen MinElute PCR Purification Kit and eluted in Buffer EB (10 mM Tris-Cl, pH 8.5).

Quality control of samples was performed by the University of North Dakota Genomics Core. DNA libraries were placed in an Agilent 2100 Bioanalyzer with the Agilent High Sensitivity DNA Kit (Agilent, catalog #5067-4626) to assess DNA fragment size and quality. Concentrations of samples were determined by a BioTek Gen5 Wellplate reader with the Quant-iT Picogreen kit (ThermoFisher, catalog #P11496). Initial concentrations of most samples were below the recommended concentration of 3nM. The concentration was increased

by reducing the volume of samples using a speed-vac. Again, samples were subjected to the well plate reader, and sufficient concentrations were established. Samples were sent to Novogene and an Illumina HiSeq 4000 was used for 150 bp paired-end sequencing across two lanes.

Data Analysis

Data was received from Novogene in FASTQ format. Initial quality control of raw data was performed by FastQC. Adaptor and low-quality base trimming were performed by trimmomatic, followed again with a quality check by FastQC – all samples passed. Alignment to the human (hg19) assembly was performed by Hisat2, version 2.1.0 and indexed by Samtools, version 1.9. Insert size calculation was performed by Picard, specifically the collectinsertsize tool, version 2.20.2. As expected, sub-nucleosome insert size (<150bp) was most predominantly enriched, with minor enrichment at mono-nucleosome (150-200bp) and di-nucleosome (200-400bp) insert sizes. As mitochondrial DNA do not form histone complexes, mitochondrial reads are typically non-negligible in ATAC-seq experiments [400]. Mitochondrial reads were removed by removeChrom.py (J. M. Gaspar; https://github.com/jsh58/harvard/blob/master/removeChrom.py). PCR artifacts, such as duplicate reads, can arise during ATAC-seq. Duplicate reads were flagged by Picard – Markduplicates, and removed during peak calling. Peaks were called by MACS2, version 2.1.2 [401].

Differential peak analysis was performed by DiffBind on the output peak files obtained by MACS2 [402]. To determine differential peaks, the following comparisons were made: 24hr infected vs control, 48hr infected vs control, 72hr

infected vs control, and 96hr infected vs control. DiffBind produces a consensus peakset, which are peaks shared between a minimum number of samples. In this analysis, a peak that was found in at least two samples was considered to be within the consensus peakset. Diffbind utilizes DESeq2 to perform differential analysis between groups that are being compared. Although the number of reads differ between our samples, DESeq2 performs read count normalization to alleviate this issue. Furthermore, the Benjamini-Hochberg adjustment is a *post-hoc* statistical test that is applied to our initial p-values, which produces a false-discovery rate (FDR). This adjusted p-value, or FDR, was set at < 0.05 for statistical significance. Each comparison produced a differential peakset. Additional analysis was performed to find overlapping differential peaks between datasets as well as to identify unique differential peaks in each condition. Using these differential peak sets, the DiffBind contrast and overlapping functions allowed us to compare differential peaksets across each group; a Venn diagram was produced to summarize these findings. To annotate peaks and assess the distance and location of peaks to genomic features, the Homer function annotatePeaks was used [403]. This function summarizes the location of peaks to genomic features (e.g. intergenic, intron, exon, promoter) and identifies specific genes associated with these peaks. Visualization of genomic distribution of peaks was performed by ChIPSeeker [404]. Gene ontology analysis was performed by the Homer function annotatePeaks with the -go option selected.

Motif enrichment analysis was performed by the findMotifsGenome.pl script of Homer. This analysis scans all peaks within the given peakset for known

motif consensus sequences to identify peaks that overlap with transcription factor binding motifs. For motif scanning, region size was set at 200 bp, centered at the peak summit; that is ±100 bp from the summit of each peak was scanned for matching sequences to known motifs. The lengths of motifs to be found were set to 8 bp, 10 bp, and 12 bp. Additionally, the number of unique motifs was limited to the top 25 enriched. The output of this analysis simply provides the most enriched motifs and their associated transcription factor. To determine the location of these motifs, annotatePeaks was used again – the differential peakset for a given comparison was paired with its motif enrichment dataset to identify peaks that contained specific motifs.

Results

As a continuation of our investigation into the epigenetic modifications that occur during *B. burgdorferi* infection, we performed ATAC-seq to profile structural changes in chromatin at four infection time points and non-infection control: 24, 48, 72, and 96 hours. Several quality control assessments were performed on our read files and compared to ENCODE standards (https://www.encodeproject.org/atac-seq/#standards). Insert size was determined for each sample. ATAC-seq utilizes a Tn5 transposase, which cleaves DNA in open chromatin, and as such, the majority of insert sizes will be small fragments, specifically subnucleosomal <150bp. Approximately 147 bp of DNA wrap around histones, in which the transposase will cleave and index reads at either end of the histone – this corresponds to a slight enrichment at 150-200bp. An additional minor enrichment in insert size is typically seen at di-nucleosome lengths,

approximately 300-400bp. In all of our samples, this pattern can be seen. Figure IV-1 shows representative images of these quality control measures. Additional quality control metrics can be found in Appendix B. In order for gene transcription to initiate, typically the transcription start site (TSS) is in the open chromatin configuration. As such, it can be expected that Tn5 accessibility at TSS's is enriched at a genome-wide level. ENCODE standards require an enrichment score > 6; all samples passed except for one technical replicate within the 96-hour group (#014). Another enrichment criterion assesses the fraction of reads in peaks (FRiP) – a fraction >0.2 is considered passable. Again, all samples passed except for the same technical replicate, #014. Mitochondrial reads and duplicate reads are two concerns that can considerably impact library complexity and usable reads. ENCODE requires 25 million non-mitochondrial, non-duplicate reads. Following the removal of these reads, only 8 samples contained >25 million aligned reads. Nevertheless, while our samples did not meet all the requirements set by ENCODE, we continued with downstream analysis.

Peaks were called by MACS2, and differential peak analysis was performed by DiffBind. As stated in the methods, DiffBind forms a consensus peakset, which characterizes a consensus peak as being found in at least two samples. A total of 120,925 unique peaks were found across all samples, of which 82,910 peaks were found in at least 2 samples and placed within the consensus peakset for additional analysis. Differential peak analysis by DiffBind

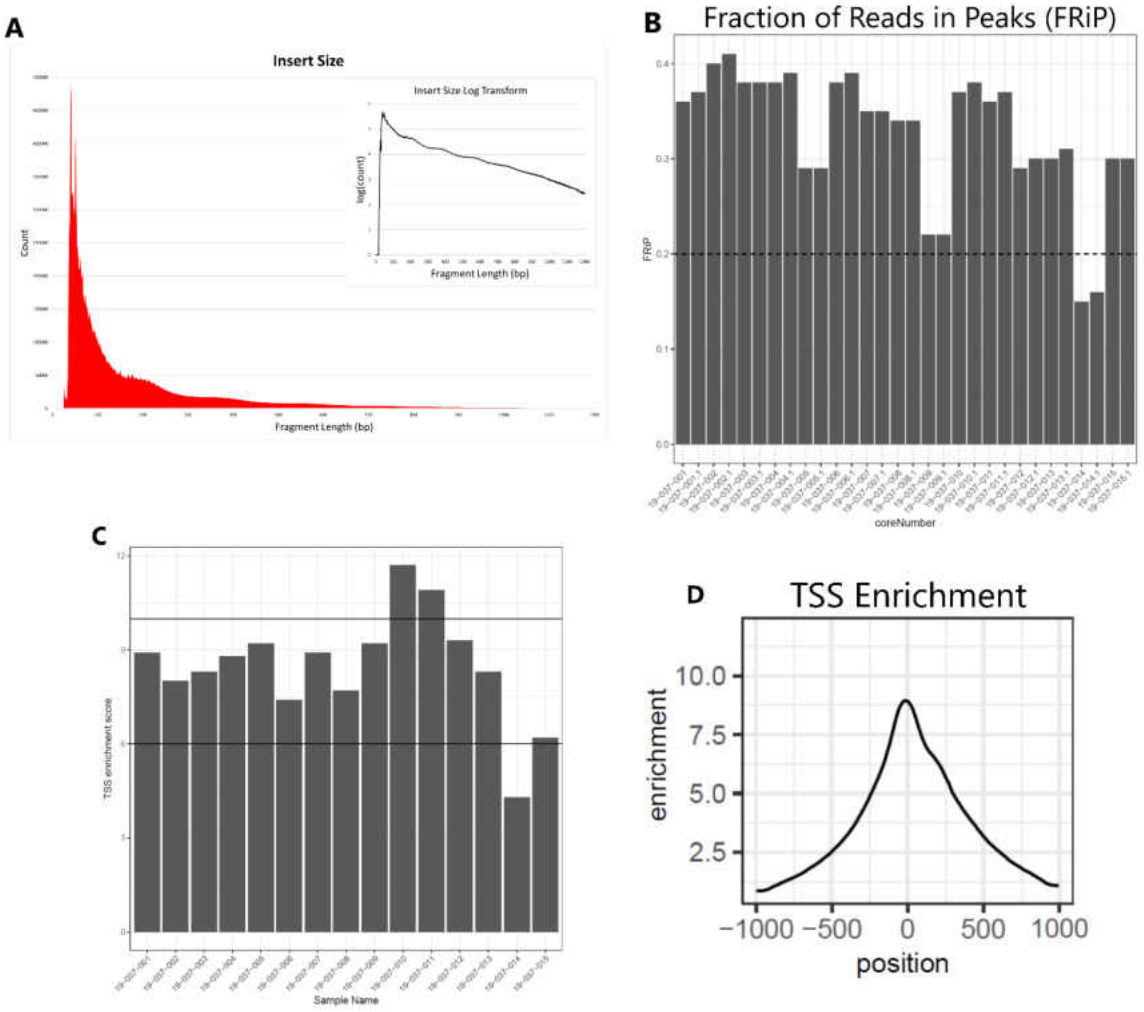

Figure IV - 1. Representative quality control metrics.
(A) The insert size of control sample #001 indicating a pattern associated with ATAC-seq. The Tn5 transposase cleaves open chromatin, producing fragments of subnucleosomal size (<150 bp). The transposases will also cleave DNA around mono-nucleosomes, producing fragments of around 150-200 bp. A second minor enrichment can be observed at the 300-400 bp range, indicated di-nucleosome fragments. The inset graph corresponds to log transformation of count numbers. (**B)** Bar graph of fraction of reads in peaks (FRiP). This is a quality control metric to determine if enrichment of reads occur within peaks. **(C)** A bar graph of transcription start site (TSS) enrichment for each sample. A minimum TSS enrichment score of 6 is required. **(D)** TSS enrichment peak graph of sample #001. Peak enrichment occurs directly above the TSS.

utilizes DESeq2 to determine significance, and an FDR < 0.05 was determined to be significant. Infected groups were compared to control and the number of differential peaks is as follows, while the number of open and closed peaks are in parentheses (Open : Closed): 24-hour – 25,464 (18,883 : 6,581); 48-hour – 7,266 (7,068 : 198); 72-hour – 3,376 (3,372 : 4); 96-hour – 3,015 (207 : 2,808). This downward trend in the number of differential peaks indicates that astrocytes are responding to *B. burgdorferi* infection much more rapidly than we had initially expected based on our previous gene expression data. Our previous data, highlighted in Chapter 3, indicates peak protein production occurring at 72 to 96 hours. However, chromatin accessibility is a requirement prior to gene expression, thus, finding a maximum peak enrichment for open chromatin at 24 hours would correspond to subsequent increase in gene expression at later time points. At each subsequent time point, the number of differential peaks continues to decrease; however, it is interesting to note that while at 24, 48, and 72 hours open chromatin predominates, while at 96 hours, the opposite is found. Additionally, overlapping analysis, displayed as a Venn diagram in Figure IV-2A, indicates peaks that are shared amongst each group and peaks that are unique to each time point. The following number of differential peaks are unique to each group: 24-Hour – 18535; 48-Hour – 1223; 72-Hour – 1355; 96-Hour – 2022. A total of 57 differential peaks were found in all groups.

The location of peaks (i.e. accessibility of chromatin) is important to determine the functional relevance of the changes that occur during infection. Generally, open chromatin is required near or within the promoter/TSS and exon

Figure IV - 2. Differential peak analysis.
(A) A Venn diagram of the number of differential peaks in each treatment group and those that overlap. The number of unique peaks of each group can be identified and the number of peaks shared amongst all groups is shown. **(B)** Differential peaks of each group were annotated, and their genomic features mapped and frequency plotted on a bar graph. 24-hour and 48-hour groups share similar patterns in genomic features – Intergenic and Intron regions were more highly enriched compared to promoter regions. The opposite is observed in 72 and 96-hour groups. **(C)** Gene Ontology analysis was performed on differential peaks; intergenic regions were removed for this analysis. The top 10 enriched biological processes for each group are shown. **(D)** 57 differential peaks were shared among all four time points. Genomic feature and biological process analysis was performed on these.

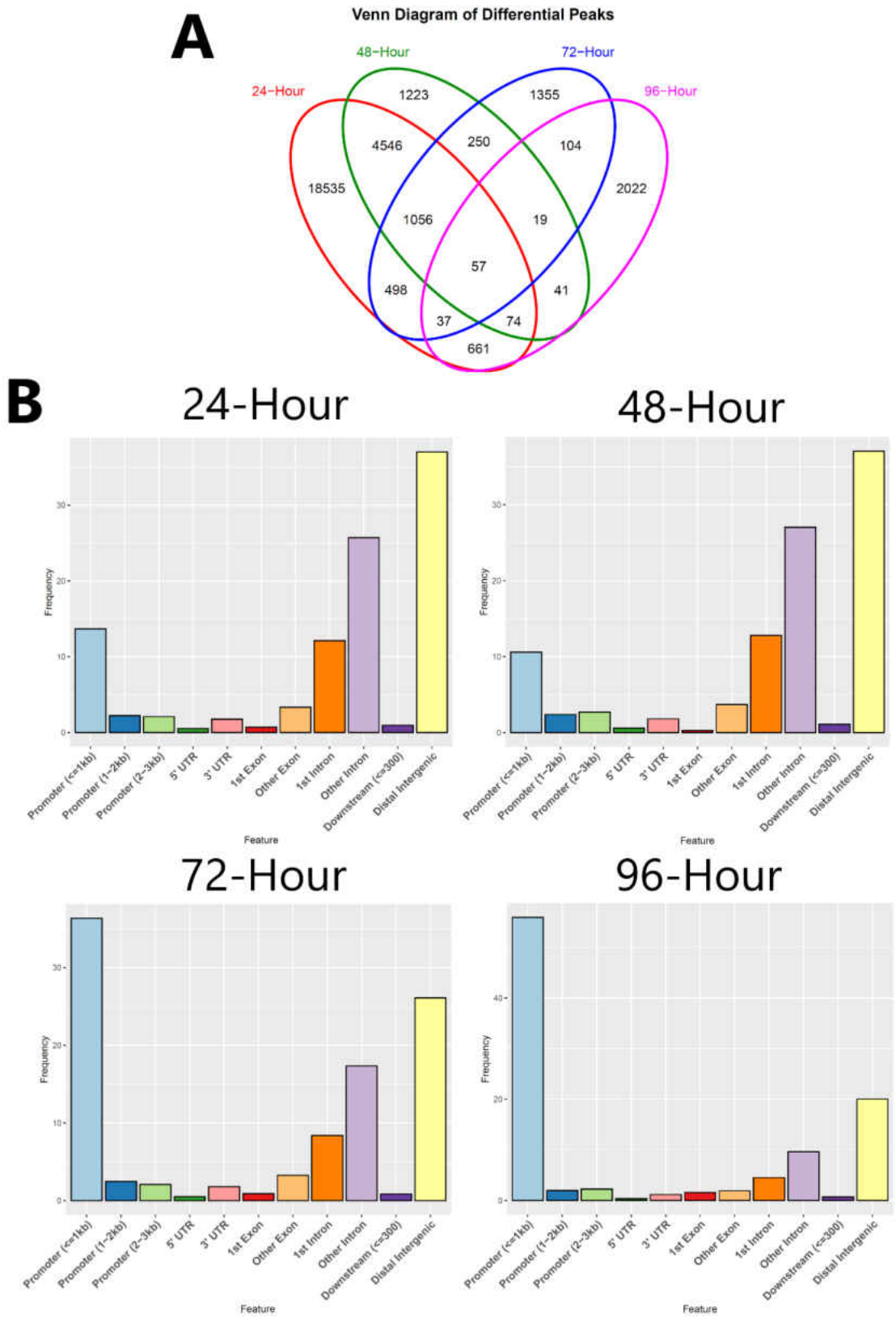
A
Venn Diagram of Differential Peaks
24-Hour
48-Hour
72-Hour
96-Hour
18535
4546
1223
1355
2022
104
250
1056
19
57
498
41
37
74
661
B
24-Hour
48-Hour
72-Hour
96-Hour
Frequency
Feature
Promoter (<=1kb)
Promoter (1~2kb)
Promoter (2~3kb)
5' UTR
3' UTR
1st Exon
Other Exon
1st Intron
Other Intron
Downstream (<=300)
Distal Intergenic

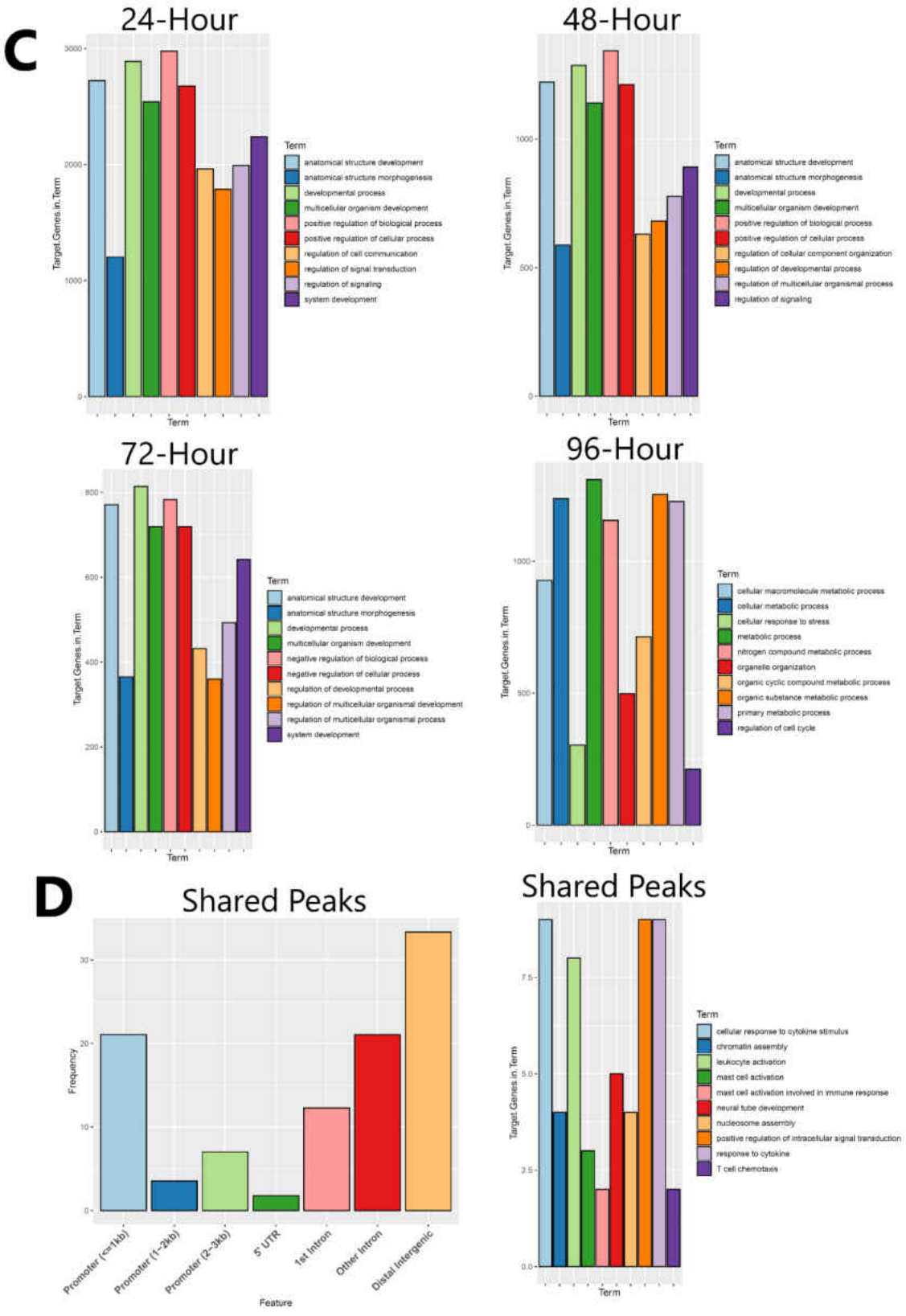
C
24-Hour
Target.Genes.in.Term
Term
anatomical structure development
anatomical structure morphogenesis
developmental process
multicellular organism development
positive regulation of biological process
positive regulation of cellular process
regulation of cell communication
regulation of signal transduction
regulation of signaling
system development
48-Hour
Target.Genes.in.Term
Term
anatomical structure development
anatomical structure morphogenesis
developmental process
multicellular organism development
positive regulation of biological process
positive regulation of cellular process
regulation of cellular component organization
regulation of developmental process
regulation of multicellular organismal process
regulation of signaling
72-Hour
Target.Genes.in.Term
Term
anatomical structure development
anatomical structure morphogenesis
developmental process
multicellular organism development
negative regulation of biological process
negative regulation of cellular process
regulation of developmental process
regulation of multicellular organismal development
regulation of multicellular organismal process
system development
96-Hour
Target.Genes.in.Term
Term
cellular macromolecule metabolic process
cellular metabolic process
cellular response to stress
metabolic process
nitrogen compound metabolic process
organelle organization
organic cyclic compound metabolic process
organic substance metabolic process
primary metabolic process
regulation of cell cycle
D
Shared Peaks
Frequency
Promoter (<=1kb)
Promoter (1~2kb)
Promoter (2~3kb)
5' UTR
1st Intron
Other Intron
Distal Intergenic
Feature
Shared Peaks
Target.Genes.in.Term
Term
cellular response to cytokine stimulus
chromatin assembly
leukocyte activation
mast cell activation
mast cell activation involved in immune response
neural tube development
nucleosome assembly
positive regulation of intracellular signal transduction
response to cytokine
T cell chemotaxis

locations for gene expression, while regulatory elements such as enhancers may be found in intergenic and intronic regions. Therefore, we sought to determine the frequency of peak enrichment within specific genomic features, highlighted in Figure 4-2B. The 24 and 48-hour groups shared similar patterns in genomic feature enrichment. The majority of peaks were found within intergenic and intron regions, with the promoter region showing less enrichment. However, at 72-hours, this trend changes, such that the greatest enrichment occurs in the promoter region, while lower enrichment was found at intergenic and intron locations. This continues and is in fact elevated in the 96-hour group, with the promoter regions containing nearly 50% of all peaks. It is important to also note that this increase in differential peaks at the promoter region corresponds to closing of accessibility, in which 2,808 out of 3,015 differential peaks were reduced following infection.

Gene ontology analysis performed by Homer provides insight into biological processes that are enriched. The top 10 enriched biological processes of differential peaks for each group and shared peaks are shown in Figure 4-2C. Multiple biological processes were shared between 24, 48, and 72-hour time points, including: Anatomical Structure development and morphogenesis, developmental process, and multicellular organism development. Signaling processes were found to be enriched within the 24-hour time point that were subsequently reduced at later time points. These include regulation of cell communication, regulation of signal transduction, and regulation of signaling. As many of the functions performed by astrocytes fall under the large umbrella of

these biological terms such as chemokine and cytokine production, this may suggest a restructuring of chromatin to promote this activated state. However, these processes change quite remarkably at the 96-hour time point; instead of structural and signaling processes, the astrocytes undergo chromatin rearrangement centered around metabolic and cellular stress. A more concise picture is found when analyzing peaks that are common amongst all groups. Biological processes based on these differential peaks indicate astrocytes undergoing immunological processes that include response to cytokines, immune cell activation (leukocytes and mast cells), and T cell chemotaxis. Furthermore, in line with the idea that astrocytes are undergoing subsequent chromatin restructuring following infection, chromatin and nucleosome assembly was found to be shared amongst these groups.

Several inflammatory and immune-related genes were found to contain differential peaks. Table IV-1 indicates genes of interest that were associated with differential peaks. It is important to note that in the table a negative fold change corresponds to an open conformation, while a positive fold change corresponds to a closed conformation. Many of these genes have previously been associated with *B. burgdorferi* infection that revolve around an inflammatory chemokine and cytokine response which function to attract and activate both innate and adaptive immune cells. In general, these peaks were found to be enriched towards the open configuration of chromatin and were predominately found within the earlier time points – 24 and 48-hours. Chemokine C-C motif ligands (CCLs) and Chemokine C-X-C motif ligands (CXCLs) are common

Table IV - 1. List of selected peaks and associated genes

Associated Gene	Peak Location	Gene Function (UniProt)	Log_2 Fold Change			
			24 Hr	48 Hr	72 Hr	96 Hr
GBP2	Promoter/TSS	Type I/II interferon signaling pathway – anti-pathogen activity (P32456)	0.63			
GBP1	Intron	Type I/II interferon signaling pathway – anti-pathogen activity (P32455)	0.46			
STAT1	Intron	Signal transducer – Mediates interferon response (P42224)	-1.48			0.81
STAT2	TSS	Signal transducer – Mediates interferon response (P52630)	0.32			
CXCL6	Exon	Chemotaxis – Neutrophils, leukocytes (P80162)	-0.89	-0.96		
CXCL13	Intron	Chemotaxis – B-lymphocytes (O43927)	-1.02	-1.2		0.65
CXCL17	Intron	Chemotaxis – Monocytes, macrophages, dendritic cells (Q6UXB2)	-1.24			
CCL2	Promoter/TSS	Chemotaxis – Monocytes, basophils (P13500)	-0.49			
CCL26	Intron	Chemotaxis – Eosinophils, basophils (Q9Y258)	-1.32			
IL6	Promoter/TSS	Cytokine - Acute inflammation, B-cell differentiation, Th-17 generation (P05231)	0.42			
TNFSF9	Exon	Cytokine – TNF superfamily, T-cell proliferation (P41273)	0.36		-0.69	0.72
TNFSF10	Intron	Cytokine – TNF superfamily, apoptosis (P50591)	-0.74	-0.79	-0.81	
TNFSF18	Promoter/TSS	Cytokine – T-cell regulation and activation, activations STAT1 phosphorylation (Q9UNG2)	1.28			
TLR5	Intron	Toll-like receptor – Innate immunity, inflammatory response (O60602)	-0.82	-0.63	-0.82	
TLR6	Promoter/TSS	Toll-like receptor – Innate immunity, inflammatory response (Q9Y2C9)		-0.62		
TLR9	TSS	Toll-like receptor – Innate and adaptive immunity (Q9NR96)	-0.53			
IRF1	Promoter/TSS	Type I/II interferon signaling pathway – Key transcriptional regulator (P10914)			-0.5	
	Intron		-0.99	-0.54		
IRF2	Intron	Type I/II interferon signaling pathway – Key transcriptional regulator (P14316)	-1.68	-0.93		
IFITM1	Promoter/TSS	Type I/II interferon signaling pathway – Inhibits entry of virus (P13164)		-1.36		
IFITM10	Intron	Interferon-induced protein (A6NMD0)	-0.55			-0.65
MMP2	Promoter/TSS	Matrix metalloproteinase – degrades extracellular matrix (P08253)			-0.51	
	Intron		-1.42	-0.83		
PLAU	TSS	Urokinase – plasminogen activator (P00749)	-1.38			
PLAT	Intron	Tissue plasminogen activation (P00750)	-0.63	-0.83	-0.49	
SERPINE1	Intron	Serine protease inhibitor – inhibits PLAU and PLAT (P05121)	-1.17			
	Promoter			-0.38	-0.52	
PLAUR	Intron	PLAU receptor (Q03405)				0.66
PIK3CD	Intron	Mediates immune cell proliferation, promotes cytokine production (O00329)	-0.85	-0.88	-0.58	1.07
GPR183	Intron	G-protein coupled receptor – chemotactic for B-cells, T-cells, macrophages, astrocytes (P32249)	-0.35	-0.49	-0.62	0.79
	Promoter/TSS		-0.65	-0.58	-0.57	0.71

signaling proteins that are released by a wide range of cells. These proteins act as chemotactic and inflammatory cytokines that aid in the attraction of peripheral immune cells such as monocytes, T-lymphocytes, and neutrophils. A peak at CCL2 was found to be enriched within the promoter-TSS region only at the 24-hour time point, which may indicate an increase in gene expression. CCL2 acts as a recruitment factor for monocytes and basophils. Similarly, CCL26, an inflammatory and eosinophil chemotactic factor, contained an enriched peak only at the 24-hour time point. Additional immune genes that were unique to the 24-hour group include TLR9, a toll-like receptor that recognizes pathogen-associated molecular patterns (PAMPs), and CXCL17, a chemoattractant for dendritic cells and monocytes. TLR5 (24, 48, and 72-hour) and TLR6 (48-hour) were found to be enriched as well throughout multiple time points. CXCL6, a neutrophilic chemoattractant was also found to be enriched at 24 and 48-hours, and gene expression has previously been shown to be elevated in astrocytes [198]. CXCL13, a B lymphocyte chemoattractant that was enriched at both of these time points, has shown to be an important factor specifically for neuroborreliosis, as it has been implicated as a possible biomarker for the neurological condition of Lyme disease [78,79]. In contrast, a reduction at this CXCL13 region was observed at 96-hours. STAT1 and STAT2 are signal transducer proteins that act as transcription factors. Both have been observed to be increased in *B. burgdorferi* infection studies and play important roles in the induction of the interferon response [234,236,237]. However, both were only observed at 24-hours and were enriched in opposite directions – STAT1 had

enrichment within an intron, STAT2 showed a reduction within the TSS. STAT1 has previously been shown to be important in mediating the inflammatory response for Lyme carditis, however, it is uncertain the possible impact the reduction of STAT2 may have within our system [405]. Though it is common for STAT1 and STAT2 to form a heterodimer, STAT1 has shown to interact with a wide range of other transcription factors including IRF1, which was shown to be enriched as well [406,407].

Under the assumption that peak enrichment within the gene corresponds to gene expression, it appears that at earlier time points, astrocytes elicit an initial inflammatory response that is later lost. This may indicate a failure in a positive paracrine feedback loop that may be dependent on the presence of additional cells and anatomical context as many of these factors function as attractants for other immune cells. This is evident in co-culture studies of glial cells and neurons in which the addition of astrocytes and microglia during *B. burgdorferi* infection led to an increase in neuronal apoptosis compared to *B. burgdorferi* infection only. In the rhesus macaque model, glial cells have been implicated in the onset and progression of neuroborreliosis due to the secretion of similar chemokine profiles including CCL2 and CXCL13 [151,283]. It is often observed that in comparison to more professional immune cells such as microglia, astrocytes do not produce a large immune and inflammatory response in regards to range and scale [141,408,409]. However, this seems to underscore the wide repertoire of supportive functions that astrocytes perform in a context dependent manner and may shed insight into the loss of inflammatory and immunological genes at later

time points. G protein-coupled receptor 183 (GPR183) was found to be enriched at both introns and promoter regions at all time points except 96-hours, in which the fold-change reversed. The function of GPRs in the context of Lyme disease is not fully understood, but they have been previously shown to be induced during infection, including GPR183, and may be associated with subsequent inflammation [168,410,411].

B. burgdorferi has long been shown to induce the production of matrix degradative proteins, specifically matrix metalloproteinases (MMP2). The induction of these proteinases leads to the degradation of the extracellular matrix such as collagen and fibronectin. These have been shown to play an important role in the manifestation of many of the inflammatory symptoms of Lyme disease, including arthritis and neuroborreliosis [161,412–416]. These factors aid in the dissemination of *B. burgdorferi* through the breakdown of barriers and lead to the exacerbation of immune cell invasion. A number of these factors were found to be enriched, including MMP2 and MMP16 at a number of time points. Importantly, the two main activators of many of these degradative proteins, PLAU (urokinase, uPa) and PLAT (tissue plasminogen activator, tPA), were found to be enriched from 24 to 72 hours. However, in contrast, the principal inhibitor of both activators, SERPINE1 (plasminogen activator inhibitor-1, PAI-1), was also found to be enriched at these time points. Furthermore, the receptor for uPA, urokinase receptor (PLAUR) was found to be reduced at 96-hours. This provides further evidence of *B. burgdorferi* induction of host extracellular matrix modulators and provides insight into the chromatin restructuring that promotes this outcome.

Motif and Transcription Factor Enrichment

One invaluable aspect of ATAC-seq is the ability to identify specific transcription factor motif enrichment based on the opening of chromatin. The Homer package and findgenomemotif function provides detailed enrichment information of these motifs, their locations, and subsequent annotations of their respective peaks. As transcription factors can bind and promote the expression of many genes of a more specific function (e.g. immune regulatory genes), we can formulate an idea of the mechanisms and expression patterns associated with our infection groups. Though our previous discussion on differential peaks were focused on enrichment of genes within the gene body, broadening the scope of motif enrichment to intergenic regions can provide insight into enhancer locations and their respective function based on the specific transcription factor that may bind to it. To this end, we sought to identify the top enriched motifs of each group, shown in Figure IV-3.

Activator protein 1 (AP-1) is a major transcription factor that regulates the expression of genes associated with stimuli from cytokines, stress signals, and infections [417]. AP-1 has been shown to play important roles in cancer, both in tumorigenesis as well as potential tumor-suppressive functions [418–421]. The transcription factor has been shown to serve as regulators of the immune response during bacterial infection, including the mediation of inflammation and persistence of *Chlamydia pneumoniae* [422,423]. Furthermore, it plays important roles in immune cell differentiation [424–426]. Activation of T cells has been shown to be dependent on a well organized opening and closing of chromatin,

Figure IV - 3. Motif enrichment analysis of differential peaks.
Motif enrichment analysis was performed on the differential peaksets for each group and shared peaks. The top 5 enriched motifs for each group are shown along with their associated transcription factor (TF). Only one motif for the shared peakset was enriched.

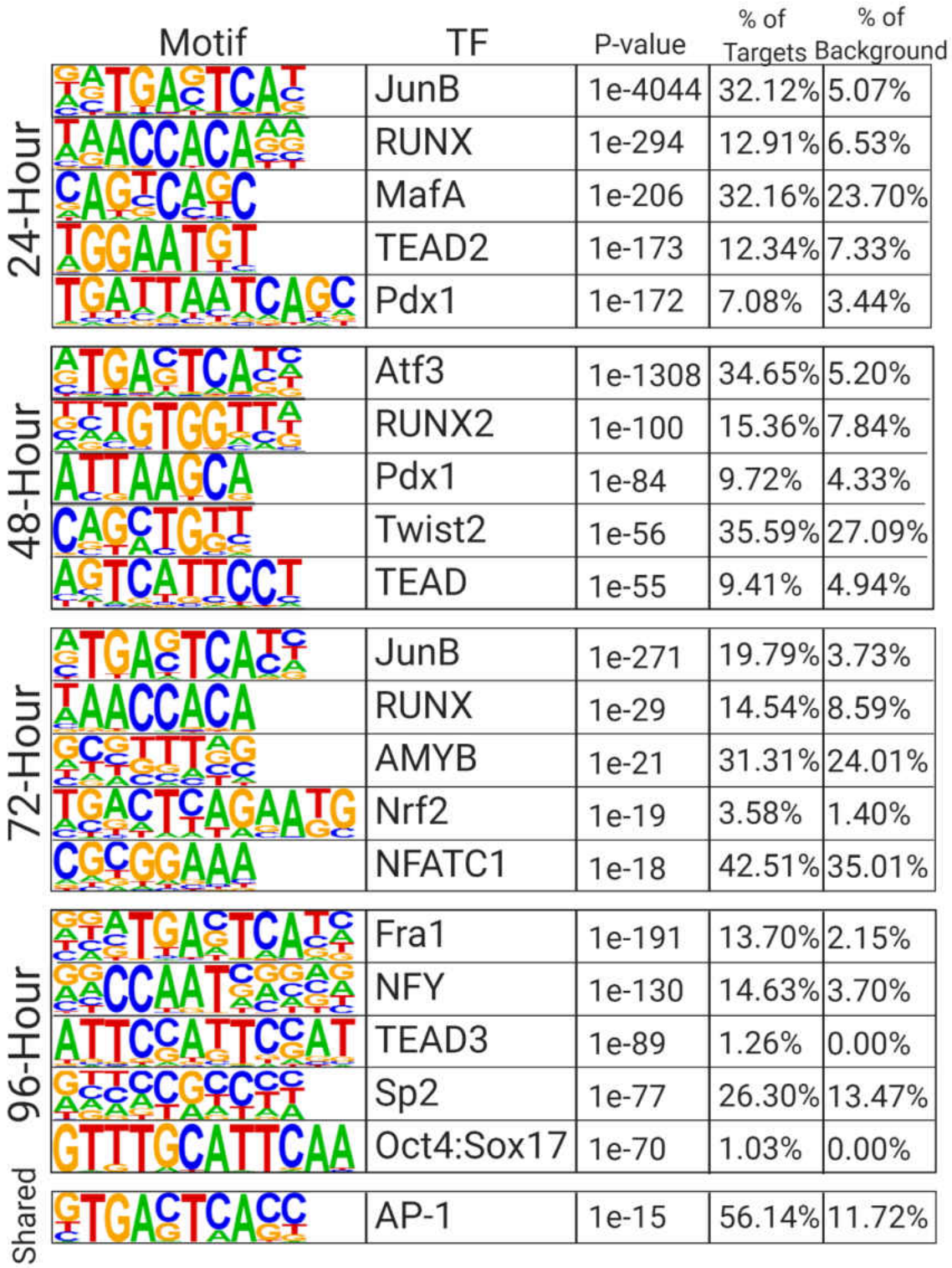
Motif
TF
P-value
% of Targets
% of Background
24-Hour
JunB 1e-4044 32.12% 5.07%
RUNX 1e-294 12.91% 6.53%
MafA 1e-206 32.16% 23.70%
TEAD2 1e-173 12.34% 7.33%
Pdx1 1e-172 7.08% 3.44%
48-Hour
Atf3 1e-1308 34.65% 5.20%
RUNX2 1e-100 15.36% 7.84%
Pdx1 1e-84 9.72% 4.33%
Twist2 1e-56 35.59% 27.09%
TEAD 1e-55 9.41% 4.94%
72-Hour
JunB 1e-271 19.79% 3.73%
RUNX 1e-29 14.54% 8.59%
AMYB 1e-21 31.31% 24.01%
Nrf2 1e-19 3.58% 1.40%
NFATC1 1e-18 42.51% 35.01%
96-Hour
Fra1 1e-191 13.70% 2.15%
NFY 1e-130 14.63% 3.70%
TEAD3 1e-89 1.26% 0.00%
Sp2 1e-77 26.30% 13.47%
Oct4:Sox17 1e-70 1.03% 0.00%
Shared
AP-1 1e-15 56.14% 11.72%

and as such, AP-1 has been identified as a required and predominant transcription factor that directs this chromatin remodeling [427]. In astrocytes, AP-1 serves to activate several pathways that include the induction of GFAP production which is a marker of astrogliosis and providing neuroprotective effects [164,428,429]. AP-1 has also been shown to play a role in MAPK and STAT pathways which have been shown to be required for the induction of MMPs (which commonly contain AP-1 motifs) during *B. burgdorferi* infection [430]. This transcription factor has a wide range of functions that generally regulate immune and stress responses to a number of stimuli, and such functions seem to have conflicting and opposite effects. An important aspect of AP-1 is that it is comprised of a heterodimer that is predominately formed by proteins of the FOS (c-FOS, FOSB, FOSL1 (Fra1), FOSL2 (Fra2)), JUN (c-Jun, JunB, JunD), and ATF (ATF1-7) families, and to a lesser extent JDP (JDP-1, JDP-2). These proteins all share a common basic leucine zipper domain (bZIP domain) that allows them to dimerize with one another. Additionally, due to this conservation in structure, the motif binding sequences share many similarities. However, minor differences in binding affinity and gene activation properties highlight differential phenotypic outcomes.

When motif enrichment analysis was performed on differential peaks of each time point, including peaks shared between all four groups, the top enriched motif in each group belonged to a member of the AP-1 transcription factor family. Furthermore, in multiple instances, the scale of difference between the top enriched and second most enriched motif was an order of magnitude in regards

to significance – 24-hour: JunB 1e-4044, RUNX 1e-294; 48-hour: ATF3 1e-1308, RUNX2 1e-100. The motif for JunB was also the most enriched at 72-hours, and Fra1 was shown to be the top motif for 96-hours. The only motif that was not flagged as a possible false positive within the group of shared peaks was the motif for AP-1. These motifs are highlighted in Figure 4-3, and the degree of enrichment can be inferred by the p-value as well as the percent of targets found vs the percent of background. The relevance of JunB within our experimental model of Lyme disease is highlighted in studies showing its role in the modulation of inflammation and its key function in the development and activation of immune cells. In T-cells, JunB is essential for the development of Th17 cells and regulatory T cells through the promotion of IL-2, and is required for the proper regulation of Th2 cell-specific cytokine profile [425,431]. In an experiment involving the stimulation of macrophage activation through LPS, JunB was confirmed to be a required factor necessary for the full expression of IL-1β, an inflammatory cytokine that highlights macrophage activation and was also observed to be increased in *B. burgdorferi* infected astrocytes [198,432]. Though its role in Lyme disease is yet to be fully elucidated, it has been previously shown to be induced in macrophages infected with *B. burgdorferi* [411]. However, in contrast to this, our differential peak analysis indicates that at 24-hours, JunB shows a Log_2FC of 0.44 at the promoter-TSS region, corresponding to a closing of chromatin, which was observed in later time points. Two conclusions can be drawn from this. If we assume that this correlates to a reduction in JunB transcription, it may underscore the closing of inflammatory genes at later time

points, inferred by the lack of differential opening. However, it is important to reiterate the similarities of motif consensus sequence between the members of the AP-1 family. As such, the Homer program places these proteins under the same or similar motifs, in which they are further ranked by matching score. However, in the case of 24-hour time point, JunB, BATF, and Atf3 had identical scores, but were ranked as such under the JunB enrichment heading. The reason I make this clarification is because BATF3, a member of the BATF/Atf family, was found to have a Log_2FC -0.39 at 24-hours within the promoter-TSS region, corresponding to an open configuration. This continued into 48-hours (-0.51) and 72-hours (-0.52) at this same peak and at additional intergenic regions. This slight distinction may shed light onto the expression of transcription factors themselves as well as their impact on gene transcription. This is again highlighted at 48-hour motif enrichment, in which the top motif corresponds to Atf3. The BATF/Atf family share similarities in function to Jun in regard to the regulation of immunity and inflammation. Atf3 has shown to negatively regulate pro-inflammatory cytokine production and its expression is elevated during the activation of several TLRs in macrophages [433–435]. Similar motif profiles are seen at 72 and 96-hours and suggest a complex mechanism of the regulation of inflammation. At this point, without direct gene expression data to overlap with our ATAC-seq data, it is difficult to expand on the functional outcomes that may be occurring, but we are able to provide potential mechanistic routes that may explain and suggest astrocyte dysregulation that may be brought upon by the alternation of multiple AP-1 motif openings and closings.

Discussion

At present, our current study has produced insight into the chromatin restructuring of astrocytes in response to *B. burgdorferi*. We have shown that at earlier time points that inflammatory chemokines and interferon-related genes show an increase in opening that may close at later time points. Through biological process enrichment, we observed large changes in anatomical restructuring and cell communication, overlapping with the broad roles that astrocytes are known to undertake – this is also highlighted in the astrocyte infection study with *B. burgdorferi* performed by the Brissette lab, which indicated differentially expressed genes that cover a wide range of biological processes [198]. Of interest for future studies is the drastic change between the earlier and later time points, notably the shift to promoter enrichment, away from potential enhancer regions, and a flip in differential peak enrichment at 96-hours. However, at the 96-hour time point, it is important to take into consideration the quality of reads, in which at least one replicate (#014) performed far worse than other samples. However, through combining the differential peaks and investigating those that are shared amongst all groups, we were able to get insight into core functional outcomes that may be taking place. When observing these peaks, a common biological process of the immune response was seen. This is highlighted by leukocyte and mast cell activation and response to cytokine stimulus. Furthermore, to lend credibility to the chromatin restructuring that takes place following infection, the biological processes of nucleosome and chromatin assembly were enriched.

Our investigation into chromatin restructuring as a potential marker and mechanism for neuroborreliosis and PTLDS stemmed from a lack of evidentiary findings and further interest was piqued by the observation of chromatin assembly processes being enriched in the aforementioned astrocyte-*Borrelia* paper by Casselli et al. From this, our initial experimental design sought to perform ATAC-seq to obtain a global, genome-wide view of the changes in chromatin structure. Additionally, based on goals, our methodology was to correlate these changes to gene expression through RNA-seq and to determine specific histone modifications as a mechanistic outcome. At the onset of this project, we had set up our experiments such that we collected enough astrocytes to be used for RNA-seq and ChIP-PCR or ChIP-seq to find direct correlations to changes in chromatin structure. Unfortunately, we had encountered numerous technical limitations during the ATAC-seq procedure. Not shown are the multiple infection experiments and subsequent ATAC-seq experiments performed on Illumina Miseq instruments to determine the efficacy of the procedure. Eventually, we were able to meet quality control prerequisites for greater coverage sequencing on Illumina HiSeq machines. However, as shown, many samples did not meet the final ENCODE data standards. With this in mind, and though the depth of coverage was not optimal, we were able to garner brief insight into alternative mechanistic routes of the astrocytic response to *B. burgdorferi*. It is hopeful that with further investigation into bacterial infections, including Lyme disease, and their impacts as epimutagens, that a more explicit pathogenesis of neuroborreliosis and PTLDS will soon be revealed.

CHAPTER V

DISCUSSION

Summary of Findings, Limitations, and Future Directions

At the beginning of my graduate career and with the *Borrelia burgdorferi* expertise of Dr. Catherine Brissette and neuroscience expertise of Dr. Watt, I had sought to investigate and expound two major gaps in knowledge that center on the neurological effects of Lyme disease. To date there is no clear evidence on the route of entry for *B. burgdorferi* into the CNS. Additionally, once within the CNS, the pathogenesis of the neurological effects of PTLDS is unknown. Though there are multiple competing theories within the field, we sought to investigate alternative and novel hypotheses for these questions.

In Chapter II, our experiments investigated an alternative route of entry into the CNS aside from the blood-brain barrier. Though previous research had been done on endothelial cells simulating this barrier, further methods on the dissemination into the CNS have yet to be performed. This uncertainty is further exacerbated by the logical conclusion that if *B. burgdorferi* enters the CNS via the blood-brain barrier, it would therefore be inferred that the bacteria will be commonly found within the brain parenchyma. However, due to obvious limitations in performing brain biopsies on living humans, and the fact that Lyme disease is rarely fatal preventing post-mortem analysis, this outcome is currently

unanswered. In defense of this approach, there is some evidence to suggest invasion of the parenchyma through the use of animal models, but such data is limited. Considering this, we sought to follow clinical evidentiary findings that would lead to a better understanding of this phenomenon. As stated previously, B. *burgdorferi* is able to enter the CNS – this is evident by lumbar puncture and direct culturing of the bacteria from the CSF of neuroborreliosis patients. Furthermore, it is well-known that the choroid plexus is highly implicated in bacterial and viral infections in allowing passage of the pathogen or peripheral immune cells directly into the CSF as the choroid plexus epithelium composes the Blood-CSF barrier. We therefore sought to use this as a system to determine the impact of *B. burgdorferi* on cultured choroid plexus epithelium cells.

Our findings had indicated what we initially hypothesized and what is in line with current research – a robust inflammatory and immune response that is produced by these epithelial cells. Furthermore, as observed in other infections, a common cytokine profile of the epithelium was that of secreted factors for the chemotaxis of peripheral immune cells. At the onset of our experiments, it was unknown how barrier related genes would be altered. As this was performed *in vitro* the choroid plexus epithelial cells lacked important physiological and anatomical context that may inhibit findings into barrier properties. However, to our surprise, we found a number of genes of barrier components and regulatory and structural factors to be downregulated. An extrapolation into an *in vivo* context would suggest that the integrity of the blood-CSF barrier may be compromised. Additionally, our downstream pathway analysis supported these

conclusions. Based on these promising results, investigating this system within an *in vivo* model is our aim for future experiments.

In Chapters III and IV, we had sought to investigate a novel mechanism behind PTLDS. Current hypotheses include the establishment of a low and undetectable infection of *B. burgdorferi* even after antibiotic treatment, and the amber hypothesis which states that the dead bacteria or debris from the bacteria is sufficient to produce a continual inflammatory response. The former hypothesis has not been well confirmed, while the later has shown promising results in which cell components of *B. burgdorferi* have been shown to elicit an immune response. Both ideas revolve around a persistent inflammatory state that would lead to deleterious outcomes. With this in mind, we sought to investigate mechanisms that would allow for inflammatory and immune genes to remain in a high transcript state that would persist after infection had been cleared. Through previous work of the epimutagen properties of other bacterial infections, we aimed to apply this to Lyme disease, specifically the neurological aspects of PTLDS. Due to the important and wide scope of astrocytic functions, we aimed to investigate the impact of *B. burgdorferi* infection of the astrocyte methylome and chromatin landscape.

In Chapter III, investigating the impact on DNA methylation, we ran into a major technical limitation within our methodology. As our primary human samples were obtained from three different individuals, our variability amongst replicates was so great that no differential methylation states were found. However, through the pooling of specific infection groups, we were able to gain limited findings that

included changes in methylation at sites of genes whose functions involved cell signaling and modulation of immune response. These genes were specifically involved in extracellular glutamate modulation and downregulation of NF-κB.

In Chapter IV, we investigated the chromatin landscape in response to *B. burgdorferi* through the use of ATAC-seq. Though we had altered our methodology to take into account the variability of primary samples, we ran into a number of technical issues that limited our access to high coverage sequencing data. However, our data was sufficient to provide a clear indication into the changes in that are occurring within astrocytes in response to infection. We observed large initial change in chromatin accessibility that predominately lead to open states throughout the genome. Interestingly, at later time points, these enriched regions continued to reduce in number. Many of the initial differential peaks were found to be involved in innate immunity, specifically cell signaling through cytokine production. However, looking at peaks shared amongst all time points, we were able to clearly see that immune cell activation and chromatin restructuring was a shared characteristic between all groups. In support of this, motif enrichment analysis indicated AP-1 transcription factor motifs were highly enriched across each group. Our conclusion indicates that an initial innate immune response is produced by astrocytes, that may not persist at later time points; however, based on motif analysis, this may just indicate a change gene profile that still remains within the inflammatory and immune response group. Our experiments were started with the expressed intent to provide correlative data of gene expression and histone modifications to our ATAC-seq data. However, due

to limitations in the ATAC-seq procedure, such analysis was not undertaken. Our future directions would aim to continue this line of thought.

Conclusion

B. burgdorferi has been around for thousands of years, inflicting pain and suffering in countless individuals, and though research has made great advances in providing medical care of patients, there are still many avenues of the disease to uncover. For the five years that span my graduate career, I had set out to add to the wealth of information within the Lyme disease field, to contribute some helpful piece of knowledge in understanding this disease. Although some experiments were met with limitations, I have felt I have met this goal to a degree. It is hopeful that with the gain in publicity, understanding of the disease will becoming even more widespread within the public. Through this education, we can ameliorate many aspects of the disease through simple administration of antibiotics. My research had focused on the aspect of the disease in which there is high correlation between a failure in timely antibiotic treatment and the onset of late stage and persistent symptoms – the effects of neuroborreliosis and PTLDS can be drastic, lowering the quality of life for a lifetime, and unfortunately at this stage, there are no current therapeutics for patients. It is my anticipation that future research will be successful in uncovering these mechanisms and provide treatment options for the endless number of patients who suffer from Lyme disease.

REFERENCES

1. Bacon RM, Kugeler KJ, Mead PS, Centers for Disease Control and Prevention (CDC). Surveillance for Lyme disease--United States, 1992-2006. MMWR Surveill Summ. 2008 Oct 3;57(10):1–9.
2. Rosenberg R. Vital Signs: Trends in Reported Vectorborne Disease Cases — United States and Territories, 2004–2016. MMWR Morb Mortal Wkly Rep [Internet]. 2018 [cited 2019 Nov 21];67. Available from: https://www.cdc.gov/mmwr/volumes/67/wr/mm6717e1.htm
3. Nelson CA, Saha S, Kugeler KJ, Delorey MJ, Shankar MB, Hinckley AF, et al. Incidence of Clinician-Diagnosed Lyme Disease, United States, 2005-2010. Emerging Infect Dis. 2015 Sep;21(9):1625–31.
4. Hinckley AF, Connally NP, Meek JI, Johnson BJ, Kemperman MM, Feldman KA, et al. Lyme Disease Testing by Large Commercial Laboratories in the United States. Clin Infect Dis. 2014 Sep 1;59(5):676–81.
5. Adrion ER, Aucott J, Lemke KW, Weiner JP. Health Care Costs, Utilization and Patterns of Care following Lyme Disease. PLOS ONE. 2015 Feb 4;10(2):e0116767.
6. Bonani G, Ivy SD, Hajdas I, Niklaus TR, Suter M. Ams 14C Age Determinations of Tissue, Bone and Grass Samples from the Ötztal Ice Man. Radiocarbon. 1994 ed;36(2):247–50.
7. Gostner P, Vigl EE. INSIGHT: Report of Radiological-Forensic Findings on the Iceman. Journal of Archaeological Science. 2002 Mar 1;29(3):323–6.

8. Kean WF, Tocchio S, Kean M, Rainsford KD. The musculoskeletal abnormalities of the Similaun Iceman ("ÖTZI"): clues to chronic pain and possible treatments. Inflammopharmacology. 2013 Feb;21(1): 11–20.

9. Keller A, Graefen A, Ball M, Matzas M, Boisguerin V, Maixner F, et al. New insights into the Tyrolean Iceman's origin and phenotype as inferred by whole-genome sequencing. Nature Communications. 2012 Feb 28;3(1):1–9.

10. Walter KS, Carpi G, Caccone A, Diuk-Wasser MA. Genomic insights into the ancient spread of Lyme disease across North America. Nat Ecol Evol. 2017 Oct;1(10):1569–76.

11. Steere AC, Malawista SE, Snydman DR, Shope RE, Andiman WA, Ross MR, et al. Lyme arthritis: an epidemic of oligoarticular arthritis in children and adults in three connecticut communities. Arthritis Rheum. 1977 Feb;20(1):7–17.

12. Elbaum-Garfinkle S. Close to Home: A History of Yale and Lyme Disease. Yale J Biol Med. 2011 Jun;84(2):103–8.

13. Steere AC, Malawista SE, Hardin JA, Ruddy S, Askenase W, Andiman WA. Erythema chronicum migrans and Lyme arthritis. The enlarging clinical spectrum. Ann Intern Med. 1977 Jun;86(6):685–98.

14. Steere AC, Broderick TF, Malawista SE. Erythema chronicum migrans and Lyme arthritis: epidemiologic evidence for a tick vector. Am J Epidemiol. 1978 Oct;108(4):312–21.

15. Burgdorfer W, Barbour AG, Hayes SF, Benach JL, Grunwaldt E, Davis JP. Lyme disease-a tick-borne spirochetosis? Science (New York, NY). 1982 Jun 1;216(4552):1317–9.

16. Centers for Disease Control and Prevention (U.S.). Center for Surveillance E and Laboratory Services National Notifiable Diseases Surveillance System. Nationally Notifiable Infectious Diseases and Conditions, United States: Annual Tables.Table 2i. Listeriosis; Lyme disease; Malaria; Measles. 2019 Nov 4;(9). Available from: https://stacks.cdc.gov/view/cdc/82392

17. Fleischmann RD, Adams MD, White O, Clayton RA, Kirkness EF, Kerlavage AR, et al. Whole-genome random sequencing and assembly of Haemophilus influenzae Rd. Science. 1995 Jul 28;269(5223):496–512.

18. Fraser CM, Gocayne JD, White O, Adams MD, Clayton RA, Fleischmann RD, et al. The minimal gene complement of Mycoplasma genitalium. Science. 1995 Oct 20;270(5235):397–403.

19. Fraser CM, Casjens S, Huang WM, Sutton GG, Clayton R, Lathigra R, et al. Genomic sequence of a Lyme disease spirochaete, Borrelia burgdorferi. Nature. 1997 Dec;390(6660):580.

20. Casjens S, Palmer N, Vugt RV, Huang WM, Stevenson B, Rosa P, et al. A bacterial genome in flux: the twelve linear and nine circular extrachromosomal DNAs in an infectious isolate of the Lyme disease spirochete Borrelia burgdorferi. Molecular Microbiology. 2000;35(3):490–516.

21. Casjens SR, Gilcrease EB, Vujadinovic M, Mongodin EF, Luft BJ, Schutzer SE, et al. Plasmid diversity and phylogenetic consistency in the Lyme disease agent Borrelia burgdorferi. BMC Genomics. 2017 15;18(1):165.

22. Grimm D, Elias AF, Tilly K, Rosa PA. Plasmid Stability during In Vitro Propagation of Borrelia burgdorferi Assessed at a Clonal Level. Infect Immun. 2003 Jun;71(6):3138–45.

23. Schwan TG, Burgdorfer W, Garon CF. Changes in infectivity and plasmid profile of the Lyme disease spirochete, Borrelia burgdorferi, as a result of in vitro cultivation. Infect Immun. 1988 Aug;56(8):1831–6.

24. Barbour AG. Plasmid analysis of Borrelia burgdorferi, the Lyme disease agent. J Clin Microbiol. 1988 Mar;26(3):475–8.

25. Purser JE, Norris SJ. Correlation between plasmid content and infectivity in Borrelia burgdorferi. Proc Natl Acad Sci U S A. 2000 Dec 5;97(25):13865–70.

26. Carroll JA, Garon CF, Schwan TG. Effects of environmental pH on membrane proteins in Borrelia burgdorferi. Infect Immun. 1999 Jul;67(7):3181–7.

27. Yang X, Goldberg MS, Popova TG, Schoeler GB, Wikel SK, Hagman KE, et al. Interdependence of environmental factors influencing reciprocal patterns of gene expression in virulent Borrelia burgdorferi. Mol Microbiol. 2000 Sep;37(6):1470–9.

28. Seshu J, Boylan JA, Gherardini FC, Skare JT. Dissolved oxygen levels alter gene expression and antigen profiles in Borrelia burgdorferi. Infect Immun. 2004 Mar;72(3):1580–6.

29. Hyde JA, Trzeciakowski JP, Skare JT. Borrelia burgdorferi alters its gene expression and antigenic profile in response to CO2 levels. J Bacteriol. 2007 Jan;189(2):437–45.

30. Drecktrah D, Lybecker M, Popitsch N, Rescheneder P, Hall LS, Samuels DS. The Borrelia burgdorferi RelA/SpoT Homolog and Stringent Response Regulate Survival in the Tick Vector and Global Gene Expression during Starvation. PLoS Pathog. 2015 Sep;11(9):e1005160.

31. Bontemps-Gallo S, Lawrence K, Gherardini FC. Two Different Virulence-Related Regulatory Pathways in Borrelia burgdorferi Are Directly Affected by Osmotic Fluxes in the Blood Meal of Feeding Ixodes Ticks. PLoS Pathog. 2016;12(8):e1005791.

32. Fisher MA, Grimm D, Henion AK, Elias AF, Stewart PE, Rosa PA, et al. Borrelia burgdorferi sigma54 is required for mammalian infection and vector transmission but not for tick colonization. Proc Natl Acad Sci USA. 2005 Apr 5;102(14):5162–7.

33. Iyer R, Caimano MJ, Luthra A, Axline D, Corona A, Iacobas DA, et al. Stage-specific global alterations in the transcriptomes of Lyme disease spirochetes during tick feeding and following mammalian host adaptation. Mol Microbiol. 2015 Feb;95(3):509–38.

34. Samuels DS. Gene regulation in Borrelia burgdorferi. Annu Rev Microbiol. 2011;65:479–99.

35. Radolf JD, Caimano MJ, Stevenson B, Hu LT. Of ticks, mice and men: understanding the dual-host lifestyle of Lyme disease spirochaetes. Nature Reviews Microbiology. 10(2):87.

36. Samuels DS, Samuels LRN. Gene Regulation During the Enzootic Cycle of the Lyme Disease Spirochete. For Immunopathol Dis Therap. 2016;7(3–4):205–12.

37. Caimano MJ, Kenedy MR, Kairu T, Desrosiers DC, Harman M, Dunham-Ems S, et al. The hybrid histidine kinase Hk1 is part of a two-component system that is essential for survival of Borrelia burgdorferi in feeding Ixodes scapularis ticks. Infect Immun. 2011 Aug;79(8):3117–30.

38. He M, Ouyang Z, Troxell B, Xu H, Moh A, Piesman J, et al. Cyclic di-GMP is Essential for the Survival of the Lyme Disease Spirochete in Ticks. PLoS Pathog [Internet]. 2011 Jun 30 [cited 2020 May 11];7(6). Available from: https://www.ncbi.nlm.nih.gov/pmc/articles/PMC3128128/

39. Pal U, Li X, Wang T, Montgomery RR, Ramamoorthi N, Desilva AM, et al. TROSPA, an Ixodes scapularis receptor for Borrelia burgdorferi. Cell. 2004 Nov 12;119(4):457–68.

40. Yang XF, Pal U, Alani SM, Fikrig E, Norgard MV. Essential Role for OspA/B in the Life Cycle of the Lyme Disease Spirochete. J Exp Med. 2004 Mar 1;199(5):641–8.

41. Battisti JM, Bono JL, Rosa PA, Schrumpf ME, Schwan TG, Policastro PF. Outer Surface Protein A Protects Lyme Disease Spirochetes from Acquired Host Immunity in the Tick Vector. Infect Immun. 2008 Nov;76(11):5228–37.

42. Pappas CJ, Iyer R, Petzke MM, Caimano MJ, Radolf JD, Schwartz I. Borrelia burgdorferi Requires Glycerol for Maximum Fitness During The Tick Phase of the Enzootic Cycle. PLoS Pathog [Internet]. 2011 Jul 7 [cited 2020 May 11];7(7). Available from: https://www.ncbi.nlm.nih.gov/pmc/articles/PMC3131272/

43. Grimm D, Tilly K, Byram R, Stewart PE, Krum JG, Bueschel DM, et al. Outer-surface protein C of the Lyme disease spirochete: A protein induced in ticks for infection of mammals. Proc Natl Acad Sci U S A. 2004 Mar 2;101(9):3142–7.

44. Tilly K, Krum JG, Bestor A, Jewett MW, Grimm D, Bueschel D, et al. Borrelia burgdorferi OspC Protein Required Exclusively in a Crucial Early Stage of Mammalian Infection. Infect Immun. 2006 Jun;74(6):3554–64.

45. Stanek G, Wormser GP, Gray J, Strle F. Lyme borreliosis. The Lancet. 2012 Feb 4;379(9814):461–73.

46. Mannelli A, Bertolotti L, Gern L, Gray J. Ecology of Borrelia burgdorferi sensu lato in Europe: transmission dynamics in multi-host systems, influence of molecular processes and effects of climate change. FEMS Microbiol Rev. 2012 Jul;36(4):837–61.

47. Schotthoefer AM, Frost HM. Ecology and Epidemiology of Lyme Borreliosis. Clin Lab Med. 2015 Dec;35(4):723–43.

48. Patrican LA. Absence of Lyme disease spirochetes in larval progeny of naturally infected Ixodes scapularis (Acari:Ixodidae) fed on dogs. J Med Entomol. 1997 Jan;34(1):52–5.

49. Brisson D, Dykhuizen DE, Ostfeld RS. Conspicuous impacts of inconspicuous hosts on the Lyme disease epidemic. Proc Biol Sci. 2008 Jan 22;275(1631):227–35.

50. Fedorova N, Kleinjan JE, James D, Hui LT, Peeters H, Lane RS. Remarkable diversity of tick or mammalian-associated Borreliae in the metropolitan San Francisco Bay Area, California. Ticks Tick Borne Dis. 2014 Oct;5(6):951–61.

51. Ogden NH, Lindsay LR, Hanincová K, Barker IK, Bigras-Poulin M, Charron DF, et al. Role of migratory birds in introduction and range expansion of Ixodes scapularis ticks and of Borrelia burgdorferi and Anaplasma phagocytophilum in Canada. Appl Environ Microbiol. 2008 Mar;74(6):1780–90.

52. Loss SR, Noden BH, Hamer GL, Hamer SA. A quantitative synthesis of the role of birds in carrying ticks and tick-borne pathogens in North America. Oecologia. 2016 Dec;182(4):947–59.

53. Ouellette J, Apperson CS, Howard P, Evans TL, Levine JF. Tick-raccoon associations and the potential for Lyme disease spirochete transmission in the coastal plain of North Carolina. J Wildl Dis. 1997 Jan;33(1):28–39.

54. Brinkerhoff RJ, Folsom-O'Keefe CM, Streby HM, Bent SJ, Tsao K, Diuk-Wasser MA. Regional Variation in Immature Ixodes scapularis Parasitism on North American Songbirds: Implications for Transmission of the Lyme Pathogen, Borrelia burgdorferi. jnl med entom. 2011 Mar 1;48(2):422–8.

55. Kollars TM, Oliver JH, Kollars PG, Durden LA. Seasonal activity and host associations of Ixodes scapularis (Acari: Ixodidae) in southeastern Missouri. J Med Entomol. 1999 Nov;36(6):720–6.

56. Gatewood AG, Liebman KA, Vourc'h G, Bunikis J, Hamer SA, Cortinas R, et al. Climate and Tick Seasonality Are Predictors of Borrelia burgdorferi Genotype Distribution. Appl Environ Microbiol. 2009 Apr;75(8):2476–83.

57. Johnson RC, Kodner C, Jarnefeld J, Eck DK, Xu Y. Agents of Human Anaplasmosis and Lyme Disease at Camp Ripley, Minnesota. Vector-Borne and Zoonotic Diseases. 2011 Aug 25;11(12):1529–34.

58. Hofmeister EK, Ellis BA, Glass GE, Childs JE. Longitudinal study of infection with Borrelia burgdorferi in a population of Peromyscus leucopus at a Lyme disease-enzootic site in Maryland. Am J Trop Med Hyg. 1999 Apr;60(4):598–609.

59. Bunikis J, Tsao J, Luke CJ, Luna MG, Fish D, Barbour AG. Borrelia burgdorferi infection in a natural population of Peromyscus Leucopus mice: a longitudinal study in an area where Lyme Borreliosis is highly endemic. J Infect Dis. 2004 Apr 15;189(8):1515–23.

60. Anderson JF, Johnson RC, Magnarelli LA. Seasonal prevalence of Borrelia burgdorferi in natural populations of white-footed mice, Peromyscus leucopus. J Clin Microbiol. 1987 Aug;25(8):1564–6.

61. Tracy KE, Baumgarth N. Borrelia burgdorferi Manipulates Innate and Adaptive Immunity to Establish Persistence in Rodent Reservoir Hosts. Front Immunol [Internet]. 2017 Feb 20 [cited 2020 May 9];8. Available from: https://www.ncbi.nlm.nih.gov/pmc/articles/PMC5316537/

62. Baum E, Hue F, Barbour AG. Experimental infections of the reservoir species Peromyscus leucopus with diverse strains of Borrelia burgdorferi, a Lyme disease agent. mBio. 2012 Dec 4;3(6):e00434-00412.

63. Wright SD, Nielsen SW. Experimental infection of the white-footed mouse with Borrelia burgdorferi. Am J Vet Res. 1990 Dec;51(12):1980–7.

64. Lane RS, Brown RN, Piesman J, Peavey CA. Vector competence of Ixodes pacificus and Dermacentor occidentalis (Acari: Ixodidae) for various isolates of Lyme disease spirochetes. J Med Entomol. 1994 May;31(3):417–24.

65. Girard YA, Travinsky B, Schotthoefer A, Fedorova N, Eisen RJ, Eisen L, et al. Population Structure of the Lyme Borreliosis Spirochete Borrelia burgdorferi in the Western Black-Legged Tick (Ixodes pacificus) in Northern California. Appl Environ Microbiol. 2009 Nov 15;75(22):7243–52.

66. Schwartz AM. Surveillance for Lyme Disease — United States, 2008–2015. MMWR Surveill Summ [Internet]. 2017 [cited 2020 Apr 20];66. Available from: https://www.cdc.gov/mmwr/volumes/66/ss/ss6622a1.htm

67. Steere AC. The Clinical Evolution of Lyme Arthritis. Ann Intern Med. 1987 Nov 1;107(5):725.

68. Steere AC, Angelis SM. Therapy for Lyme arthritis: Strategies for the treatment of antibiotic-refractory arthritis. Arthritis Rheum. 2006 Oct;54(10):3079–86.

69. Bartůněk P, Gorican K, Veiser T, Táborský M, Hulínská D. Significance of Borrelia infection in development of dilated cardiomypathy (a pilot study). Prague Med Rep. 2007;108(4):339–47.

70. Silver E, Pass RH, Kaufman S, Hordof AJ, Liberman L. Complete Heart Block Due to Lyme Carditis in Two Pediatric Patients and a Review of the Literature. Congenital Heart Disease. 2007 Sep;2(5):338–41.

71. Biesiada G, Czepiel J, Leśniak MR, Garlicki A, Mach T. Lyme disease: review. Arch Med Sci. 2012 Dec 20;8(6):978–82.

72. Pachner AR, Steere AC. The triad of neurologic manifestations of Lyme disease. Neurology. 1985 Jan 1;35(1):47.

73. Schmidt H, Djukic M, Jung K, Holzgraefe M, Dechent P, Steinbüchel N von, et al. Neurocognitive functions and brain atrophy after proven neuroborreliosis: a case-control study. BMC Neurol [Internet]. 2015 Aug 19 [cited 2019 Nov 21];15. Available from: https://www.ncbi.nlm.nih.gov/pmc/articles/PMC4545711/

74. Thaisetthawatkul P, Logigian E. Peripheral Nervous System Manifestations of Lyme Borreliosis. Journal of Clinical Neuromuscular Disease. 2002 Jun;3(4):165–71.

75. Luft BJ, Steinman CR, Neimark HC, Muralidhar B, Rush T, Finkel MF, et al. Invasion of the central nervous system by Borrelia burgdorferi in acute disseminated infection. JAMA. 1992 Mar 11;267(10):1364–7.

76. Djukic M, Schmidt-Samoa C, Lange P, Spreer A, Neubieser K, Eiffert H, et al. Cerebrospinal fluid findings in adults with acute Lyme neuroborreliosis. J Neurol. 2012 Apr;259(4):630–6.

77. Wormser GP, Dattwyler RJ, Shapiro ED, Halperin JJ, Steere AC, Klempner MS, et al. The Clinical Assessment, Treatment, and Prevention of Lyme Disease, Human Granulocytic Anaplasmosis, and Babesiosis: Clinical Practice Guidelines by the Infectious Diseases Society of America. Clin Infect Dis. 2006 Nov 1;43(9):1089–134.

78. Rupprecht TA, Pfister HW, Angele B, Kastenbauer S, Wilske B, Koedel U. The chemokine CXCL13 (BLC): a putative diagnostic marker for neuroborreliosis. Neurology. 2005 Aug 9;65(3):448–50.

79. Senel M, Rupprecht TA, Tumani H, Pfister HW, Ludolph AC, Brettschneider J. The chemokine CXCL13 in acute neuroborreliosis. J Neurol Neurosurg Psychiatry. 2010 Aug;81(8):929–33.

80. Ramesh G, Santana-Gould L, Inglis FM, England JD, Philipp MT. The Lyme disease spirochete Borrelia burgdorferi induces inflammation and apoptosis in cells from dorsal root ganglia. J Neuroinflammation. 2013 Jul 18;10:88.

81. Ramesh G, Benge S, Pahar B, Philipp MT. A possible role for inflammation in mediating apoptosis of oligodendrocytes as induced by the Lyme disease spirochete Borrelia burgdorferi. Journal of Neuroinflammation. 2012 Apr 23;9(1):72.

82. Liba Z, Kayserova J, Komarek V. Th1 and Th17 but no Th2-related cytokine spectrum in the cerebrospinal fluid of children with Borrelia-related facial nerve palsy. Fluids Barriers CNS. 2013 Oct 4;10:30.

83. Gyllemark P, Forsberg P, Ernerudh J, Henningsson AJ. Intrathecal Th17- and B cell-associated cytokine and chemokine responses in relation to clinical outcome in Lyme neuroborreliosis: a large retrospective study. J Neuroinflammation [Internet]. 2017 Feb 1 [cited 2019 Nov 25];14. Available from: https://www.ncbi.nlm.nih.gov/pmc/articles/PMC5286657/

84. Pietikäinen A, Maksimow M, Kauko T, Hurme S, Salmi M, Hytönen J. Cerebrospinal fluid cytokines in Lyme neuroborreliosis. J Neuroinflammation [Internet]. 2016 Oct 18 [cited 2019 Nov 25];13. Available from: https://www.ncbi.nlm.nih.gov/pmc/articles/PMC5070144/

85. Steere AC, Grodzicki RL, Kornblatt AN, Craft JE, Barbour AG, Burgdorfer W, et al. The spirochetal etiology of Lyme disease. N Engl J Med. 1983 Mar 31;308(13):733–40.

86. Hildenbrand P, Craven DE, Jones R, Nemeskal P. Lyme Neuroborreliosis: Manifestations of a Rapidly Emerging Zoonosis. American Journal of Neuroradiology. 2009 Jun 1;30(6):1079–87.

87. Wormser GP, McKenna D, Carlin J, Nadelman RB, Cavaliere LF, Holmgren D, et al. Brief communication: hematogenous dissemination in early Lyme disease. Ann Intern Med. 2005 May 3;142(9):751–5.

88. Wormser GP. Hematogenous dissemination in early Lyme disease. Wien Klin Wochenschr. 2006 Nov;118(21–22):634–7.

89. Grab DJ, Perides G, Dumler JS, Kim KJ, Park J, Kim YV, et al. Borrelia burgdorferi, Host-Derived Proteases, and the Blood-Brain Barrier. Infect Immun. 2005 Feb;73(2):1014–22.

90. Szczepanski A, Furie MB, Benach JL, Lane BP, Fleit HB. Interaction between Borrelia burgdorferi and endothelium in vitro. J Clin Invest. 1990 May;85(5):1637–47.

91. Comstock LE, Thomas DD. Penetration of endothelial cell monolayers by Borrelia burgdorferi. Infect Immun. 1989 May;57(5):1626–8.

92. Smith RP, Schoen RT, Rahn DW, Sikand VK, Nowakowski J, Parenti DL, et al. Clinical characteristics and treatment outcome of early Lyme disease in patients with microbiologically confirmed erythema migrans. Ann Intern Med. 2002 Mar 19;136(6):421–8.

93. Nowakowski J, Nadelman RB, Sell R, McKenna D, Cavaliere LF, Holmgren D, et al. Long-term follow-up of patients with culture-confirmed Lyme disease. Am J Med. 2003 Aug 1;115(2):91–6.

94. Wormser GP, Ramanathan R, Nowakowski J, McKenna D, Holmgren D, Visintainer P, et al. Duration of antibiotic therapy for early Lyme disease. A randomized, double-blind, placebo-controlled trial. Ann Intern Med. 2003 May 6;138(9):697–704.

95. Dattwyler RJ, Halperin JJ, Volkman DJ, Luft BJ. Treatment of late Lyme borreliosis--randomised comparison of ceftriaxone and penicillin. Lancet. 1988 May 28;1(8596):1191–4.

96. Pfister H-W, Preac-Mursic V, Wilske B, Schielke E, Sörgel F, Einhaupl KM. Randomized Comparison of Ceftriaxone and Cefotaxime in Lyme Neuroborreliosis. J Infect Dis. 1991 Feb 1;163(2):311–8.

97. Dattwyler RJ, Wormser GP, Rush TJ, Finkel MF, Schoen RT, Grunwaldt E, et al. A comparison of two treatment regimens of ceftriaxone in late Lyme disease. Wien Klin Wochenschr. 2005 Jun;117(11–12):393–7.

98. Aucott JN, Rebman AW, Crowder LA, Kortte KB. Post-treatment Lyme disease syndrome symptomatology and the impact on life functioning: is there something here? Qual Life Res. 2013 Feb;22(1):75–84.

99. Marques A. Chronic Lyme Disease: An appraisal. Infect Dis Clin North Am. 2008 Jun;22(2):341–60.

100. Pícha D, Moravcova L, Lasikova S, Holeckova D, Maresova V. Symptoms of post-Lyme syndrome in long-term outcome of patients with neuroborreliosis. Scandinavian Journal of Infectious Diseases. 2006 Jan 1;38(8):747–8.

101. Rebman AW, Bechtold KT, Yang T, Mihm EA, Soloski MJ, Novak CB, et al. The Clinical, Symptom, and Quality-of-Life Characterization of a Well-Defined Group of Patients with Posttreatment Lyme Disease Syndrome. Front Med (Lausanne) [Internet]. 2017 Dec 14 [cited 2020 May 7];4. Available from: https://www.ncbi.nlm.nih.gov/pmc/articles/PMC5735370/

102. Asch ES, Bujak DI, Weiss M, Peterson MG, Weinstein A. Lyme disease: an infectious and postinfectious syndrome. J Rheumatol. 1994 Mar;21(3):454–61.

103. Shadick NA, Phillips CB, Logigian EL, Steere AC, Kaplan RF, Berardi VP, et al. The long-term clinical outcomes of Lyme disease. A population-based retrospective cohort study. Ann Intern Med. 1994 Oct 15;121(8):560–7.

104. Krupp LB, Hyman LG, Grimson R, Coyle PK, Melville P, Ahnn S, et al. Study and treatment of post Lyme disease (STOP-LD): A randomized double masked clinical trial. Neurology. 2003 Jun 24;60(12):1923–30.

105. Fallon BA, Keilp JG, Corbera KM, Petkova E, Britton CB, Dwyer E, et al. A randomized, placebo-controlled trial of repeated IV antibiotic therapy for Lyme encephalopathy. Neurology. 2008 Mar 25;70(13):992–1003.

106. Klempner MS, Hu LT, Evans J, Schmid CH, Johnson GM, Trevino RP, et al. Two Controlled Trials of Antibiotic Treatment in Patients with Persistent Symptoms and a History of Lyme Disease. New England Journal of Medicine. 2001 Jul 12;345(2):85–92.

107. Middelveen MJ, Sapi E, Burke J, Filush KR, Franco A, Fesler MC, et al. Persistent Borrelia Infection in Patients with Ongoing Symptoms of Lyme Disease. Healthcare (Basel) [Internet]. 2018 Apr 14 [cited 2020 May 7];6(2). Available from: https://www.ncbi.nlm.nih.gov/pmc/articles/PMC6023324/

108. Wormser GP, Nadelman RB, Schwartz I. The amber theory of Lyme arthritis: initial description and clinical implications. Clin Rheumatol. 2012 Jun 1;31(6):989–94.

109. Greenmyer JR, Gaultney RA, Brissette CA, Watt JA. Primary Human Microglia Are Phagocytically Active and Respond to Borrelia burgdorferi With Upregulation of Chemokines and Cytokines. Front Microbiol [Internet]. 2018 Apr 25 [cited 2019 Nov 4];9. Available from: https://www.ncbi.nlm.nih.gov/pmc/articles/PMC5996889/

110. Spielman A, Ribeiro JMC, Mather TN, Piesman J. Dissemination and Salivary Delivery of Lyme Disease Spirochetes in Vector Ticks (Acari: Ixodidae). Journal of Medical Entomology. 1987 Mar 1;24(2):201–5.

111. Kotsyfakis M, Sá-Nunes A, Francischetti IMB, Mather TN, Andersen JF, Ribeiro JMC. Antiinflammatory and immunosuppressive activity of sialostatin L, a salivary cystatin from the tick Ixodes scapularis. J Biol Chem. 2006 Sep 8;281(36):26298–307.

112. Das S, Banerjee G, DePonte K, Marcantonio N, Kantor FS, Fikrig E. Salp25D, an Ixodes scapularis antioxidant, is 1 of 14 immunodominant antigens in engorged tick salivary glands. J Infect Dis. 2001 Oct 15;184(8):1056–64.

113. Hourcade DE, Akk AM, Mitchell LM, Zhou H, Hauhart R, Pham CTN. Anti-complement activity of the Ixodes scapularis salivary protein Salp20. Mol Immunol. 2016 Jan;69:62–9.

114. Ribeiro JM, Weis JJ, Telford SR. Saliva of the tick Ixodes dammini inhibits neutrophil function. Exp Parasitol. 1990 May;70(4):382–8.

115. Guo X, Booth CJ, Paley MA, Wang X, DePonte K, Fikrig E, et al. Inhibition of Neutrophil Function by Two Tick Salivary Proteins. Infect Immun. 2009 Jun;77(6):2320–9.

116. Sá-Nunes A, Bafica A, Lucas DA, Conrads TP, Veenstra TD, Andersen JF, et al. Prostaglandin E2 is a major inhibitor of dendritic cell maturation and function in Ixodes scapularis saliva. J Immunol. 2007 Aug 1;179(3):1497–505.

117. Skallová A, Iezzi G, Ampenberger F, Kopf M, Kopecky J. Tick saliva inhibits dendritic cell migration, maturation, and function while promoting development of Th2 responses. J Immunol. 2008 May 1;180(9):6186–92.

118. Banchereau J, Steinman RM. Dendritic cells and the control of immunity. Nature. 1998 Mar 19;392(6673):245–52.

119. Patente TA, Pinho MP, Oliveira AA, Evangelista GCM, Bergami-Santos PC, Barbuto JAM. Human Dendritic Cells: Their Heterogeneity and Clinical Application Potential in Cancer Immunotherapy. Front Immunol [Internet]. 2019 [cited 2020 May 2];9. Available from: https://www.frontiersin.org/articles/10.3389/fimmu.2018.03176/full

120. Filgueira L, Nestlé FO, Rittig M, Joller HI, Groscurth P. Human dendritic cells phagocytose and process Borrelia burgdorferi. The Journal of Immunology. 1996 Oct 1;157(7):2998–3005.

121. Mason LMK, Veerman CC, Geijtenbeek TBH, Hovius JWR. Ménage à trois: Borrelia, dendritic cells, and tick saliva interactions. Trends in Parasitology. 2014 Feb;30(2):95–103.

122. Hartiala P, Hytönen J, Pelkonen J, Kimppa K, West A, Penttinen MA, et al. Transcriptional response of human dendritic cells to Borrelia garinii—defective CD38 and CCR7 expression detected. Journal of Leukocyte Biology. 2007;82(1):33–43.

123. Suhonen J, Komi J, Soukka J, Lassila O, Viljanen MK. Interaction Between Borrelia burgdorferi and Immature Human Dendritic Cells. Scandinavian Journal of Immunology. 2003;58(1):67–75.

124. Rouault C, Pellegrinelli V, Schilch R, Cotillard A, Poitou C, Tordjman J, et al. Roles of Chemokine Ligand-2 (CXCL2) and Neutrophils in Influencing Endothelial Cell Function and Inflammation of Human Adipose Tissue. Endocrinology. 2013 Mar 1;154(3):1069–79.

125. Moser B, Ckark-Lewis I, Zwahlen R, Baggiolini M. Neutrophil-activating properties of the melanoma growth-stimulatory activity. J Exp Med. 1990 May 1;171(5):1797–802.

126. Burdon PCE, Martin C, Rankin SM. The CXC chemokine MIP-2 stimulates neutrophil mobilization from the rat bone marrow in a CD49d-dependent manner. Blood. 2005 Mar 15;105(6):2543–8.

127. Ritzman AM, Hughes-Hanks JM, Blaho VA, Wax LE, Mitchell WJ, Brown CR. The Chemokine Receptor CXCR2 Ligand KC (CXCL1) Mediates Neutrophil Recruitment and Is Critical for Development of Experimental Lyme Arthritis and Carditis. Infect Immun. 2010 Nov;78(11):4593–600.

128. Jones CV, Ricardo SD. Macrophages and CSF-1. Organogenesis. 2013 Oct 1;9(4):249–60.

129. Nemunaitis J. Macrophage function activating cytokines: potential clinical application. Critical Reviews in Oncology/Hematology. 1993 Apr 1;14(2):153–71.

130. Fritsche J, Moser M, Faust S, Peuker A, Büttner R, Andreesen R, et al. Molecular cloning and characterization of a human metalloprotease disintegrin--a novel marker for dendritic cell differentiation. Blood. 2000 Jul 15;96(2):732–9.

131. Aerts-Toegaert C, Heirman C, Tuyaerts S, Corthals J, Aerts JL, Bonehill A, et al. CD83 expression on dendritic cells and T cells: correlation with effective immune responses. Eur J Immunol. 2007 Mar;37(3):686–95.

132. Li Z, Ju X, Silveira PA, Abadir E, Hsu W-H, Hart DNJ, et al. CD83: Activation Marker for Antigen Presenting Cells and Its Therapeutic Potential. Front Immunol [Internet]. 2019 [cited 2020 May 3];10. Available from: https://www.frontiersin.org/articles/10.3389/fimmu.2019.01312/full

133. Kruse M, Meinl E, Henning G, Kuhnt C, Berchtold S, Berger T, et al. Signaling lymphocytic activation molecule is expressed on mature CD83+ dendritic cells and is up-regulated by IL-1 beta. J Immunol. 2001 Aug 15;167(4):1989–95.

134. Partida-Sánchez S, Goodrich S, Kusser K, Oppenheimer N, Randall TD, Lund FE. Regulation of dendritic cell trafficking by the ADP-ribosyl cyclase CD38: impact on the development of humoral immunity. Immunity. 2004 Mar;20(3):279–91.

135. Fedele G, Frasca L, Palazzo R, Ferrero E, Malavasi F, Ausiello CM. CD38 is expressed on human mature monocyte-derived dendritic cells and is functionally involved in CD83 expression and IL-12 induction. Eur J Immunol. 2004 May;34(5):1342–50.

136. MartIn-Fontecha A, Sebastiani S, Höpken UE, Uguccioni M, Lipp M, Lanzavecchia A, et al. Regulation of dendritic cell migration to the draining lymph node: impact on T lymphocyte traffic and priming. J Exp Med. 2003 Aug 18;198(4):615–21.

137. Mason LMK, Wagemakers A, Veer C van ‘t, Oei A, Pot WJ van der, Ahmed K, et al. Borrelia burgdorferi Induces TLR2-Mediated Migration of Activated Dendritic Cells in an Ex Vivo Human Skin Model. PLOS ONE. 2016 Oct 3;11(10):e0164040.

138. Gottschalk C, Kurts C. The Debate about Dendritic Cells and Macrophages in the Kidney. Front Immunol [Internet]. 2015 [cited 2020 May 3];6. Available from: https://www.frontiersin.org/articles/10.3389/fimmu.2015.00435/full

139. Ferenbach D, Hughes J. Macrophages and dendritic cells: what is the difference? Kidney International. 2008 Jul 1;74(1):5–7.

140. Berende A, Oosting M, Kullberg B-J, Netea MG, Joosten LA. Activation of innate host defense mechanisms by Borrelia. European Cytokine Network. 2010 Feb 12;21(1):7–18.

141. Bernardino ALF, Myers TA, Alvarez X, Hasegawa A, Philipp MT. Toll-Like Receptors: Insights into Their Possible Role in the Pathogenesis of Lyme Neuroborreliosis. Infect Immun. 2008 Oct;76(10):4385–95.

142. Wooten RM, Ma Y, Yoder RA, Brown JP, Weis JH, Zachary JF, et al. Toll-like receptor 2 is required for innate, but not acquired, host defense to Borrelia burgdorferi. J Immunol. 2002 Jan 1;168(1): 348–55.

143. Yoder A, Wang X, Ma Y, Philipp MT, Heilbrun M, Weis JH, et al. Tripalmitoyl-S-Glyceryl-Cysteine-Dependent OspA Vaccination of Toll-Like Receptor 2-Deficient Mice Results in Effective Protection from Borrelia burgdorferi Challenge. Infection and Immunity. 2003 Jul 1;71(7):3894–900.

144. Hirschfeld M, Kirschning CJ, Schwandner R, Wesche H, Weis JH, Wooten RM, et al. Cutting Edge: Inflammatory Signaling by Borrelia burgdorferi Lipoproteins Is Mediated by Toll-Like Receptor 2. The Journal of Immunology. 1999 Sep 1;163(5):2382–6.

145. Roe K, Gibot S, Verma S. Triggering receptor expressed on myeloid cells-1 (TREM-1): a new player in antiviral immunity? Front Microbiol [Internet]. 2014 [cited 2020 May 17];5. Available from: https://www.frontiersin.org/articles/10.3389/fmicb.2014.00627/full

146. Colonna M. TREM1 Blockade: Killing Two Birds with One Stone. Trends in Immunology. 2019 Sep 1;40(9):781–3.

147. Wooten RM, Weis JJ. Host-pathogen interactions promoting inflammatory Lyme arthritis: use of mouse models for dissection of disease processes. Curr Opin Microbiol. 2001 Jun;4(3):274–9.

148. Wang X-M, Hamza M, Wu T-X, Dionne RA. UP-REGULATION OF IL-6, IL-8 AND CCL2 GENE EXPRESSION AFTER ACUTE INFLAMMATION: CORRELATION TO CLINICAL PAIN. Pain. 2009 Apr;142(3):275–83.

149. Weber B, Schuster S, Zysset D, Rihs S, Dickgreber N, Schürch C, et al. TREM-1 Deficiency Can Attenuate Disease Severity without Affecting Pathogen Clearance. PLOS Pathogens. 2014 Jan 16;10(1):e1003900.

150. Bouquet J, Soloski MJ, Swei A, Cheadle C, Federman S, Billaud J-N, et al. Longitudinal Transcriptome Analysis Reveals a Sustained Differential Gene Expression Signature in Patients Treated for Acute Lyme Disease. mBio [Internet]. 2016 Feb 12 [cited 2020 May 17];7(1). Available from: https://www.ncbi.nlm.nih.gov/pmc/articles/PMC4791844/

151. Myers TA, Kaushal D, Philipp MT. Microglia Are Mediators of Borrelia burgdorferi–Induced Apoptosis in SH-SY5Y Neuronal Cells. PLoS Pathog [Internet]. 2009 Nov 13 [cited 2020 May 17];5(11). Available from: https://www.ncbi.nlm.nih.gov/pmc/articles/PMC2771360/

152. Castelli E, Caputo V, Morello V, Tomasino RM. Local reactions to tick bites. Am J Dermatopathol. 2008 Jun;30(3):241–8.

153. Vasudevan B, Chatterjee M. Lyme Borreliosis and Skin. Indian J Dermatol. 2013;58(3):167–74.

154. Schramm F, Kern A, Barthel C, Nadaud S, Meyer N, Jaulhac B, et al. Microarray Analyses of Inflammation Response of Human Dermal Fibroblasts to Different Strains of Borrelia burgdorferi Sensu Stricto. PLoS One [Internet]. 2012 Jun 29 [cited 2020 May 4];7(6). Available from: https://www.ncbi.nlm.nih.gov/pmc/articles/PMC3386942/

155. Sorrell JM, Caplan AI. Fibroblasts-a diverse population at the center of it all. Int Rev Cell Mol Biol. 2009;276:161–214.

156. Saalbach A, Klein C, Sleeman J, Sack U, Kauer F, Gebhardt C, et al. Dermal fibroblasts induce maturation of dendritic cells. J Immunol. 2007 Apr 15;178(8):4966–74.

157. Steere AC, Duray PH, Butcher EC. Spirochetal antigens and lymphoid cell surface markers in Lyme synovitis. Comparison with rheumatoid synovium and tonsillar lymphoid tissue. Arthritis Rheum. 1988 Apr;31(4):487–95.

158. Cawston TE, Mercer E, de Silva M, Hazleman BL. Metalloproteinases and collagenase inhibitors in rheumatoid synovial fluid. Arthritis Rheum. 1984 Mar;27(3):285–90.

159. Hu LT, Eskildsen MA, Masgala C, Steere AC, Arner EC, Pratta MA, et al. Host metalloproteinases in Lyme arthritis. Arthritis Rheum. 2001 Jun;44(6):1401–10.

160. Lin B, Kidder JM, Noring R, Steere AC, Klempner MS, Hu LT. Differences in synovial fluid levels of matrix metalloproteinases suggest separate mechanisms of pathogenesis in Lyme arthritis before and after antibiotic treatment. J Infect Dis. 2001 Jul 15;184(2):174–80.

161. Behera AK, Hildebrand E, Scagliotti J, Steere AC, Hu LT. Induction of Host Matrix Metalloproteinases by Borrelia burgdorferi Differs in Human and Murine Lyme Arthritis. Infect Immun. 2005 Jan;73(1): 126–34.

162. Gebbia JA, Coleman JL, Benach JL. Borrelia Spirochetes Upregulate Release and Activation of Matrix Metalloproteinase Gelatinase B (MMP-9) and Collagenase 1 (MMP-1) in Human Cells. Infect Immun. 2001 Jan;69(1):456–62.

163. Parsonage G, Filer AD, Haworth O, Nash GB, Rainger GE, Salmon M, et al. A stromal address code defined by fibroblasts. Trends Immunol. 2005 Mar;26(3):150–6.

164. Ebnet K, Brown KD, Siebenlist UK, Simon MM, Shaw S. Borrelia burgdorferi activates nuclear factor-kappa B and is a potent inducer of chemokine and adhesion molecule gene expression in endothelial cells and fibroblasts. J Immunol. 1997 Apr 1;158(7):3285–92.

165. Jones NC, Germain A, Riley KE, Bautista C, Taylor W, Wells AF. Borrelia burgdorferi decreases hyaluronan synthesis but increases IL-6 production by fibroblasts. Microb Pathog. 1994 Apr;16(4):261–7.

166. Müllegger RR, Means TK, Shin JJ, Lee M, Jones KL, Glickstein LJ, et al. Chemokine signatures in the skin disorders of Lyme borreliosis in Europe: predominance of CXCL9 and CXCL10 in erythema migrans and acrodermatitis and CXCL13 in lymphocytoma. Infect Immun. 2007 Sep;75(9):4621–8.

167. de Koning J. Histopathologic patterns of erythema migrans and borrelial lymphocytoma. Clin Dermatol. 1993 Sep;11(3):377–83.

168. Dame TM, Orenzoff BL, Palmer LE, Furie MB. IFN-γ Alters the Response of Borrelia burgdorferi-Activated Endothelium to Favor Chronic Inflammation. The Journal of Immunology. 2007 Jan 15;178(2): 1172–9.

169. Salazar JC, Pope CD, Sellati TJ, Feder HM, Kiely TG, Dardick KR, et al. Coevolution of Markers of Innate and Adaptive Immunity in Skin and Peripheral Blood of Patients with Erythema Migrans. The Journal of Immunology. 2003 Sep 1;171(5):2660–70.

170. Gross DM, Steere AC, Huber BT. T Helper 1 Response Is Dominant and Localized to the Synovial Fluid in Patients with Lyme Arthritis. The Journal of Immunology. 1998 Jan 15;160(2):1022–8.

171. Gergel EI, Furie MB. Populations of Human T Lymphocytes That Traverse the Vascular Endothelium Stimulated by Borrelia burgdorferi Are Enriched with Cells That Secrete Gamma Interferon. Infection and Immunity. 2004 Mar 1;72(3):1530–6.

172. Burns MJ, Sellati TJ, Teng EI, Furie MB. Production of interleukin-8 (IL-8) by cultured endothelial cells in response to Borrelia burgdorferi occurs independently of secreted [corrected] IL-1 and tumor necrosis factor alpha and is required for subsequent transendothelial migration of neutrophils. Infection and Immunity. 1997 Apr 1;65(4):1217–22.

173. Burns MJ, Furie MB. Borrelia burgdorferi and Interleukin-1 Promote the Transendothelial Migration of Monocytes In Vitro by Different Mechanisms. Infection and Immunity. 1998 Oct 1;66(10):4875–83.

174. Böggemeyer E, Stehle T, Schaible UE, Hahne M, Vestweber D, Simon MM. Borrelia burgdorferi upregulates the adhesion molecules E-selectin, P-selectin, ICAM-1 and VCAM-1 on mouse endothelioma cells in vitro. Cell Adhes Commun. 1994 Jun;2(2):145–57.

175. Sellati TJ, Burns MJ, Ficazzola MA, Furie MB. Borrelia burgdorferi upregulates expression of adhesion molecules on endothelial cells and promotes transendothelial migration of neutrophils in vitro. Infection and Immunity. 1995 Nov 1;63(11):4439–47.

176. Loetscher P, Seitz M, Clark-Lewis I, Baggiolini M, Moser B. Monocyte chemotactic proteins MCP-1, MCP-2, and MCP-3 are major attractants for human CD4+ and CD8+ T lymphocytes. The FASEB Journal. 1994 Oct 1;8(13):1055–60.

177. Liao F, Rabin RL, Yannelli JR, Koniaris LG, Vanguri P, Farber JM. Human Mig chemokine: biochemical and functional characterization. J Exp Med. 1995 Nov 1;182(5):1301–14.

178. Taub DD, Lloyd AR, Conlon K, Wang JM, Ortaldo JR, Harada A, et al. Recombinant human interferon-inducible protein 10 is a chemoattractant for human monocytes and T lymphocytes and promotes T cell adhesion to endothelial cells. J Exp Med. 1993 Jun 1;177(6):1809–14.

179. Cole KE, Strick CA, Paradis TJ, Ogborne KT, Loetscher M, Gladue RP, et al. Interferon–inducible T Cell Alpha Chemoattractant (I-TAC): A Novel Non-ELR CXC Chemokine with Potent Activity on Activated T Cells through Selective High Affinity Binding to CXCR3. J Exp Med. 1998 Jun 15;187(12):2009–21.

180. Bazan JF, Bacon KB, Hardiman G, Wang W, Soo K, Rossi D, et al. A new class of membrane-bound chemokine with a CX3C motif. Nature. 1997 Feb 13;385(6617):640–4.

181. Moro-García MA, Mayo JC, Sainz RM, Alonso-Arias R. Influence of Inflammation in the Process of T Lymphocyte Differentiation: Proliferative, Metabolic, and Oxidative Changes. Front Immunol [Internet]. 2018 Mar 1 [cited 2020 May 19];9. Available from: https://www.ncbi.nlm.nih.gov/pmc/articles/PMC5839096/

182. Cope AP. Studies of T-cell activation in chronic inflammation. Arthritis Res. 2002;4(Suppl 3):S197–211.

183. Skapenko A, Leipe J, Lipsky PE, Schulze-Koops H. The role of the T cell in autoimmune inflammation. Arthritis Res Ther. 2005;7(Suppl 2): S4–14.

184. Divan A, Budd RC, Tobin RP, Newell-Rogers MK. γδ T Cells and dendritic cells in refractory Lyme arthritis. J Leukoc Biol. 2015 Apr;97(4):653–63.

185. Duray PH, Steere AC. Clinical pathologic correlations of Lyme disease by stage. Ann N Y Acad Sci. 1988;539:65–79.

186. Duray PH. Histopathology of clinical phases of human Lyme disease. Rheum Dis Clin North Am. 1989 Nov;15(4):691–710.

187. Forsberg P, Ernerudh J, Ekerfelt C, Roberg M, Vrethem M, Bergström S. The outer surface proteins of Lyme disease borrelia spirochetes stimulate T cells to secrete interferon-gamma (IFN-gamma): diagnostic and pathogenic implications. Clin Exp Immunol. 1995 Sep;101(3):453–60.

188. Acosta Davila JA, Hernandez De Los Rios A. An Overview of Peripheral Blood Mononuclear Cells as a Model for Immunological Research of Toxoplasma gondii and Other Apicomplexan Parasites. Front Cell Infect Microbiol [Internet]. 2019 [cited 2020 May 20];9. Available from: https://www.frontiersin.org/articles/10.3389/fcimb.2019.00024/full

189. Autissier P, Soulas C, Burdo TH, Williams KC. Evaluation of a 12-color flow cytometry panel to study lymphocyte, monocyte, and dendritic cell subsets in humans. Cytometry A. 2010 May;77(5):410–9.

190. Park S-H, Moon Y. Integrated stress response-altered pro-inflammatory signals in mucosal immune-related cells. Immunopharmacol Immunotoxicol. 2013 Apr;35(2):205–14.

191. Fontana MF, Banga S, Barry KC, Shen X, Tan Y, Luo Z-Q, et al. Secreted bacterial effectors that inhibit host protein synthesis are critical for induction of the innate immune response to virulent Legionella pneumophila. PLoS Pathog. 2011 Feb;7(2):e1001289.

192. Shrestha N, Bahnan W, Wiley DJ, Barber G, Fields KA, Schesser K. Eukaryotic Initiation Factor 2 (eIF2) Signaling Regulates Proinflammatory Cytokine Expression and Bacterial Invasion. J Biol Chem. 2012 Aug 17;287(34):28738–44.

193. Arvikar SL, Steere AC. Diagnosis and Treatment of Lyme Arthritis. Infectious Disease Clinics of North America. 2015 Jun 1;29(2):269–80.

194. Crandall H, Dunn DM, Ma Y, Wooten RM, Zachary JF, Weis JH, et al. Gene Expression Profiling Reveals Unique Pathways Associated with Differential Severity of Lyme Arthritis. The Journal of Immunology. 2006 Dec 1;177(11):7930–42.

195. Ma Y, Seiler KP, Eichwald EJ, Weis JH, Teuscher C, Weis JJ. Distinct Characteristics of Resistance toBorrelia burgdorferi-Induced Arthritis in C57BL/6N Mice. Infection and Immunity. 1998 Jan 1;66(1):161–8.

196. Brown CR, Reiner SL. Clearance of Borrelia burgdorferi May Not Be Required for Resistance to Experimental Lyme Arthritis. Infection and Immunity. 1998 May 1;66(5):2065–71.

197. Petzke MM, Brooks A, Krupna MA, Mordue D, Schwartz I. Recognition of Borrelia burgdorferi, the Lyme Disease Spirochete, by TLR7 and TLR9 Induces a Type I IFN Response by Human Immune Cells. The Journal of Immunology. 2009 Oct 15;183(8):5279–92.

198. Casselli T, Qureshi H, Peterson E, Perley D, Blake E, Jokinen B, et al. MicroRNA and mRNA Transcriptome Profiling in Primary Human Astrocytes Infected with Borrelia burgdorferi. PLoS One [Internet]. 2017 Jan 30;12(1). Available from: http://www.ncbi.nlm.nih.gov/pmc/articles/PMC5279786/

199. Pekny M, Pekna M. Astrocyte Reactivity and Reactive Astrogliosis: Costs and Benefits. Physiological Reviews. 2014 Oct 1;94(4):1077–98.

200. Khakh BS, Sofroniew MV. Diversity of astrocyte functions and phenotypes in neural circuits. Nature Neuroscience. 2015 Jul;18(7):942–52.

201. Castro L de, A J. How ERAP1 and ERAP2 Shape the Peptidomes of Disease-Associated MHC-I Proteins. Front Immunol [Internet]. 2018 [cited 2020 May 21];9. Available from: https://www.frontiersin.org/articles/10.3389/fimmu.2018.02463/full

202. Baker PJ. Chronic Lyme disease: in defense of the scientific enterprise. FASEB J. 2010 Nov;24(11):4175–7.

203. Feder HM, Johnson BJB, O'Connell S, Shapiro ED, Steere AC, Wormser GP. A Critical Appraisal of "Chronic Lyme Disease." N Engl J Med. 2007 Oct 4;357(14):1422–30.

204. Maloney EL. Controversies in Persistent (Chronic) Lyme Disease. J Infus Nurs. 2016 Nov;39(6):369–75.

205. Milhorat TH, Hammock MK, Fenstermacher JD, Rall DP, Levin VA. Cerebrospinal Fluid Production by the Choroid Plexus and Brain. Science. 1971 Jul 23;173(3994):330–2.

206. Damkier HH, Brown PD, Praetorius J. Cerebrospinal Fluid Secretion by the Choroid Plexus. Physiological Reviews. 2013 Oct 1;93(4): 1847–92.

207. Redzic ZB, Segal MB. The structure of the choroid plexus and the physiology of the choroid plexus epithelium. Advanced Drug Delivery Reviews. 2004 Oct 14;56(12):1695–716.

208. Hanly A, Petito CK. HLA-DR-positive dendritic cells of the normal human choroid plexus: A potential reservoir of HIV in the central nervous system. Human Pathology. 1998 Jan 1;29(1):88–93.

209. Quintana E, Fernández A, Velasco P, Andrés B de, Liste I, Sancho D, et al. DNGR-1+ dendritic cells are located in meningeal membrane and choroid plexus of the noninjured brain. Glia. 2015;63(12):2231–48.

210. Matyszak MK, Lawson LJ, Perry VH, Gordon S. Stromal macrophages of the choroid plexus situated at an interface between the brain and peripheral immune system constitutively express major histocompatibility class II antigens. Journal of Neuroimmunology. 1992 Oct 1;40(2):173–81.

211. Chinnery HR, Ruitenberg MJ, McMenamin PG. Novel Characterization of Monocyte-Derived Cell Populations in the Meninges and Choroid Plexus and Their Rates of Replenishment in Bone Marrow Chimeric Mice. J Neuropathol Exp Neurol. 2010 Sep 1;69(9):896–909.

212. Steffen BJ, Breier G, Butcher EC, Schulz M, Engelhardt B. ICAM-1, VCAM-1, and MAdCAM-1 are expressed on choroid plexus epithelium but not endothelium and mediate binding of lymphocytes in vitro. Am J Pathol. 1996 Jun;148(6):1819–38.

213. Meeker RB, Bragg DC, Poulton W, Hudson L. Transmigration of macrophages across the choroid plexus epithelium in response to the feline immunodeficiency virus. Cell Tissue Res. 2012 Feb;347(2):443–55.

214. Grandgirard D, Gäumann R, Coulibaly B, Dangy J-P, Sie A, Junghanss T, et al. The causative pathogen determines the inflammatory profile in cerebrospinal fluid and outcome in patients with bacterial meningitis. Mediators Inflamm. 2013;2013:312476.

215. Thuong NTT, Vinh DN, Hai HT, Thu DDA, Nhat LTH, Heemskerk D, et al. Pretreatment Cerebrospinal Fluid Bacterial Load Correlates With Inflammatory Response and Predicts Neurological Events During Tuberculous Meningitis Treatment. J Infect Dis. 2019 Feb 23;219(6):986–95.

216. Knudtzen FC, Andersen NS, Jensen TG, Skarphédinsson S. Characteristics and Clinical Outcome of Lyme Neuroborreliosis in a High Endemic Area, 1995–2014: A Retrospective Cohort Study in Denmark. Clin Infect Dis. 2017 Oct 16;65(9):1489–95.

217. Miller JC, von Lackum K, Babb K, McAlister JD, Stevenson B. Temporal Analysis of Borrelia burgdorferi Erp Protein Expression throughout the Mammal-Tick Infectious Cycle. Infect Immun. 2003 Dec;71(12): 6943–52.

218. Andrews S. FastQC: a quality control tool for high throughput sequence data. Available online at: https://www.bioinformatics.babraham.ac.uk/projects/fastqc/. 2019;

219. Bolger AM, Lohse M, Usadel B. Trimmomatic: a flexible trimmer for Illumina sequence data. Bioinformatics. 2014 Aug 1;30(15):2114–20.

220. Kim D, Paggi JM, Park C, Bennett C, Salzberg SL. Graph-based genome alignment and genotyping with HISAT2 and HISAT-genotype. Nature Biotechnology. 2019 Aug;37(8):907–15.

221. Li H, Handsaker B, Wysoker A, Fennell T, Ruan J, Homer N, et al. The Sequence Alignment/Map format and SAMtools. Bioinformatics. 2009 Aug 15;25(16):2078–9.

222. Love MI, Huber W, Anders S. Moderated estimation of fold change and dispersion for RNA-seq data with DESeq2. Genome Biology. 2014 Dec 5;15(12):550.

223. Szklarczyk D, Gable AL, Lyon D, Junge A, Wyder S, Huerta-Cepas J, et al. STRING v11: protein–protein association networks with increased coverage, supporting functional discovery in genome-wide experimental datasets. Nucleic Acids Res. 2019 Jan 8;47(Database issue):D607–13.

224. Mi H, Muruganujan A, Ebert D, Huang X, Thomas PD. PANTHER version 14: more genomes, a new PANTHER GO-slim and improvements in enrichment analysis tools. Nucleic Acids Res. 2019 Jan 8;47(D1):D419–26.

225. Ashburner M, Ball CA, Blake JA, Botstein D, Butler H, Cherry JM, et al. Gene Ontology: tool for the unification of biology. Nat Genet. 2000 May;25(1):25–9.

226. The Gene Ontology Consortium. The Gene Ontology Resource: 20 years and still GOing strong. Nucleic Acids Res. 2019 Jan 8;47(D1):D330–8.

227. Tarca AL, Kathri P, Draghici S. SPIA: Signaling Pathway Impact Analysis (SPIA) using combined evidence of pathway over-representation and unusual signaling perturbations. 2019; Available from: http://bioinformatics.oxfordjournals.org/cgi/reprint/btn577v1

228. Tarca AL, Draghici S, Khatri P, Hassan SS, Mittal P, Kim J, et al. A novel signaling pathway impact analysis. Bioinformatics. 2009 Jan 1;25(1):75–82.

229. Kanehisa M, Goto S. KEGG: Kyoto Encyclopedia of Genes and Genomes. Nucleic Acids Res. 2000 Jan 1;28(1):27–30.

230. Benjamini Y, Krieger AM, Yekutieli D. Adaptive linear step-up procedures that control the false discovery rate. Biometrika. 2006 Sep 1;93(3):491–507.

231. Herbert J, Wilcox JN, Pham KT, Fremeau RT, Zeviani M, Dwork A, et al. Transthyretin: a choroid plexus-specific transport protein in human brain. The 1986 S. Weir Mitchell award. Neurology. 1986 Jul;36(7):900–11.

232. Love AC, Schwartz I, Petzke MM. Borrelia burgdorferi RNA Induces Type I and III Interferons via Toll-Like Receptor 7 and Contributes to Production of NF-κB-Dependent Cytokines. Infection and Immunity. 2014 Jun 1;82(6):2405–16.

233. Miller JC, Maylor-Hagen H, Ma Y, Weis JH, Weis JJ. The Lyme Disease Spirochete Borrelia burgdorferi Utilizes Multiple Ligands, Including RNA, for Interferon Regulatory Factor 3-Dependent Induction of Type I Interferon-Responsive Genes. Infection and Immunity. 2010 Jul 1;78(7):3144–53.

234. Petzke MM, Iyer R, Love AC, Spieler Z, Brooks A, Schwartz I. Borrelia burgdorferi induces a type I interferon response during early stages of disseminated infection in mice. BMC Microbiol [Internet]. 2016 Mar 8 [cited 2019 Dec 2];16. Available from: https://www.ncbi.nlm.nih.gov/pmc/articles/PMC4784397/

235. Petnicki-Ocwieja T, Chung E, Acosta DI, Ramos LT, Shin OS, Ghosh S, et al. TRIF Mediates Toll-Like Receptor 2-Dependent Inflammatory Responses to Borrelia burgdorferi. Infection and Immunity. 2013 Feb 1;81(2):402–10.

236. Boxx GM, Cheng G. The Roles of Type I Interferon in Bacterial Infection. Cell Host Microbe. 2016 Jun 8;19(6):760–9.

237. Pietras EM, Saha SK, Cheng G. The interferon response to bacterial and viral infections. J Endotoxin Res. 2006;12(4):246–50.

238. Rothfuchs AG, Trumstedt C, Wigzell H, Rottenberg ME. Intracellular Bacterial Infection-Induced IFN-γ Is Critically but Not Solely Dependent on Toll-Like Receptor 4-Myeloid Differentiation Factor 88-IFN-αβ-STAT1 Signaling. The Journal of Immunology. 2004 May 15;172(10):6345–53.

239. Shtrichman R, Samuel CE. The role of gamma interferon in antimicrobial immunity. Curr Opin Microbiol. 2001 Jun;4(3):251–9.

240. Charo IF, Ransohoff RM. The Many Roles of Chemokines and Chemokine Receptors in Inflammation. New England Journal of Medicine. 2006 Feb 9;354(6):610–21.

241. Sprenger H, Krause A, Kaufmann A, Priem S, Fabian D, Burmester GR, et al. Borrelia burgdorferi induces chemokines in human monocytes. Infect Immun. 1997 Nov;65(11):4384–8.

242. Dwinell MB, Eckmann L, Leopard JD, Varki NM, Kagnoff MF. Chemokine receptor expression by human intestinal epithelial cells. Gastroenterology. 1999 Aug 1;117(2):359–67.

243. Schmaußer B, Endrich S, Brändlein S, Schär J, Beier D, Müller-Hermelink H-K, et al. The chemokine receptor CCR7 is expressed on epithelium of non-inflamed gastric mucosa, Helicobacter pylori gastritis, gastric carcinoma and its precursor lesions and up-regulated by H. pylori. Clin Exp Immunol. 2005 Feb;139(2):323–7.

244. Tietz S, Engelhardt B. Brain barriers: Crosstalk between complex tight junctions and adherens junctions. J Cell Biol. 2015 May 25;209(4):493–506.

245. Christensen IB, Mogensen EN, Damkier HH, Praetorius J. Choroid plexus epithelial cells express the adhesion protein P-cadherin at cell-cell contacts and syntaxin-4 in the luminal membrane domain. Am J Physiol Cell Physiol. 2018 May 1;314(5):C519–33.

246. Belman AL, Reynolds L, Preston T, Postels D, Grimson R, Coyle PK. Cerebrospinal Fluid Findings in Children With Lyme Disease-Associated Facial Nerve Palsy. Arch Pediatr Adolesc Med. 1997 Dec 1;151(12):1224–8.

247. Angel TE, Jacobs JM, Smith RP, Pasternack MS, Elias S, Gritsenko MA, et al. Cerebrospinal fluid proteome of patients with acute Lyme disease. J Proteome Res. 2012 Oct 5;11(10):4814–22.

248. Cerar T, Ogrinc K, Lotrič-Furlan S, Kobal J, Levičnik-Stezinar S, Strle F, et al. Diagnostic Value of Cytokines and Chemokines in Lyme Neuroborreliosis. Clin Vaccine Immunol. 2013 Oct 1;20(10):1578–84.

249. Spector R, Keep RF, Robert Snodgrass S, Smith QR, Johanson CE. A balanced view of choroid plexus structure and function: Focus on adult humans. Experimental Neurology. 2015 May 1;267:78–86.

250. Chung Y, Zhang N, Wooten RM. Borrelia burgdorferi Elicited-IL-10 Suppresses the Production of Inflammatory Mediators, Phagocytosis, and Expression of Co-Stimulatory Receptors by Murine Macrophages and/or Dendritic Cells. PLOS ONE. 2013 Dec 19;8(12):e84980.

251. Dennis VA, Dixit S, O'Brien SM, Alvarez X, Pahar B, Philipp MT. Live Borrelia burgdorferi Spirochetes Elicit Inflammatory Mediators from Human Monocytes via the Toll-Like Receptor Signaling Pathway. Infection and Immunity. 2009 Mar 1;77(3):1238–45.

252. Krupna-Gaylord MA, Liveris D, Love AC, Wormser GP, Schwartz I, Petzke MM. Induction of Type I and Type III Interferons by Borrelia burgdorferi Correlates with Pathogenesis and Requires Linear Plasmid 36. PLoS One [Internet]. 2014 Jun 19 [cited 2019 Dec 24];9(6). Available from: https://www.ncbi.nlm.nih.gov/pmc/articles/PMC4063763/

253. de Graaf MT, Smitt PAES, Luitwieler RL, van Velzen C, van den Broek PDM, Kraan J, et al. Central memory CD4+ T cells dominate the normal cerebrospinal fluid. Cytometry B Clin Cytom. 2011 Jan;80(1):43–50.

254. Meeker RB, Williams K, Killebrew DA, Hudson LC. Cell trafficking through the choroid plexus. Cell Adh Migr. 2012 Sep 1;6(5):390–6.

255. Smith DF, Galkina E, Ley K, Huo Y. GRO family chemokines are specialized for monocyte arrest from flow. American Journal of Physiology-Heart and Circulatory Physiology. 2005 Nov 1;289(5):H1976–84.

256. Ahuja SK, Murphy PM. The CXC Chemokines Growth-regulated Oncogene (GRO) α, GROβ, GROγ, Neutrophil-activating Peptide-2, and Epithelial Cell-derived Neutrophil-activating Peptide-78 Are Potent Agonists for the Type B, but Not the Type A, Human Interleukin-8 Receptor. J Biol Chem. 1996 Aug 23;271(34):20545–50.

257. Schumacher C, Clark-Lewis I, Baggiolini M, Moser B. High- and low-affinity binding of GRO alpha and neutrophil-activating peptide 2 to interleukin 8 receptors on human neutrophils. Proc Natl Acad Sci U S A. 1992 Nov 1;89(21):10542–6.

258. Roche JK, Keepers TR, Gross LK, Seaner RM, Obrig TG. CXCL1/KC and CXCL2/MIP-2 Are Critical Effectors and Potential Targets for Therapy of Escherichia coli O157:H7-Associated Renal Inflammation. Am J Pathol. 2007 Feb;170(2):526–37.

259. Brown CR, Blaho VA, Loiacono CM. Susceptibility to Experimental Lyme Arthritis Correlates with KC and Monocyte Chemoattractant Protein-1 Production in Joints and Requires Neutrophil Recruitment Via CXCR2. The Journal of Immunology. 2003 Jul 15;171(2):893–901.

260. Steinmann U, Borkowski J, Wolburg H, Schröppel B, Findeisen P, Weiss C, et al. Transmigration of polymorphnuclear neutrophils and monocytes through the human blood-cerebrospinal fluid barrier after bacterial infection in vitro. Journal of Neuroinflammation. 2013 Feb 28;10(1):832.

261. Borkowski J, Li L, Steinmann U, Quednau N, Stump-Guthier C, Weiss C, et al. Neisseria meningitidiselicits a pro-inflammatory response involving IκBζ in a human blood-cerebrospinal fluid barrier model. Journal of Neuroinflammation. 2014 Sep 13;11(1):163.

262. Schwerk C, Adam R, Borkowski J, Schneider H, Klenk M, Zink S, et al. In vitro transcriptome analysis of porcine choroid plexus epithelial cells in response to Streptococcus suis: release of pro-inflammatory cytokines and chemokines. Microbes and Infection. 2011 Oct 1;13(11):953–62.

263. Schneider H, Weber CE, Schoeller J, Steinmann U, Borkowski J, Ishikawa H, et al. Chemotaxis of T-cells after infection of human choroid plexus papilloma cells with Echovirus 30 in an in vitro model of the blood-cerebrospinal fluid barrier. Virus Res. 2012 Dec;170(1–2):66–74.

264. Cepok S, Zhou D, Vogel F, Rosche B, Grummel V, Sommer N, et al. The Immune Response at Onset and During Recovery From Borrelia burgdorferi Meningoradiculitis. Arch Neurol. 2003 Jun 1;60(6):849–55.

265. Rupprecht TA, Koedel U, Fingerle V, Pfister H-W. The Pathogenesis of Lyme Neuroborreliosis: From Infection to Inflammation. Mol Med. 2008;14(3–4):205–12.

266. Schwerk C, Tenenbaum T, Kim KS, Schroten H. The choroid plexus—a multi-role player during infectious diseases of the CNS. Front Cell Neurosci [Internet]. 2015 Mar 12 [cited 2019 Mar 26];9. Available from: https://www.ncbi.nlm.nih.gov/pmc/articles/PMC4357259/

267. Wolburg H, Wolburg-Buchholz K, Liebner S, Engelhardt B. Claudin-1, claudin-2 and claudin-11 are present in tight junctions of choroid plexus epithelium of the mouse. Neurosci Lett. 2001 Jul 13;307(2):77–80.

268. Steinemann A, Galm I, Chip S, Nitsch C, Maly IP. Claudin-1, -2 and -3 Are Selectively Expressed in the Epithelia of the Choroid Plexus of the Mouse from Early Development and into Adulthood While Claudin-5 is Restricted to Endothelial Cells. Front Neuroanat [Internet]. 2016 [cited 2019 Nov 4];10. Available from: https://www.frontiersin.org/articles/10.3389/fnana.2016.00016/full

269. Marques F, Sousa JC, Coppola G, Falcao AM, Rodrigues AJ, Geschwind DH, et al. Kinetic Profile of the Transcriptome Changes Induced in the Choroid Plexus by Peripheral Inflammation. J Cereb Blood Flow Metab. 2009 May 1;29(5):921–32.

270. Hayashi S, Takeichi M. Emerging roles of protocadherins: from self-avoidance to enhancement of motility. J Cell Sci. 2015 Apr 15;128(8):1455–64.

271. Lobas MA, Helsper L, Vernon CG, Schreiner D, Zhang Y, Holtzman MJ, et al. Molecular heterogeneity in the choroid plexus epithelium: the 22-member γ-protocadherin family is differentially expressed, apically localized, and implicated in CSF regulation. Journal of Neurochemistry. 2012;120(6):913–27.

272. Rajasekaran SA, Barwe SP, Rajasekaran AK. Multiple Functions of Na,K-ATPase in Epithelial Cells. Seminars in Nephrology. 2005 Sep 1;25(5):328–34.

273. Vagin O, Tokhtaeva E, Sachs G. The role of the beta1 subunit of the Na,K-ATPase and its glycosylation in cell-cell adhesion. J Biol Chem. 2006 Dec 22;281(51):39573–87.

274. Rajasekaran SA, Palmer LG, Quan K, Harper JF, Ball WJ, Bander NH, et al. Na,K-ATPase beta-subunit is required for epithelial polarization, suppression of invasion, and cell motility. Mol Biol Cell. 2001 Feb;12(2):279–95.

275. Rajasekaran SA, Hu J, Gopal J, Gallemore R, Ryazantsev S, Bok D, et al. Na,K-ATPase inhibition alters tight junction structure and permeability in human retinal pigment epithelial cells. American Journal of Physiology-Cell Physiology. 2003 Jun 1;284(6):C1497–507.

276. Schwerk C, Papandreou T, Schuhmann D, Nickol L, Borkowski J, Steinmann U, et al. Polar Invasion and Translocation of Neisseria meningitidis and Streptococcus suis in a Novel Human Model of the Blood-Cerebrospinal Fluid Barrier. PLOS ONE. 2012 Jan 11;7(1):e30069.

277. Coleman JL, Roemer EJ, Benach JL. Plasmin-Coated Borrelia burgdorferi Degrades Soluble and Insoluble Components of the Mammalian Extracellular Matrix. Infect Immun. 1999 Aug;67(8):3929–36.

278. Yang Y, Estrada EY, Thompson JF, Liu W, Rosenberg GA. Matrix metalloproteinase-mediated disruption of tight junction proteins in cerebral vessels is reversed by synthetic matrix metalloproteinase inhibitor in focal ischemia in rat. J Cereb Blood Flow Metab. 2007 Apr;27(4):697–709.

279. Steere AC, Duray PH, Butcher EC. Spirochetal antigens and lymphoid cell surface markers in lyme synovitis. Arthritis & Rheumatism. 1988;31(4):487–95.

280. Coyle PK, Schutzer SE, Deng Z, Krupp LB, Belman AL, Benach JL, et al. Detection of Borrelia burgdorferi-specific antigen in antibody-negative cerebrospinal fluid in neurologic Lyme disease. Neurology. 1995 Nov;45(11):2010–5.

281. Parthasarathy G, Fevrier HB, Philipp MT. Non-viable Borrelia burgdorferi induce inflammatory mediators and apoptosis in human oligodendrocytes. Neuroscience Letters. 2013 Nov 27;556:200–3.

282. Crossland NA, Alvarez X, Embers ME. Late Disseminated Lyme Disease: Associated Pathology and Spirochete Persistence Posttreatment in Rhesus Macaques. The American Journal of Pathology. 2018 Mar 1;188(3):672–82.

283. Ramesh G, Borda JT, Gill A, Ribka EP, Morici LA, Mottram P, et al. Possible role of glial cells in the onset and progression of Lyme neuroborreliosis. J Neuroinflammation. 2009 Aug 25;6:23.

284. Coughlin JM, Yang T, Rebman AW, Bechtold KT, Du Y, Mathews WB, et al. Imaging glial activation in patients with post-treatment Lyme disease symptoms: a pilot study using [11C]DPA-713 PET. Journal of Neuroinflammation. 2018 Dec 19;15(1):346.

285. Giaume C, McCarthy KD. Control of gap-junctional communication in astrocytic networks. Trends Neurosci. 1996 Aug;19(8):319–25.

286. Rouach N, Koulakoff A, Abudara V, Willecke K, Giaume C. Astroglial Metabolic Networks Sustain Hippocampal Synaptic Transmission. Science. 2008 Dec 5;322(5907):1551–5.

287. Allaman I, Bélanger M, Magistretti PJ. Astrocyte–neuron metabolic relationships: for better and for worse. Trends in Neurosciences. 2011 Feb;34(2):76–87.

288. Christopherson KS, Ullian EM, Stokes CCA, Mullowney CE, Hell JW, Agah A, et al. Thrombospondins are astrocyte-secreted proteins that promote CNS synaptogenesis. Cell. 2005 Feb 11;120(3):421–33.

289. Eroglu C, Barres BA. Regulation of synaptic connectivity by glia. Nature. 2010 Nov 11;468(7321):223–31.

290. Ullian EM, Christopherson KS, Barres BA. Role for glia in synaptogenesis. Glia. 2004 Aug 15;47(3):209–16.

291. Ullian EM, Sapperstein SK, Christopherson KS, Barres BA. Control of synapse number by glia. Science. 2001 Jan 26;291(5504):657–61.

292. Mederos S, González-Arias C, Perea G. Astrocyte–Neuron Networks: A Multilane Highway of Signaling for Homeostatic Brain Function. Front Synaptic Neurosci [Internet]. 2018 Nov 27 [cited 2020 May 29];10. Available from: https://www.ncbi.nlm.nih.gov/pmc/articles/PMC6277918/

293. Liebner S, Czupalla CJ, Wolburg H. Current concepts of blood-brain barrier development. Int J Dev Biol. 2011;55(4–5):467–76.

294. Abbott NJ, Rönnbäck L, Hansson E. Astrocyte-endothelial interactions at the blood-brain barrier. Nat Rev Neurosci. 2006 Jan;7(1):41–53.

295. Silver J, Miller JH. Regeneration beyond the glial scar. Nature Reviews Neuroscience. 2004 Feb;5(2):146–56.

296. Sofroniew MV, Vinters HV. Astrocytes: biology and pathology. Acta Neuropathol. 2010 Jan;119(1):7–35.

297. Schiweck J, Eickholt BJ, Murk K. Important Shapeshifter: Mechanisms Allowing Astrocytes to Respond to the Changing Nervous System During Development, Injury and Disease. Front Cell Neurosci [Internet]. 2018 [cited 2020 May 30];12. Available from: https://www.frontiersin.org/articles/10.3389/fncel.2018.00261/full

298. Eng LF, Ghirnikar RS, Lee YL. Glial fibrillary acidic protein: GFAP-thirty-one years (1969-2000). Neurochem Res. 2000 Oct;25(9–10): 1439–51.

299. Burda JE, Bernstein AM, Sofroniew MV. Astrocyte roles in traumatic brain injury. Exp Neurol. 2016 Jan;275(0 3):305–15.

300. Sofroniew MV. Astrogliosis. Cold Spring Harb Perspect Biol [Internet]. 2015 Feb [cited 2020 May 30];7(2). Available from: https://www.ncbi.nlm.nih.gov/pmc/articles/PMC4315924/

301. Becerra-Calixto A, Cardona-Gómez GP. The Role of Astrocytes in Neuroprotection after Brain Stroke: Potential in Cell Therapy. Front Mol Neurosci [Internet]. 2017 [cited 2020 May 30];10. Available from: https://www.frontiersin.org/articles/10.3389/fnmol.2017.00088/full

302. Dong Y, Benveniste EN. Immune function of astrocytes. Glia. 2001;36(2):180–90.

303. Wong GH, Bartlett PF, Clark-Lewis I, Battye F, Schrader JW. Inducible expression of H-2 and Ia antigens on brain cells. Nature. 1984 Aug 23;310(5979):688–91.

304. Vidovic M, Sparacio SM, Elovitz M, Benveniste EN. Induction and regulation of class II major histocompatibility complex mRNA expression in astrocytes by interferon-gamma and tumor necrosis factor-alpha. J Neuroimmunol. 1990 Dec;30(2–3):189–200.

305. Sofroniew MV. Astrocyte barriers to neurotoxic inflammation. Nat Rev Neurosci. 2015 May;16(5):249–63.

306. Zamanian JL, Xu L, Foo LC, Nouri N, Zhou L, Giffard RG, et al. Genomic Analysis of Reactive Astrogliosis. J Neurosci. 2012 May 2;32(18):6391–410.

307. Hamby ME, Coppola G, Ao Y, Geschwind DH, Khakh BS, Sofroniew MV. Inflammatory mediators alter the astrocyte transcriptome and calcium signaling elicited by multiple G-protein-coupled receptors. J Neurosci. 2012 Oct 17;32(42):14489–510.

308. John GR, Lee SC, Song X, Rivieccio M, Brosnan CF. IL-1-regulated responses in astrocytes: relevance to injury and recovery. Glia. 2005 Jan 15;49(2):161–76.

309. Halassa MM, Haydon PG. Integrated brain circuits: astrocytic networks modulate neuronal activity and behavior. Annu Rev Physiol. 2010;72:335–55.

310. Hansen RR, Malcangio M. Astrocytes--multitaskers in chronic pain. Eur J Pharmacol. 2013 Sep 15;716(1–3):120–8.

311. Czéh B, Di Benedetto B. Antidepressants act directly on astrocytes: evidences and functional consequences. Eur Neuropsychopharmacol. 2013 Mar;23(3):171–85.

312. Paradise MB, Naismith SL, Norrie LM, Graeber MB, Hickie IB. The role of glia in late-life depression. Int Psychogeriatr. 2012 Dec;24(12):1878–90.

313. Klose RJ, Bird AP. Genomic DNA methylation: the mark and its mediators. Trends Biochem Sci. 2006 Feb;31(2):89–97.

314. Robertson KD. DNA methylation and human disease. Nat Rev Genet. 2005 Aug;6(8):597–610.

315. Bird A. DNA methylation patterns and epigenetic memory. Genes Dev. 2002 Jan 1;16(1):6–21.

316. Arechederra M, Daian F, Yim A, Bazai SK, Richelme S, Dono R, et al. Hypermethylation of gene body CpG islands predicts high dosage of functional oncogenes in liver cancer. Nature Communications. 2018 Aug 8;9(1):3164.

317. Yang X, Han H, De Carvalho DD, Lay FD, Jones PA, Liang G. Gene body methylation can alter gene expression and is a therapeutic target in cancer. Cancer Cell. 2014 Oct 13;26(4):577–90.

318. Jjingo D, Conley AB, Yi SV, Lunyak VV, Jordan IK. On the presence and role of human gene-body DNA methylation. Oncotarget. 2012 May 9;3(4):462–74.

319. Razin A, Riggs AD. DNA methylation and gene function. Science. 1980 Nov 7;210(4470):604–10.

320. Morgan HD, Santos F, Green K, Dean W, Reik W. Epigenetic reprogramming in mammals. Hum Mol Genet. 2005 Apr 15;14 Spec No 1:R47-58.

321. Li E, Bestor TH, Jaenisch R. Targeted mutation of the DNA methyltransferase gene results in embryonic lethality. Cell. 1992 Jun 12;69(6):915–26.

322. Okano M, Bell DW, Haber DA, Li E. DNA methyltransferases Dnmt3a and Dnmt3b are essential for de novo methylation and mammalian development. Cell. 1999 Oct 29;99(3):247–57.

323. Mayer W, Niveleau A, Walter J, Fundele R, Haaf T. Demethylation of the zygotic paternal genome. Nature. 2000 Feb 3;403(6769):501–2.

324. Riggs AD. X inactivation, differentiation, and DNA methylation. Cytogenet Cell Genet. 1975;14(1):9–25.

325. Goll MG, Bestor TH. Eukaryotic cytosine methyltransferases. Annu Rev Biochem. 2005;74:481–514.

326. Pradhan S, Bacolla A, Wells RD, Roberts RJ. Recombinant human DNA (cytosine-5) methyltransferase. I. Expression, purification, and comparison of de novo and maintenance methylation. J Biol Chem. 1999 Nov 12;274(46):33002–10.

327. Chen T, Li E. Structure and Function of Eukaryotic DNA Methyltransferases. In: Current Topics in Developmental Biology [Internet]. Academic Press; 2004 [cited 2020 May 31]. p. 55–89. (Stem Cells in Development and Disease; vol. 60). Available from: http://www.sciencedirect.com/science/article/pii/S0070215304600032

328. Chen T, Ueda Y, Dodge JE, Wang Z, Li E. Establishment and maintenance of genomic methylation patterns in mouse embryonic stem cells by Dnmt3a and Dnmt3b. Mol Cell Biol. 2003 Aug;23(16):5594–605.

329. Liang G, Chan MF, Tomigahara Y, Tsai YC, Gonzales FA, Li E, et al. Cooperativity between DNA methyltransferases in the maintenance methylation of repetitive elements. Mol Cell Biol. 2002 Jan;22(2):480–91.

330. Jones PA, Liang G. Rethinking how DNA methylation patterns are maintained. Nat Rev Genet. 2009;10(11):805–11.

331. Ji H, Ehrlich LIR, Seita J, Murakami P, Doi A, Lindau P, et al. A comprehensive methylome map of lineage commitment from hematopoietic progenitors. Nature. 2010 Sep 16;467(7313):338–42.

332. Chen Z, Riggs AD. DNA Methylation and Demethylation in Mammals. J Biol Chem. 2011 May 27;286(21):18347–53.

333. Bierne H, Hamon M, Cossart P. Epigenetics and Bacterial Infections. Cold Spring Harb Perspect Med [Internet]. 2012 Dec;2(12). Available from: http://www.ncbi.nlm.nih.gov/pmc/articles/PMC3543073/

334. Maekita T, Nakazawa K, Mihara M, Nakajima T, Yanaoka K, Iguchi M, et al. High levels of aberrant DNA methylation in Helicobacter pylori-infected gastric mucosae and its possible association with gastric cancer risk. Clin Cancer Res. 2006 Feb 1;12(3 Pt 1):989–95.

335. Ding S-Z, Goldberg JB, Hatakeyama M. Helicobacter pylori infection, oncogenic pathways and epigenetic mechanisms in gastric carcinogenesis. Future Oncol. 2010 May;6(5):851–62.

336. Ushijima T, Hattori N. Molecular pathways: involvement of Helicobacter pylori-triggered inflammation in the formation of an epigenetic field defect, and its usefulness as cancer risk and exposure markers. Clin Cancer Res. 2012 Feb 15;18(4):923–9.

337. Bussière FI, Michel V, Mémet S, Avé P, Vivas JR, Huerre M, et al. H. pylori-induced promoter hypermethylation downregulates USF1 and USF2 transcription factor gene expression. Cell Microbiol. 2010 Aug;12(8):1124–33.

338. Yao Y, Tao H, Park DI, Sepulveda JL, Sepulveda AR. Demonstration and characterization of mutations induced by Helicobacter pylori organisms in gastric epithelial cells. Helicobacter. 2006 Aug;11(4):272–86.

339. Stylianou E. Epigenetics of chronic inflammatory diseases. J Inflamm Res. 2018 Dec 20;12:1–14.

340. Nakajima T, Enomoto S, Yamashita S, Ando T, Nakanishi Y, Nakazawa K, et al. Persistence of a component of DNA methylation in gastric mucosae after Helicobacter pylori eradication. J Gastroenterol. 2010;45(1):37–44.

341. Babb K, McAlister JD, Miller JC, Stevenson B. Molecular Characterization of Borrelia burgdorferi erp Promoter/Operator Elements. Journal of Bacteriology. 2004 May 1;186(9):2745–56.

342. Schutzer SE, Fraser-Liggett CM, Casjens SR, Qiu W-G, Dunn JJ, Mongodin EF, et al. Whole-Genome Sequences of Thirteen Isolates of Borrelia burgdorferi. J Bacteriol. 2011 Feb;193(4):1018–20.

343. Barbour AG. Isolation and cultivation of Lyme disease spirochetes. Yale J Biol Med. 1984;57(4):521–5.

344. Zückert WR. Laboratory Maintenance of Borrelia burgdorferi. Current Protocols in Microbiology. 2007;4(1):12C.1.1-12C.1.10.

345. Li H, Dai Y, Luo Z, Nie D. Cloning of a new testis-enriched gene C4orf22 and its role in cell cycle and apoptosis in mouse spermatogenic cells. Mol Biol Rep. 2019 Apr;46(2):2029–38.

346. Singh K, Loreth D, Pöttker B, Hefti K, Innos J, Schwald K, et al. Neuronal Growth and Behavioral Alterations in Mice Deficient for the Psychiatric Disease-Associated Negr1 Gene. Front Mol Neurosci [Internet]. 2018 [cited 2020 Jun 2];11. Available from: https://www.frontiersin.org/articles/10.3389/fnmol.2018.00030/full

347. Hyde CL, Nagle MW, Tian C, Chen X, Paciga SA, Wendland JR, et al. Identification of 15 genetic loci associated with risk of major depression in individuals of European descent. Nature Genetics. 2016 Sep;48(9):1031–6.

348. Noh K, Lee H, Choi T-Y, Joo Y, Kim S-J, Kim H, et al. Negr1 controls adult hippocampal neurogenesis and affective behaviors. Molecular Psychiatry. 2019 Aug;24(8):1189–205.

349. Newell-Litwa KA, Horwitz R, Lamers ML. Non-muscle myosin II in disease: mechanisms and therapeutic opportunities. Dis Model Mech. 2015 Dec 1;8(12):1495–515.

350. Vicente-Manzanares M, Ma X, Adelstein RS, Horwitz AR. Non-muscle myosin II takes centre stage in cell adhesion and migration. Nat Rev Mol Cell Biol. 2009 Nov;10(11):778–90.

351. Luo R, Bai C, Yang L, Zheng Z, Su G, Gao G, et al. DNA methylation subpatterns at distinct regulatory regions in human early embryos. Open Biology. 8(10):180131.

352. Martino D, Saffery R. Characteristics of DNA methylation and gene expression in regulatory features on the Infinium 450k Beadchip [Internet]. Genetics; 2015 Nov [cited 2020 Jun 2]. Available from: http://biorxiv.org/lookup/doi/10.1101/032862

353. Jiménez-Garza O, Linares-Segovia B, Ruiz-García L, Monroy-Torres R, Hernández-Luna MA. 5'UTR methylation in different genes from workers exposed to volatile organic compounds: A new insight for considering an epigenetic mark as a functional correlate. Toxicology Letters. 2020 Sep;330:59–64.

354. Kasai K, Suga K, Izumi T, Akagawa K. Syntaxin 8 has two functionally distinct di-leucine-based motifs. Cell Mol Biol Lett. 2007 Oct 29;13(1):144–54.

355. Bhat SS, Friedmann KS, Knörck A, Hoxha C, Leidinger P, Backes C, et al. Syntaxin 8 is required for efficient lytic granule trafficking in cytotoxic T lymphocytes. Biochimica et Biophysica Acta (BBA) - Molecular Cell Research. 2016 Jul 1;1863(7, Part A):1653–64.

356. Ma MPC, Chircop M. SNX9, SNX18 and SNX33 are required for progression through and completion of mitosis. J Cell Sci. 2012 Sep 15;125(18):4372–82.

357. Zhang J, Zhang X, Guo Y, Xu L, Pei D. Sorting Nexin 33 Induces Mammalian Cell Micronucleated Phenotype and Actin Polymerization by Interacting with Wiskott-Aldrich Syndrome Protein. J Biol Chem. 2009 Aug 7;284(32):21659–69.

358. Dimitrov A, Paupe V, Gueudry C, Sibarita J-B, Raposo G, Vielemeyer O, et al. The gene responsible for Dyggve-Melchior-Clausen syndrome encodes a novel peripheral membrane protein dynamically associated with the Golgi apparatus. Hum Mol Genet. 2009 Feb 1;18(3):440–53.

359. Osipovich AB, Jennings JL, Lin Q, Link AJ, Ruley HE. Dyggve–Melchior–Clausen syndrome: Chondrodysplasia resulting from defects in intracellular vesicle traffic. PNAS. 2008 Oct 21;105(42):16171–6.

360. Yazaki S, Koga M, Ishiguro H, Inada T, Ujike H, Itokawa M, et al. An association study between the dymeclin gene and schizophrenia in the Japanese population. Journal of Human Genetics. 2010 Sep;55(9):631–4.

361. Rothstein JD, Martin L, Levey AI, Dykes-Hoberg M, Jin L, Wu D, et al. Localization of neuronal and glial glutamate transporters. Neuron. 1994 Sep;13(3):713–25.

362. Perego C, Vanoni C, Bossi M, Massari S, Basudev H, Longhi R, et al. The GLT-1 and GLAST Glutamate Transporters Are Expressed on Morphologically Distinct Astrocytes and Regulated by Neuronal Activity in Primary Hippocampal Cocultures. Journal of Neurochemistry. 2000;75(3):1076–84.

363. Lehre KP, Levy LM, Ottersen OP, Storm-Mathisen J, Danbolt NC. Differential expression of two glial glutamate transporters in the rat brain: quantitative and immunocytochemical observations. J Neurosci. 1995 Mar;15(3 Pt 1):1835–53.

364. Mahmoud S, Gharagozloo M, Simard C, Gris D. Astrocytes Maintain Glutamate Homeostasis in the CNS by Controlling the Balance between Glutamate Uptake and Release. Cells [Internet]. 2019 Feb 20 [cited 2020 Jun 2];8(2). Available from: https://www.ncbi.nlm.nih.gov/pmc/articles/PMC6406900/

365. Eulenburg V, Gomeza J. Neurotransmitter transporters expressed in glial cells as regulators of synapse function. Brain Res Rev. 2010 May;63(1–2):103–12.

366. Anderson CM, Swanson RA. Astrocyte glutamate transport: review of properties, regulation, and physiological functions. Glia. 2000 Oct;32(1):1–14.

367. Bechtholt-Gompf AJ, Walther HV, Adams MA, Carlezon WA, Ongür D, Cohen BM. Blockade of astrocytic glutamate uptake in rats induces signs of anhedonia and impaired spatial memory. Neuropsychopharmacology. 2010 Sep;35(10):2049–59.

368. Disorders I of M (US) F on N and NS. Overview of the Glutamatergic System [Internet]. Glutamate-Related Biomarkers in Drug Development for Disorders of the Nervous System: Workshop Summary. National Academies Press (US); 2011 [cited 2020 Jun 2]. Available from: https://www.ncbi.nlm.nih.gov/books/NBK62187/

369. Mei Y-Y, Wu DC, Zhou N. Astrocytic Regulation of Glutamate Transmission in Schizophrenia. Front Psychiatry [Internet]. 2018 Nov 6 [cited 2020 Jun 2];9. Available from: https://www.ncbi.nlm.nih.gov/pmc/articles/PMC6232167/

370. Lawrence T. The Nuclear Factor NF-κB Pathway in Inflammation. Cold Spring Harb Perspect Biol [Internet]. 2009 Dec [cited 2020 Jun 2];1(6). Available from: https://www.ncbi.nlm.nih.gov/pmc/articles/PMC2882124/

371. Korn T, Magnus T, Jung S. Autoantigen specific T cells inhibit glutamate uptake in astrocytes by decreasing expression of astrocytic glutamate transporter GLAST: a mechanism mediated by tumor necrosis factor-alpha. FASEB J. 2005 Nov;19(13):1878–80.

372. Lin C-H, You J-R, Wei K-C, Gean P-W. Stimulating ERK/PI3K/NFκB signaling pathways upon activation of mGluR2/3 restores OGD-induced impairment in glutamate clearance in astrocytes. Eur J Neurosci. 2014 Jan;39(1):83–96.

373. Schepers M, Tiane A, Paes D, Sanchez S, Rombaut B, Piccart E, et al. Targeting Phosphodiesterases—Towards a Tailor-Made Approach in Multiple Sclerosis Treatment. Front Immunol [Internet]. 2019 [cited 2020 Jun 2];10. Available from: https://www.frontiersin.org/articles/10.3389/fimmu.2019.01727/full

374. Li L, Yee C, Beavo JA. CD3- and CD28-Dependent Induction of PDE7 Required for T Cell Activation. Science. 1999 Feb 5;283(5403):848–51.

375. Smith SJ, Brookes-Fazakerley S, Donnelly LE, Barnes PJ, Barnette MS, Giembycz MA. Ubiquitous expression of phosphodiesterase 7A in human proinflammatory and immune cells. American Journal of Physiology-Lung Cellular and Molecular Physiology. 2003 Feb 1;284(2):L279–89.

376. Yang G, McIntyre KW, Townsend RM, Shen HH, Pitts WJ, Dodd JH, et al. Phosphodiesterase 7A-Deficient Mice Have Functional T Cells. The Journal of Immunology. 2003 Dec 15;171(12):6414–20.

377. Li KK, Li F, Li QS, Yang K, Jin B. DNA methylation as a target of epigenetic therapeutics in cancer. Anticancer Agents Med Chem. 2013 Feb;13(2):242–7.

378. Szyf M. Therapeutic implications of DNA methylation. Future Oncol. 2005 Feb;1(1):125–35.

379. Cole J, Morris P, Dickman MJ, Dockrell DH. The therapeutic potential of epigenetic manipulation during infectious diseases. Pharmacol Ther. 2016 Nov;167:85–99.

380. Kelly TK, De Carvalho DD, Jones PA. Epigenetic Modifications as Therapeutic Targets. Nat Biotechnol. 2010 Oct;28(10):1069–78.

381. Luger K, Mäder AW, Richmond RK, Sargent DF, Richmond TJ. Crystal structure of the nucleosome core particle at 2.8 Å resolution. Nature. 1997 Sep;389(6648):251–60.

382. Kornberg RD, Lorch Y. Twenty-Five Years of the Nucleosome, Fundamental Particle of the Eukaryote Chromosome. Cell. 1999 Aug 6;98(3):285–94.

383. Tropberger P, Schneider R. Scratching the (lateral) surface of chromatin regulation by histone modifications. Nat Struct Mol Biol. 2013 Jun;20(6):657–61.

384. Mersfelder EL, Parthun MR. The tale beyond the tail: histone core domain modifications and the regulation of chromatin structure. Nucleic Acids Res. 2006;34(9):2653–62.

385. Bannister AJ, Kouzarides T. Regulation of chromatin by histone modifications. Cell Research. 2011 Mar;21(3):381–95.

386. Strahl BD, Allis CD. The language of covalent histone modifications. Nature. 2000 Jan 6;403(6765):41–5.

387. Jenuwein T, Allis CD. Translating the histone code. Science. 2001 Aug 10;293(5532):1074–80.

388. Benevolenskaya EV. Histone H3K4 demethylases are essential in development and differentiation. Biochem Cell Biol. 2007 Aug;85(4):435–43.

389. Guillemette B, Drogaris P, Lin H-HS, Armstrong H, Hiragami-Hamada K, Imhof A, et al. H3 lysine 4 is acetylated at active gene promoters and is regulated by H3 lysine 4 methylation. PLoS Genet. 2011 Mar;7(3):e1001354.

390. Barski A, Cuddapah S, Cui K, Roh T-Y, Schones DE, Wang Z, et al. High-resolution profiling of histone methylations in the human genome. Cell. 2007 May 18;129(4):823–37.

391. Creyghton MP, Cheng AW, Welstead GG, Kooistra T, Carey BW, Steine EJ, et al. Histone H3K27ac separates active from poised enhancers and predicts developmental state. Proc Natl Acad Sci USA. 2010 Dec 14;107(50):21931–6.

392. Hamon MA, Cossart P. Histone Modifications and Chromatin Remodeling during Bacterial Infections. Cell Host & Microbe. 2008 Aug 14;4(2):100–9.

393. Basak C, Pathak SK, Bhattacharyya A, Pathak S, Basu J, Kundu M. The Secreted Peptidyl Prolyl cis,trans-Isomerase HP0175 of Helicobacter pylori Induces Apoptosis of Gastric Epithelial Cells in a TLR4- and Apoptosis Signal-Regulating Kinase 1-Dependent Manner. The Journal of Immunology. 2005 May 1;174(9):5672–80.

394. Schmeck B, Beermann W, van Laak V, Zahlten J, Opitz B, Witzenrath M, et al. Intracellular bacteria differentially regulated endothelial cytokine release by MAPK-dependent histone modification. J Immunol. 2005 Sep 1;175(5):2843–50.

395. Hamon MA, Batsché E, Régnault B, Tham TN, Seveau S, Muchardt C, et al. Histone modifications induced by a family of bacterial toxins. PNAS. 2007 Aug 14;104(33):13467–72.

396. Grabiec AM, Potempa J. Epigenetic regulation in bacterial infections: targeting histone deacetylases. Critical Reviews in Microbiology. 2018 May 4;44(3):336–50.

397. Edmunds JW, Mahadevan LC. MAP kinases as structural adaptors and enzymatic activators in transcription complexes. Journal of Cell Science. 2004 Aug 1;117(17):3715–23.

398. Pennini ME, Pai RK, Schultz DC, Boom WH, Harding CV. Mycobacterium tuberculosis 19-kDa Lipoprotein Inhibits IFN-γ-Induced Chromatin Remodeling of MHC2TA by TLR2 and MAPK Signaling. The Journal of Immunology. 2006 Apr 1;176(7):4323–30.

399. Buenrostro J, Wu B, Chang H, Greenleaf W. ATAC-seq: A Method for Assaying Chromatin Accessibility Genome-Wide. Curr Protoc Mol Biol. 2015 Jan 5;109:21.29.1-21.29.9.

400. Bogenhagen DF. Mitochondrial DNA nucleoid structure. Biochimica et Biophysica Acta (BBA) - Gene Regulatory Mechanisms. 2012 Sep 1;1819(9):914–20.

401. Zhang Y, Liu T, Meyer CA, Eeckhoute J, Johnson DS, Bernstein BE, et al. Model-based Analysis of ChIP-Seq (MACS). Genome Biology. 2008 Sep 17;9(9):R137.

402. Stark R, Brown G. DiffBind: Differential binding analysis of ChIP-Seq peak data. :33.

403. Heinz S, Benner C, Spann N, Bertolino E, Lin YC, Laslo P, et al. Simple combinations of lineage-determining transcription factors prime cis-regulatory elements required for macrophage and B cell identities. Mol Cell. 2010 May 28;38(4):576–89.

404. Yu G, Wang L-G, He Q-Y. ChIPseeker: an R/Bioconductor package for ChIP peak annotation, comparison and visualization. Bioinformatics. 2015 Jul 15;31(14):2382–3.

405. Brown CR, Blaho VA, Fritsche KL, Loiacono CM. Stat1 deficiency exacerbates carditis but not arthritis during experimental lyme borreliosis. J Interferon Cytokine Res. 2006 Jun;26(6):390–9.

406. Zenke K, Muroi M, Tanamoto K-I. IRF1 supports DNA binding of STAT1 by promoting its phosphorylation. Immunol Cell Biol. 2018;96(10):1095–103.

407. Abou El Hassan M, Huang K, Eswara MBK, Xu Z, Yu T, Aubry A, et al. Properties of STAT1 and IRF1 enhancers and the influence of SNPs. BMC Mol Biol [Internet]. 2017 Mar 9 [cited 2020 Jun 18];18. Available from: https://www.ncbi.nlm.nih.gov/pmc/articles/PMC5343312/

408. Cassiani-Ingoni R, Cabral ES, Lünemann JD, Garza Z, Magnus T, Gelderblom H, et al. Borrelia burgdorferi Induces TLR1 and TLR2 in Human Microglia and Peripheral Blood Monocytes but Differentially Regulates HLA-Class II Expression. J Neuropathol Exp Neurol. 2006 Jun 1;65(6):540–8.

409. Saura J. Microglial cells in astroglial cultures: a cautionary note. Journal of Neuroinflammation. 2007 Oct 15;4(1):26.

410. Parthasarathy G, Philipp MT. Receptor tyrosine kinases play a significant role in human oligodendrocyte inflammation and cell death associated with the Lyme disease bacterium Borrelia burgdorferi. J Neuroinflammation [Internet]. 2017 May 30 [cited 2020 Jun 18];14. Available from: https://www.ncbi.nlm.nih.gov/pmc/articles/PMC5450372/

411. Gautam A, Dixit S, Philipp MT, Singh SR, Morici LA, Kaushal D, et al. Interleukin-10 alters effector functions of multiple genes induced by Borrelia burgdorferi in macrophages to regulate Lyme disease inflammation. Infect Immun. 2011 Dec;79(12):4876–92.

412. Kirchner A, Koedel U, Fingerle V, Paul R, Wilske B, Pfister HW. Upregulation of matrix metalloproteinase-9 in the cerebrospinal fluid of patients with acute Lyme neuroborreliosis. J Neurol Neurosurg Psychiatry. 2000 Mar;68(3):368–71.

413. Perides G, Charness ME, Tanner LM, Péter O, Satz N, Steere AC, et al. Matrix metalloproteinases in the cerebrospinal fluid of patients with Lyme neuroborreliosis. J Infect Dis. 1998 Feb;177(2):401–8.

414. Di Domenico EG, Cavallo I, Bordignon V, D'Agosto G, Pontone M, Trento E, et al. The Emerging Role of Microbial Biofilm in Lyme Neuroborreliosis. Front Neurol [Internet]. 2018 [cited 2020 Jun 18];9. Available from: https://www.frontiersin.org/articles/10.3389/fneur.2018.01048/full

415. Perides G, Tanner-Brown LM, Eskildsen MA, Klempner MS. Borrelia burgdorferi induces matrix metalloproteinases by neural cultures. Journal of Neuroscience Research. 1999;58(6):779–90.

416. Heilpern AJ, Wertheim W, He J, Perides G, Bronson RT, Hu LT. Matrix Metalloproteinase 9 Plays a Key Role in Lyme Arthritis but Not in Dissemination of Borrelia burgdorferi. Infect Immun. 2009 Jul;77(7):2643–9.

417. Hess J, Angel P, Schorpp-Kistner M. AP-1 subunits: quarrel and harmony among siblings. Journal of Cell Science. 2004 Dec 1;117(25):5965–73.

418. Eferl R, Wagner EF. AP-1: a double-edged sword in tumorigenesis. Nature Reviews Cancer. 2003 Nov;3(11):859–68.

419. Ibrahim SAE-F, Abudu A, Jonhson E, Aftab N, Conrad S, Fluck M. The role of AP-1 in self-sufficient proliferation and migration of cancer cells and its potential impact on an autocrine/paracrine loop. Oncotarget. 2018 Sep 28;9(76):34259–78.

420. Ashida R, Tominaga K, Sasaki E, Watanabe T, Fujiwara Y, Oshitani N, et al. AP-1 and colorectal cancer. Inflammopharmacology. 2005;13(1–3):113–25.

421. Kharman-Biz A, Gao H, Ghiasvand R, Zhao C, Zendehdel K, Dahlman-Wright K. Expression of activator protein-1 (AP-1) family members in breast cancer. BMC Cancer. 2013 Sep 28;13(1):441.

422. Krämer S, Crauwels P, Bohn R, Radzimski C, Szaszák M, Klinger M, et al. AP-1 Transcription Factor Serves as a Molecular Switch between Chlamydia pneumoniae Replication and Persistence. Infection and Immunity. 2015 Jul 1;83(7):2651–60.

423. Wang A, Al-Kuhlani M, Johnston SC, Ojcius DM, Chou J, Dean D. Transcription factor complex AP-1 mediates inflammation initiated by Chlamydia pneumoniae infection. Cell Microbiol. 2013 May;15(5):779–94.

424. Grötsch B, Brachs S, Lang C, Luther J, Derer A, Schlötzer-Schrehardt U, et al. The AP-1 transcription factor Fra1 inhibits follicular B cell differentiation into plasma cells. J Exp Med. 2014 Oct 20;211(11):2199–212.

425. Hartenstein B, Teurich S, Hess J, Schenkel J, Schorpp-Kistner M, Angel P. Th2 cell-specific cytokine expression and allergen-induced airway inflammation depend on JunB. The EMBO Journal. 2002 Dec 1;21(23):6321–9.

426. Angel P, Karin M. The role of Jun, Fos and the AP-1 complex in cell-proliferation and transformation. Biochim Biophys Acta. 1991 Dec 10;1072(2–3):129–57.

427. Yukawa M, Jagannathan S, Vallabh S, Kartashov AV, Chen X, Weirauch MT, et al. AP-1 activity induced by co-stimulation is required for chromatin opening during T cell activation. J Exp Med [Internet]. 2020 Jan 6 [cited 2020 Jun 18];217(1). Available from: https://rupress.org/jem/article/217/1/e20182009/132593/AP-1-activity-induced-by-co-stimulation-is

428. Gao K, Wang CR, Jiang F, Wong AYK, Su N, Jiang JH, et al. Traumatic scratch injury in astrocytes triggers calcium influx to activate the JNK/c-Jun/AP-1 pathway and switch on GFAP expression: Calcium Upregulates GFAP Via the JNK/c-Jun/AP-1 Pathway. Glia. 2013 Dec;61(12):2063–77.

429. Dhandapani KM, Hadman M, Sevilla LD, Wade MF, Mahesh VB, Brann DW. Astrocyte Protection of Neurons ROLE OF TRANSFORMING GROWTH FACTOR-β SIGNALING VIA A c-Jun-AP-1 PROTECTIVE PATHWAY. J Biol Chem. 2003 Oct 31;278(44):43329–39.

430. Behera AK, Thorpe CM, Kidder JM, Smith W, Hildebrand E, Hu LT. Borrelia burgdorferi-induced expression of matrix metalloproteinases from human chondrocytes requires mitogen-activated protein kinase and Janus kinase/signal transducer and activator of transcription signaling pathways. Infect Immun. 2004 May;72(5):2864–71.

431. Katagiri T, Yamazaki S, Fukui Y, Aoki K, Yagita H, Nishina T, et al. JunB plays a crucial role in development of regulatory T cells by promoting IL-2 signaling. Mucosal Immunology. 2019 Sep;12(5):1104–17.

432. Fontana MF, Baccarella A, Pancholi N, Pufall MA, Herbert DR, Kim CC. JUNB is a Key Transcriptional Modulator of Macrophage Activation. J Immunol. 2015 Jan 1;194(1):177–86.

433. Thompson M, Xu D, Williams BRG. ATF3 transcription factor and its emerging roles in immunity and cancer. J Mol Med (Berl). 2009 Nov;87(11):1053–60.

434. Jadhav K, Zhang Y. Activating transcription factor 3 in immune response and metabolic regulation. Liver Research. 2017 Sep 1;1(2):96–102.

435. Thompson MR, Xu D, Williams BRG. Activating transcription factor 3 contributes to Toll-like receptor-mediated macrophage survival via repression of Bax and Bak. J Interferon Cytokine Res. 2013 Nov;33(11):682–93.

APPENDIX A

Table 1 Full list of significant differentially expressed genes for choroid plexus epithelial cells infected with *B. burgdorferi* – Chapter 2

Gene Names	Base Mean	log2FoldChange	padj	Control Mean	Treated 48 Mean
OASL	448.17	1.9238	7.63E-18	93.654	802.687
RSAD2	764.51	1.4247	7.87E-09	230.775	1298.247
IFIT1	8346.65	1.4001	1.51E-10	3453.899	13239.393
CCL5	430.80	1.3553	4.67E-09	174.752	686.852
IFITM1	27173.06	1.3364	1.99E-13	13318.547	41027.568
IFIT3	12167.59	1.2283	6.81E-11	6356.379	17978.807
PPP1R1B	241.47	1.1815	9.29E-07	108.641	374.307
CMPK2	1451.15	1.1521	7.77E-06	588.991	2313.305
HERC6	4050.63	1.0908	2.80E-08	2287.800	5813.465
HERC5	188.00	1.0886	2.14E-07	103.688	272.312
OAS2	10016.30	1.0649	3.93E-06	5325.848	14706.761
OAS1	6135.39	1.0618	1.35E-05	3142.753	9128.029
RTP4	221.62	0.9955	0.000254	104.579	338.651
HSD11B1	718.06	0.9951	1.70E-08	443.592	992.533
USP18	2146.79	0.9890	1.70E-05	1222.883	3070.692
XAF1	2054.46	0.9762	1.13E-07	1271.616	2837.299
INMT	1711.12	0.9706	1.70E-05	999.312	2422.929
IFI44L	2995.77	0.9699	3.27E-07	1845.838	4145.700
ISG15	21665.63	0.9699	0.000247	11334.942	31996.328
SECTM1	79.24	0.9674	0.000655	30.397	128.073
PARP9	4958.89	0.9354	2.80E-08	3192.496	6725.287
NGF	153.50	0.9319	0.00033	85.767	221.243
CXCL2	2684.76	0.9276	3.00E-07	1716.511	3653.008
CDKN1C	1645.23	0.9239	3.66E-06	1033.178	2257.291
SPOCK2	455.73	0.9175	6.00E-05	276.124	635.345
BATF2	240.06	0.9165	0.000655	132.148	347.970
IDO1	68.63	0.9158	0.001608	31.734	105.521
IFI27	1735.28	0.9145	0.00125	889.410	2581.152
GAS1	6260.61	0.8966	1.19E-06	4058.639	8462.586
LRG1	112.72	0.8912	0.000847	64.483	160.947
EPSTI1	4404.34	0.8881	9.00E-07	2880.335	5928.340
CXCL3	364.31	0.8654	0.000102	231.804	496.815
ODF3B	642.22	0.8466	0.001328	389.511	894.921
PLSCR1	3923.08	0.8455	5.73E-07	2654.131	5192.032
ELANE	23.80	0.8378	0.005424	8.920	38.672
CRLF1	398.20	0.8353	0.000538	253.603	542.789
AP3B2	30.46	0.8275	0.00616	11.530	49.387

CD38	311.03	0.8235	8.32E-05	205.946	416.114
MX1	21861.91	0.8191	0.007334	8805.820	34917.998
SMOC1	2802.39	0.8188	0.00248	1721.887	3882.899
LGALS9	2257.86	0.7920	0.008757	1319.674	3196.040
IRF7	4832.52	0.7805	0.002187	3159.848	6505.187
PDK4	452.86	0.7759	0.006053	285.628	620.089
CAMK1G	157.80	0.7704	0.001414	105.371	210.235
EFNA1	38.45	0.7647	0.015876	16.329	60.564
IFI35	9889.28	0.7647	0.004436	6442.943	13335.619
ATOH8	450.69	0.7617	3.52E-05	317.181	584.195
ISG20	170.06	0.7598	0.012529	103.827	236.303
PF4V1	431.88	0.7551	0.009922	273.020	590.735
GBP4	203.89	0.7533	0.013558	125.275	282.513
CDH23	105.83	0.7532	0.01992	59.603	152.055
CYP26B1	3324.10	0.7459	3.12E-05	2365.098	4283.106
SIGLEC17P	15.10	0.7455	0.007334	2.980	27.220
CEBPD	13416.80	0.7417	8.23E-08	9756.188	17077.418
PDE4B	453.60	0.7397	0.018726	276.549	630.641
CXCL1	24802.58	0.7349	1.35E-05	17850.741	31754.418
STAT1	24312.97	0.7346	1.89E-05	17469.009	31156.939
TNFSF10	45.87	0.7335	0.028897	24.007	67.731
OAS3	11840.52	0.7259	0.008201	7931.005	15750.037
IGFBP5	6435.36	0.7204	0.01255	4253.875	8616.835
NGFR	103.34	0.7162	0.032294	61.544	145.129
MYT1L	19.93	0.7161	0.022778	7.255	32.607
CCL13	31.53	0.7147	0.032672	14.274	48.789
LOC101929412	20.08	0.7132	0.01231	4.563	35.602
SMTNL2	21.59	0.7107	0.025255	7.871	35.317
SAMHD1	4581.76	0.7051	8.13E-09	3411.478	5752.051
KCNG2	163.54	0.7048	0.021866	106.579	220.496
TRIM25	7492.37	0.6973	0.000481	5423.863	9560.882
SOCS3	4237.99	0.6951	4.60E-05	3112.299	5363.684
DACT2	199.21	0.6905	0.005831	140.424	257.992
C3	413.70	0.6893	0.037701	264.141	563.268
CA8	25.93	0.6879	0.04867	12.722	39.129
FGFR4	342.51	0.6878	0.032358	223.631	461.395
LINC00475	143.98	0.6859	0.020191	97.426	190.537
C1QTNF1	4196.86	0.6800	2.77E-07	3153.018	5240.702
IFITM3	134616.32	0.6778	2.45E-05	100183.682	169048.962
CPZ	7805.47	0.6735	0.0019	5679.915	9931.032
DHX58	3020.72	0.6698	0.006368	2167.513	3873.921

HELZ2	11186.20	0.6676	0.007739	8014.161	14358.236
KCNJ8	265.72	0.6624	0.013697	188.958	342.483
CCR7	158.55	0.6597	0.009835	113.688	203.407
AMPH	247.46	0.6571	0.002201	181.992	312.937
ENPP2	1627.81	0.6568	0.024745	1138.721	2116.909
G0S2	562.19	0.6562	0.001042	416.806	707.580
CXCL6	37203.61	0.6550	2.30E-05	28074.261	46332.957
CXCL5	884.05	0.6525	0.009551	640.126	1127.972
APOC1	658.41	0.6506	0.010323	476.348	840.480
ISYNA1	29489.12	0.6481	3.17E-07	22525.219	36453.014
PAQR5	694.55	0.6479	0.016003	498.674	890.436
FAM65C	3790.29	0.6446	3.80E-05	2873.558	4707.021
ALG9	6918.94	0.6427	0.00616	5089.152	8748.729
DDX58	2349.17	0.6413	0.019759	1687.631	3010.712
SELENBP1	1305.74	0.6399	0.00025	986.655	1624.817
TLE2	212.86	0.6376	0.046517	148.204	277.519
THEMIS2	713.55	0.6253	0.010589	528.144	898.959
ZP1	97.82	0.6251	0.038453	70.043	125.591
IFIH1	1398.22	0.6235	0.002252	1054.007	1742.431
RAB20	611.30	0.6202	0.000668	465.030	757.576
SLC1A3	1256.51	0.6195	0.029817	913.147	1599.882
SOD2	8623.19	0.6129	0.000137	6635.243	10611.145
PARP10	8678.95	0.6118	0.042829	6278.935	11078.964
ADAMTS15	20417.38	0.6101	0.000254	15704.121	25130.643
SLC15A3	2246.48	0.6071	0.049637	1624.078	2868.879
TGFB3	2571.68	0.6051	0.001641	1967.566	3175.788
ID1	1018.16	0.6027	0.00616	772.151	1264.159
OLFM2	552.76	0.6020	0.004436	421.328	684.199
DTX3L	4507.30	0.5998	0.000723	3474.141	5540.461
IGFBP4	323911.54	0.5998	8.23E-08	254032.810	393790.277
CFB	2104.02	0.5988	0.003654	1607.879	2600.170
SAMD11	307.62	0.5956	0.006791	234.535	380.711
UNC93B1	6459.08	0.5929	0.014694	4882.722	8035.439
RGMA	679.66	0.5897	0.000466	528.371	830.955
IFI44	1716.37	0.5832	0.004908	1322.751	2109.992
APOE	94745.90	0.5739	0.006346	73314.091	116177.699
IFITM2	18767.24	0.5717	0.000815	14705.382	22829.098
SERPINA3	7499.36	0.5659	0.023579	5752.195	9246.524
NDUFA4L2	1429.86	0.5589	0.007507	1116.554	1743.163
CLEC3B	7705.91	0.5588	0.001414	6071.223	9340.600
CYP4X1	3141.67	0.5517	0.023579	2436.368	3846.969

IGFBP3	14520.21	0.5425	0.001586	11542.732	17497.698
C19orf66	6649.66	0.5393	0.034535	5178.861	8120.457
THOC6	1333.77	0.5382	0.002789	1060.170	1607.363
ASS1	12719.21	0.5371	4.11E-05	10222.203	15216.216
UBE2L6	16178.97	0.5343	0.034193	12652.521	19705.421
BEST1	464.03	0.5297	0.041217	363.008	565.059
TRIM21	4075.79	0.5291	0.046668	3184.880	4966.697
APOL6	3085.57	0.5244	0.003758	2470.408	3700.736
PPAP2B	2533.78	0.5238	0.006346	2024.429	3043.132
PODN	804.54	0.5188	0.042954	634.538	974.538
RNF213	14441.39	0.5183	0.008846	11553.140	17329.644
AKR1C1	1478.84	0.5124	0.02802	1177.365	1780.305
NR1H3	1265.29	0.5122	0.007334	1017.278	1513.298
TNFRSF1B	17682.52	0.5020	6.92E-05	14452.644	20912.388
AKR1C3	1193.07	0.5017	0.017555	960.488	1425.651
CA11	1516.51	0.4992	0.002759	1232.563	1800.450
COLEC11	4957.41	0.4960	0.016607	4004.743	5910.071
HES4	4140.44	0.4911	0.038453	3333.376	4947.503
C11orf96	5527.48	0.4877	0.001058	4531.730	6523.222
CCL2	25983.24	0.4794	0.002206	21356.008	30610.466
PDGFRL	6152.46	0.4766	0.002187	5064.676	7240.238
KCNE4	4198.15	0.4705	0.000655	3474.862	4921.445
VWCE	451.84	0.4647	0.018312	371.498	532.186
PISD	10446.39	0.4610	0.001201	8678.277	12214.495
DDIT4	16547.00	0.4602	0.005091	13710.057	19383.947
C10orf10	4334.99	0.4586	0.030155	3567.986	5101.989
SP110	2553.40	0.4581	0.011885	2111.436	2995.357
STAT2	19287.98	0.4566	0.026725	15905.159	22670.802
COL5A3	14742.58	0.4564	0.003422	12251.194	17233.967
HSPA2	2392.15	0.4497	0.038887	1976.499	2807.804
PHYHD1	754.55	0.4420	0.009585	629.842	879.259
MPZ	1948.44	0.4240	0.00894	1642.458	2254.427
GBP2	3103.50	0.4001	0.049661	2633.342	3573.661
PLEKHG3	2343.67	0.3895	0.009922	2008.383	2678.957
TXNIP	14707.53	0.3848	0.042325	12587.712	16827.341
PAMR1	67991.66	0.3830	0.008846	58469.176	77514.136
CHST7	2414.89	0.3733	0.028897	2081.125	2748.655
GGT5	48308.77	0.3662	0.014077	41840.675	54776.864
RASL10B	2537.26	0.3604	0.034321	2199.725	2874.805
CHST2	59735.18	0.3296	0.042954	52523.474	66946.882
CPT1A	7587.48	0.3285	0.034825	6677.758	8497.195

PALLD	35487.29	-0.3054	0.041217	39421.193	31553.388
CAPN2	111661.34	-0.3376	0.047708	125532.075	97790.597
SORT1	20012.41	-0.3431	0.014077	22505.069	17519.752
FRMD4A	10217.04	-0.3571	0.017093	11550.012	8884.064
OSBPL10	3241.84	-0.3674	0.042705	3684.217	2799.458
DKK1	3380.17	-0.3707	0.019039	3840.965	2919.377
BHLHE40	13633.08	-0.3747	0.020191	15515.633	11750.530
CCND1	121589.23	-0.3768	0.008102	138294.436	104884.033
PCDH7	3082.73	-0.3969	0.011885	3533.661	2631.802
CLCN4	650.56	-0.4071	0.034193	750.239	550.886
FRMD5	1238.87	-0.4245	0.01386	1434.914	1042.835
NES	21224.21	-0.4246	0.008757	24564.138	17884.290
MAGI1	1725.13	-0.4272	0.03935	2006.774	1443.490
FAM92A1	1212.11	-0.4273	0.014354	1405.986	1018.234
MYLK	1346.72	-0.4353	0.014211	1566.508	1126.924
C12orf75	7263.94	-0.4509	0.001852	8467.286	6060.595
KIAA1549L	2019.21	-0.4637	0.040845	2384.735	1653.690
NTN4	8292.00	-0.4644	0.001042	9704.817	6879.174
CSPG4	25934.42	-0.4668	0.034321	30644.203	21224.646
LTBP2	49121.85	-0.4692	0.010762	57848.256	40395.452
ATP1B1	1279.56	-0.4777	0.034878	1519.140	1039.990
ARL4C	7714.00	-0.4842	0.000847	9089.598	6338.397
CDKN2B	16386.28	-0.4957	1.70E-05	19317.945	13454.622
MMP1	947.51	-0.4965	0.01112	1127.636	767.376
DIRAS3	5886.67	-0.5023	0.005859	7008.484	4764.856
FLT1	962.05	-0.5036	0.01255	1149.131	774.978
PDGFC	3292.89	-0.5057	4.18E-05	3897.518	2688.269
TM6SF1	494.04	-0.5059	0.015561	591.441	396.640
LAMA3	761.06	-0.5083	0.015414	911.261	610.855
ITGBL1	14063.57	-0.5090	0.000512	16706.643	11420.504
LXN	7618.86	-0.5133	0.002481	9091.339	6146.387
SIGLEC15	524.95	-0.5184	0.032672	634.177	415.728
KCNMA1	570.93	-0.5206	0.046696	692.577	449.279
FGF1	588.74	-0.5241	0.042964	714.932	462.558
COMMD8	1395.17	-0.5248	0.031748	1690.895	1099.450
SERPIND1	733.45	-0.5264	0.03935	890.764	576.129
TPD52L1	598.81	-0.5268	0.024515	724.842	472.773
SERPINE1	346899.04	-0.5281	0.006053	417291.420	276506.653
ZDHHC2	1273.03	-0.5282	0.019212	1539.857	1006.212
MTSS1	2163.89	-0.5315	0.000231	2587.983	1739.797
MYOZ2	384.74	-0.5350	0.017172	466.460	303.025

LMO7	10944.04	-0.5480	0.022213	13372.659	8515.425
ANKRD1	7067.23	-0.5549	2.29E-06	8485.715	5648.743
VEGFC	1349.71	-0.5697	0.000961	1641.112	1058.300
4-Mar	944.63	-0.5788	0.001857	1154.753	734.505
AHNAK2	23919.03	-0.5840	0.002201	29322.810	18515.250
C5orf28	621.66	-0.5869	0.033145	778.005	465.316
EDN1	162.77	-0.5913	0.03609	204.381	121.166
MAMDC2	1053.76	-0.5924	0.000301	1288.716	818.809
ANXA1	21179.88	-0.5933	0.02466	26497.676	15862.085
PTPRR	126.07	-0.5997	0.047248	160.023	92.124
PLAT	113441.44	-0.6000	0.01255	141402.940	85479.930
TMEM200A	7045.78	-0.6032	1.08E-06	8591.029	5500.521
CRHBP	600.20	-0.6160	0.001694	744.354	456.054
SMURF2	3482.59	-0.6220	0.001857	4333.109	2632.067
PDCD10	1390.63	-0.6326	0.017432	1770.018	1011.236
NEXN	3077.42	-0.6339	0.015809	3914.026	2240.813
STXBP3	1218.20	-0.6358	0.018604	1554.927	881.469
WNT5B	2835.30	-0.6366	0.001201	3542.047	2128.549
TNFRSF10D	13044.79	-0.6375	0.003695	16396.121	9693.465
7-Sep	9071.48	-0.6386	0.039818	11785.485	6357.479
LCA5	166.00	-0.6390	0.047248	217.154	114.838
GIPC2	84.82	-0.6396	0.047708	111.147	58.484
PLCH2	616.93	-0.6406	0.005979	778.841	455.019
C15orf65	181.02	-0.6412	0.009835	229.828	132.219
LARP7	1740.54	-0.6486	0.014077	2228.296	1252.792
CDH2	4337.00	-0.6500	3.70E-07	5365.299	3308.703
VRK2	316.24	-0.6502	0.022213	408.638	223.846
STAG2	1086.30	-0.6585	0.04535	1444.038	728.566
AKAP5	227.55	-0.6617	0.029817	298.536	156.555
BLZF1	707.74	-0.6668	0.044212	948.297	467.174
SCOC	2913.60	-0.6781	0.025915	3856.985	1970.217
TWF1	2914.00	-0.6790	0.038453	3925.453	1902.548
ST6GAL2	170.75	-0.6803	0.017615	223.927	117.564
NXT2	253.22	-0.6803	0.020191	333.674	172.771
MAP3K7CL	4170.24	-0.6852	1.44E-05	5244.675	3095.805
STK38L	897.36	-0.6925	0.019776	1191.938	602.788
NEK7	5457.83	-0.7038	0.014441	7246.618	3669.044
PCDH10	8287.41	-0.7054	0.000243	10579.977	5994.834
TRIM23	367.97	-0.7088	0.020113	496.282	239.650
SMC6	1013.08	-0.7107	0.011535	1343.726	682.430
ZDHHC20	1586.52	-0.7108	0.016003	2124.814	1048.218

DYNLT3	2962.65	-0.7199	0.004263	3884.350	2040.952
ASPN	489.31	-0.7234	0.020191	670.258	308.358
DNAJB4	4610.34	-0.7244	0.006346	6097.170	3123.502
E2F7	426.92	-0.7248	0.00033	550.295	303.549
ARPP21	405.79	-0.7273	3.34E-05	519.482	292.093
LOC100126784	562.67	-0.7275	1.70E-05	718.673	406.659
NAV2	2237.87	-0.7299	5.46E-07	2844.299	1631.446
GREM1	5666.75	-0.7448	3.15E-07	7232.619	4100.881
PTPRB	813.68	-0.7568	4.60E-05	1054.405	572.949
LACC1	361.02	-0.7597	0.008256	492.903	229.139
FGF5	119.94	-0.7660	0.004125	161.680	78.201
KRT34	148.20	-0.7737	0.002252	198.858	97.552
CLDN14	41.45	-0.7785	0.014354	64.146	18.763
DCSTAMP	128.12	-0.7895	0.001852	172.890	83.356
KCNN4	262.98	-0.7953	0.00493	363.743	162.214
PODXL	2583.24	-0.9762	6.91E-07	3594.753	1571.733

APPENDIX B

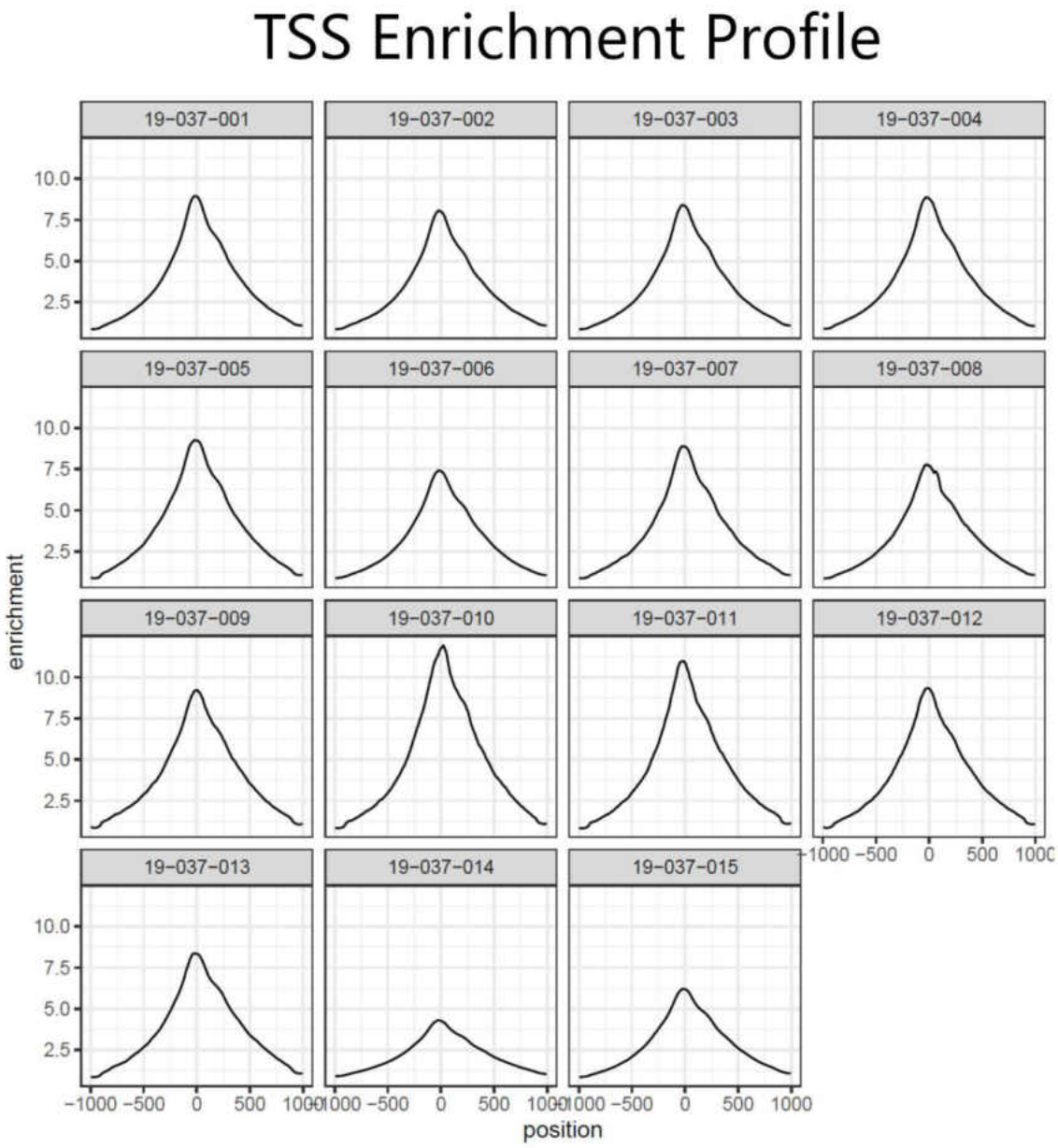

Figure Appendix B – 1: TSS enrichment – Chapter IV

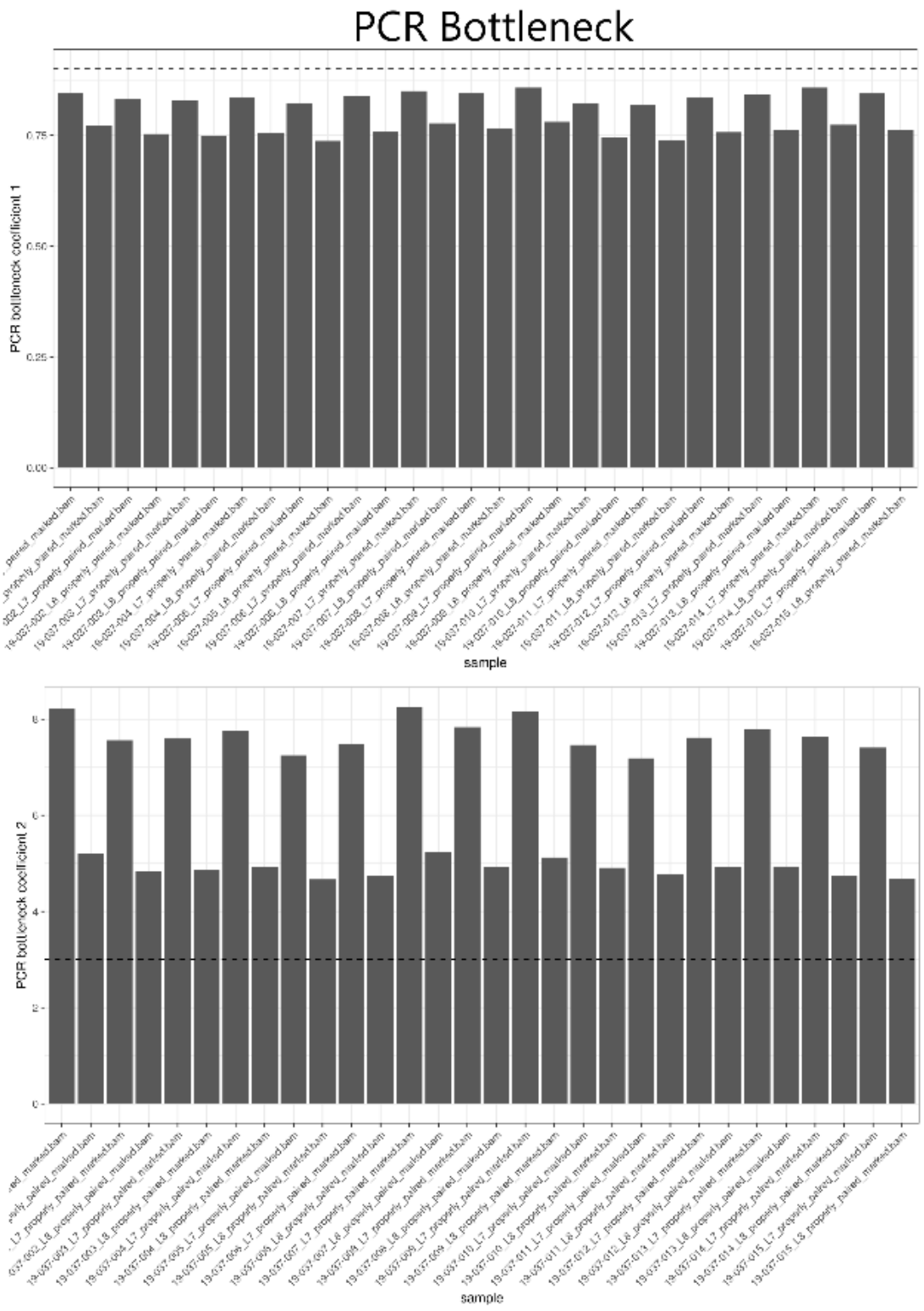

Figure Appendix B – 2: PCR Bottleneck Coefficient – Chapter IV

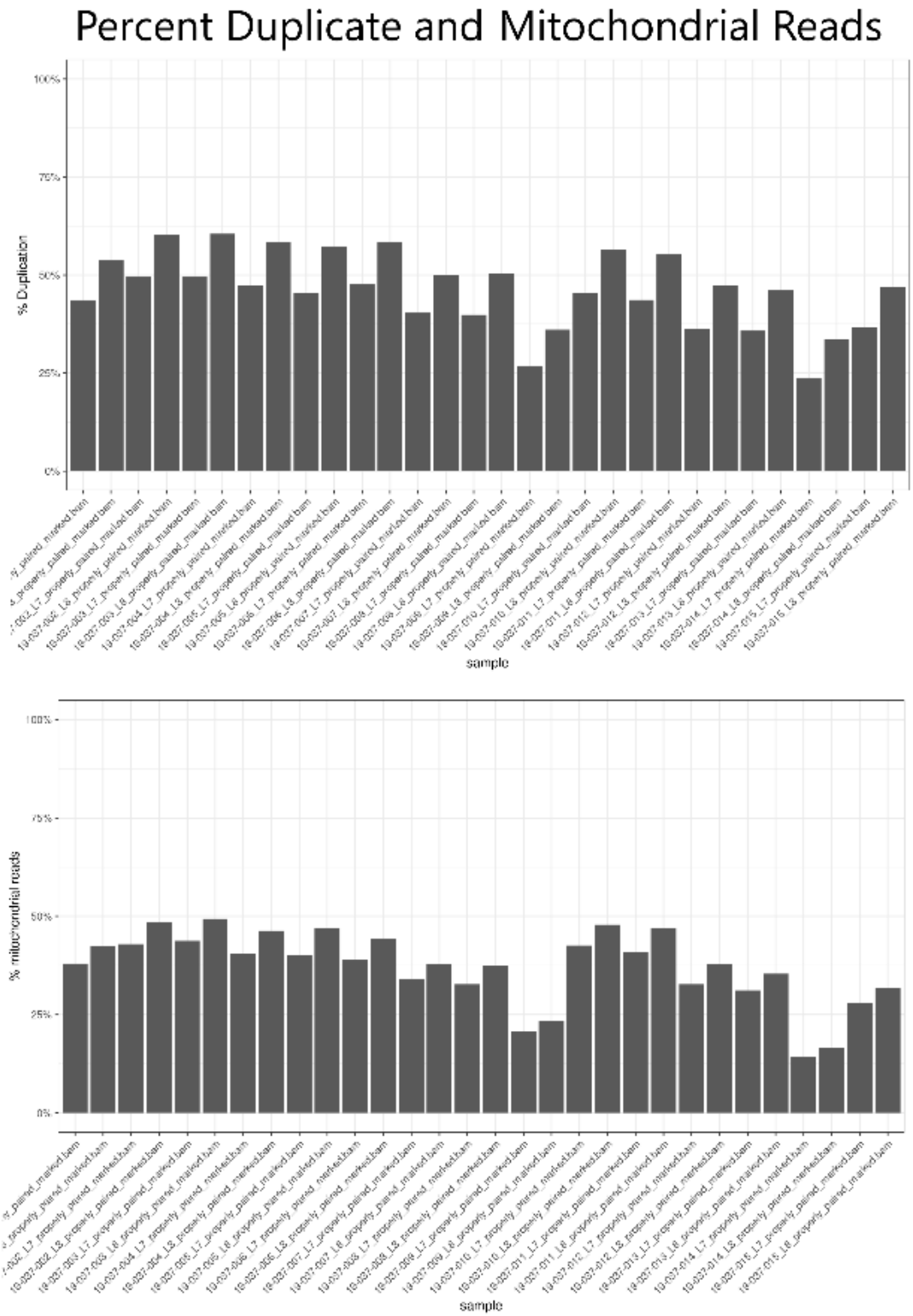

Figure Appendix B – 3: Percent of duplicate and mitochondrial reads – Chapter IV